Universidade Federal Fluminense

Instituto de Física

Coordenação do Curso de Pós-Graduação em Física

Tese de doutorado

Adiabatic dynamics and shortcuts to adiabaticity in many-body systems.

Ivan Berbert Coulamy

Niterói-RJ

Maio de 2018

Universidade Federal Fluminense

Instituto de Física

Coordenação do Curso de Pós-Graduação em Física

Adiabatic dynamics and shortcuts to adiabaticity in many-body systems.

Ivan Berbert Coulamy

Tese realizada sob orientação do Prof. Dr. Marcelo Silva Sarandy, apresentada ao Programa de Posgraduação em Física da Universidade Federal Fluminense, em complementação aos requisitos para obtenção da titulação de Doutor em Física.

Niterói

Maio de 2018

Ficha catalográfica automática - SDC/BIF

C855a Coulamy, Ivan Berbert
Adiabatic dynamics and shortcuts to adiabaticity in many-bodysystems. / Ivan Berbert Coulamy ; Marcelo Sarandy, orientador. Niterói, 2018.
107 f. : il.

Tese (doutorado)-Universidade Federal Fluminense, Niterói, 2018.

DOI: http://dx.doi.org/10.22409/PPGF.2018.d.1192596807

1. Mecânica quântica. 2. Informação quântica. 3. Adiabaticidade quântica. 4. Busca quântica. 5. Produção intelectual. I. Título II. Sarandy,Marcelo, orientador. III. Universidade Federal Fluminense. Instituto de Física.

CDD -

Bibliotecária responsável: Danieli Brabo de Moraes - CRB7/5805

Universidade Federal Fluminense

Instituto de física

Coordenação do Curso de Pós-Graduação em Física

Tese de doutorado

Adiabatic dynamics and shortcuts to adiabaticity in many-body systems.

Ivan Berbert Coulamy

Banca Examinadora:

Prof. Dr. Marcelo Silva Sarandy (Orientador-UFF)

Prof. Dr. Frederico Borges de Brito (USP-São Carlos)

Prof. Dr. Roberto Silva Sarthour Júnior (CBPF)

Prof. Dr. Ernesto Fagundes Galvão (UFF)

Prof. Dr. Jose Augusto Oliveira Huguenin (UFF)

Prof. Dr. Fernando da Rocha Vaz Bandeira de Melo (CBPF-Suplente)

Prof. Dr. Marcos Sérgio Figueira da Silva (UFF-Suplente)

Prof. Dr. Thiago Rodrigues de Oliveira (UFF-Suplente)

Niterói

Maio de 2018

Agradecimentos

Agradeço primeiro meus pais e minha família, sem seu contínuo, generoso e carinhoso apoio nada dessa jornada teria sido possível.

Agradeço também meu orientador Marcelo, que com muita paciência me ajudou a aprender tanto nesses últimos cinco anos. Um agradecimento especial ao Adolfo, que me recebeu em Boston e me ajudou a me adaptar à cidade e ao país, além de me ensinar muito sobre física. Agradeço também ao prof. Sérgio Duarte, que orientou minha primeira iniciação cientifica, literalmente abrindo novos horizontes para mim.

Agradeço também a todos outros bons professores que tive a sorte de encontrar ao longo de minha vida acadêmica. Desde muito jovem fui fascinado pelas boas aulas que assisti e trago várias lembranças de momentos que até hoje me inspiram a tentar entender mais sobre o nosso misterioso e magnifico universo.

"Do or do not, there is no try."

-Master Yoda

List of Figures

List of Abbreviations

AQC	Adiabatic Quantum Computation
AT	Adiabatic Theorem
CD	Counterdiabatic Driving
QA	Quantum Annealing
KZM	Kibble-Zurek mechanism
LCD	Local Counterdiabatic Driving
LQU	Local Quantum Uncertainty
QD	Quantum Decoherence
QPT	Quantum Phase Transition
STA	Shortcuts to Adiabaticity

Contents

Citations to Previously Published Work

Chapter 3 has been previously published [35] as

I.B. Coulamy, J.H. Warnes, M.S. Sarandy, and A. Saguia. Scaling of the local quantum uncertainty at quantum phase transitions. *Physics Letters A*, 380(20):1724 – 1728, 2016, DOI: 10.1016/j.physleta.2016.03.026.

Chapter 4 has been previously published [36] as

I. B. Coulamy, A. Saguia, and M. S. Sarandy. Dynamics of the quantum search and quench-induced first-order phase transitions. *Phys. Rev. E*, 95:022127, Feb 2017, DOI: 10.1103/PhysRevE.95.022127.

Chapter 5 has been previously published [37] as

Shujin Deng, Aurélia Chenu, Pengpeng Diao, Fang Li, Shi Yu, Ivan Coulamy, Adolfo del Campo, and Haibin Wu. Superadiabatic quantum friction suppression in finite-time thermodynamics. *Science Advances*, 4(4), 2018. DOI: 10.1126/sciadv.aar5909.

And Chapter 2 has made references to [31] as

I. B. Coulamy, A. C. Santos, I. Hen, and M. S. Sarandy. Energetic cost of superadiabatic quantum computation. *Frontiers in ICT*, 3:19, 2016, DOI: 10.3389/fict.2016.00019.

Resumo

Nessa tese estudamos propriedades das dinâmicas adiabática e diabática de sistemas quânticos de muitos corpos. Como aplicação, investigamos formulações Hamiltonianas para o problema da busca quântica e a aplicação de atalhos para adiabaticidade em um gás unitário quântico que imita em tempo finito exatamente uma evolução adiabática.

Primeiro examinamos as correlações quânticas mensuradas pela local quantum uncertainty (LQU) em uma cadeia de spins implementando a versão adiabática da busca quântica. Obtemos o valor exato da correlação entre um spin e um bloco de L spins para diversos valores de L ao longo da evolução. Nós mostramos que a LQU apresenta um comportamento característico no ponto de transição de fase quântica.

Em seguida estudamos os erros ocorridos numa implementação em tempo finito da busca quântica com uma forma análoga ao mecanismo de Kibbe-Zurek (KZM em inglês) porém aplicada a transições quânticas de primeira ordem. É demonstrado que a formação de kinks segue uma lei exponencial, e são comparadas as dinâmicas de estrategias local e global para adiabaticidade.

Finalmente, encontramos um sistema em que atalhos para adiabaticidade podem ser implementados em laboratório com tecnologia atual e os erros causados por excitações são suprimidos. Isso é demonstrado ao estudarmos a implementação em tempo finito da expansão de uma nuvem de gás quântico unitário em um motor termodinâmico.

Abstract

In this thesis we study properties of the adiabatic and diabatic dynamics of many body quantum systems. As a test bed, we investigate Hamiltonian formulations for the quantum search algorithm and the application of shortcuts to adiabaticity in a unitary quantum gas to mimic an exact adiabatic evolution in finite time.

First we examine the quantum correlations as measured by the local quantum uncertainty (LQU) in a spin chain implementing the adiabatic quantum search algorithm. We obtain the exact value of the correlation measure between a single spin and a block of L spins with many different values of L throughout the evolution. We show that the LQU exhibits pronounced behaviour at the quantum phase transition.

Next we study the errors occurring in a finite-time implementation of the quantum search with an analogy to the Kibble-Zurek mechanism but related to first order quantum phase transitions. We show that the formation of kinks follow an exponential law, we also compare the exact dynamic of global and local adibaticity strategies.

Finally we find a system where shortcuts to adiabaticity can be implemented with current technology and the errors due to excitations are thus removed. We show this by examining a finite-time expansion stroke of a thermodynamic engine operating on a cloud of a unitary quantum gas.

Chapter 1

Introduction

In 1980 Paul Benioff published his pioneering work on Hamiltonian models of computers [1] and in 1981 Feynman gave his famous lecture 'Simulating physics with computers' [2], in both it was made clear what is one of the greatest difficulties in simulating quantum physical phenomena with classical computers: the exponential scaling of classical physical resources to describe quantum phenomena. This exponential scaling is also the motivation for its own solution: to use quantum resources to manipulate information in physical systems. Soon after Feynman's lecture great advances started being made towards understanding what a quantum computer was and what it could offer: Deutsch proposed the first description of a universal quantum computer [3], Shor created his algorithm for factoring large numbers [4] and Grover created an optimal algorithm for searching through unstructured lists [5, 6].

As it became clear that quantum computers would be able to offer superior performance in some tasks, compared to the best known classical algorithms, the field gained more and more interest and soon several new ways of doing quantum computation were proposed. One proposal was to build adiabatic quantum computers [7]. This approach offers equivalent performance (up to some polynomial overhead) compared to the more traditional circuit-based quantum computers [8]. On the other hand, there are several advantages, including robustness against some kinds of errors [9] and the provision of a more natural language to physicists since it deals with the evolution of Hamiltonians instead of the logic gate truth tables more natural to computer scientists. But being analog

has brought its own problems, like difficulty in error-correction and chaos [10].

Adiabatic Quantum Computation (AQC) has been successfully implemented in Nitrogen-vacancies in diamond [11], superconducting flux qubits [12, 13], Rydberg atoms [14], NMR [15–18], ion traps [19], etc. In the commercial arena D-Wave Inc. has brought a great deal of attention to AQC by selling quantum annealers implemented through adiabatic evolution [20–22] which helped bring up the seemly innocuous but deep question of how to recognize quantum speedup [23, 24].

In trying to find better ways to build a quantum computer and make it work, it pays to go into more detail over what exactly we want it to do. From about 1600 to just before the advent of the first electronic computers, "computer" was a person who worked doing calculations [25]. So computation was the act of following a rigid set of instructions to do a specific mathematical calculation. With the advent of modern electronic computers this has remained the same, just the human execution of the basic operations has been removed.

It is clear that to define what computation is we have first to see what a computer (of the modern kind) is. After defining a general computer we will be able to define a classical computer (in short: the ones we use nowadays) and a quantum computer.

A computer, in general, is a device that:

- receives information as input,
- stores that input,
- manipulates that information,
- and outputs the result.

Information is stored by setting some measurable physical quantity of a system to a predefined value. In the binary digital logic favored nowadays only two values are necessary, so that we can represent 0 and 1. Each of these zeros and ones represents a unit of information called a "bit".

Quantum computers use physical resources that need quantum mechanics to describe their behavior when storing and operating on information, like an electron's magnetic

spin instead of a current of electrons as in classical computers. This different physical implementation opens the possibility to explore uniquely quantum phenomena that are not available to classical computers. Two quantum phenomena of great import are state superpositions and quantum correlations.

Classical bits, or just bits, only have two available states, 0 and 1. Quantum bits, or qubits, also have two available states, 0 and 1, but they can also exist in what physicists call a superposition: a state that operates like an overlap of them but when measured shows up as being only one of them. Superposed states are useful for any operation executed on the system acts on all of the superposed states, leading to a high level of parallelism.

Quantum correlations is a name used to collect a broad range of interactions between subsystems that cannot be explained by classical physics. One example of quantum correlation is entanglement. Entangled pairs of qubits have the property that even if they are both described by a pure global state, their individual states are mixed and thus have some uncertainty inherently. It has been verified that entanglement plays a role on some important quantum algorithms [26]. It has also been verified that there are some quantum algorithms that perform better than classical analogues without using any entanglement [27]. As a consequence, quantum computers have access to operations on their physical qubits that have no analogue on classical computers. These new operations open many new possibilities for faster algorithms that we are still learning to exploit.

So, what is quantum computing? In short, now that we know what a quantum computer is, we can define what quantum computation is by saying: "it is what quantum computers do: storing and manipulating quantum mechanical quantities to represent and operate on information".

As already said, quantum computers manipulate some quantum properties of a system to store and operate on information. But doing that can be tricky for several reasons, and not only quantum computers but quantum thermal machines face the same problem: design and correctly implement a reliable quantum process.

Adiabatic quantum computers are protected from some sources of errors, but the com-

putational process must be realized at a time that is long enough compared to the energy gap of the system, which may expose the quantum computer to a phenomenon known as quantum decoherence (QD). In short, QD is the effect a quantum system undergoes as its degrees of freedom get unpredictably entangled with the degrees of freedom of the surrounding environment as time passes by, so that the superpositions originally in the system are spread out through the environment due the system-environment interaction.

In this thesis, we will explore correlations and excitation dynamics in adiabatic algorithms, as well as one possible solution to overcoming QD, which is provided by shortcuts to adiabaticity. Shortcuts to adiabaticity can be achieved when a system's evolution is tailored to mimic an infinite time adiabatic evolution, but in a finite amount of time. Usually this is experimentally hindered by the resulting Hamiltonian's complexity and non-locality of interactions, but we have found a system where this was overcome and the resulting many-body evolution could be precisely controlled. The particular system found was a unitary quantum gas, which is characterized by having only 2-body interactions with infinite scattering length and null range. These three characteristics together greatly simplify the dynamics allowing us to control the necessary quantities just by modulating the trap potential.

1.1 Outline of this Thesis

The thesis is organized as follows. We first introduce in chapter 2 the fundamental concepts and theories of adiabatic computation [7], the simplest adiabatic condition [28], quantum phase transitions [29], shortcuts to adiabaticity [30], the quantum search algorithm [31, 32] and quantum correlations [33].

In chapter 3 we investigate a quantum correlation measure called local quantum uncertainty (LQU) [34]. More specifically, we consider the LQU between a block of L qubits and one single qubit in a composite system of n qubits driven through a quantum phase transition (QPT) [35]. A first-order QPT is analytically considered via a Hamiltonian implementation of the quantum search. We compute the LQU for finite-sizes as a function of L and of the coupling parameter, analyzing its pronounced behavior at the QPT and

its consequences for the adiabatic implementation of the quantum search.

In chapter 4 we investigate the effects of the finite-time evolution over adiabaticity, considering the excitation dynamics at a first-order QPT in the quantum search algorithm [36]. We begin by deriving the exact dynamics of the model, which is shown to obey a Riccati differential equation. Then, we discuss the probabilities of success by adopting either global or local adiabaticity strategies. Moreover, we determine the disturbance of the quantum criticality as a function of the system size. In particular, we show that the critical point exponentially converges to its thermodynamic limit even in a fast evolution regime, which is characterized by both entanglement QPT estimators and the Schmidt gap. The excitation pattern is manifested in terms of quantum domain walls separated by kinks. The kink density is then shown to follow an exponential scaling as a function of the evolution speed, which can be interpreted as a Kibble-Zurek mechanism for first-order QPTs.

Looking beyond the adiabatic dynamics, we also consider shortcuts to adiabaticity, which mimic the effect of the adiabatic evolution by adding counter-fields in the dynamics so that they can be implemented in finite time [37]. In particular, this can be investigated in the context of thermal machines. Optimal performance of thermal machines is reached by suppressing friction. Friction in quantum thermodynamics results from fast driving schemes that generate nonadiabatic excitations. The far-from-equilibrium dynamics of quantum devices can be tailored by shortcuts to adiabaticity to suppress quantum friction. In chapter 5 we experimentally demonstrate friction-free superadiabatic strokes with a trapped unitary Fermi gas as a working substance and establish the equivalence between the superadiabatic mean work and its adiabatic value.

Finally, in chapter 6 we present our conclusions and remarks on future work.

Chapter 2

Fundamentals

In this chapter some well known results are presented. These are necessary for the understanding of the new results shown in later chapters.

2.1 Adiabatic Quantum Computation

The first ideas on how to build quantum computers were extensions of the highly successful ideas used to build classical computers from electronic circuits [38]. Quantum circuits computation proposed that series of quantum gates could act in sequence on qubits to transform their state according to the chosen algorithm. A quantum gate being an operation that interacts with a number of qubits (usually one or two) in a fixed way.

Computation by quantum gate circuitry was proven universal (capable of implementing any algorithm) [3]. It was also experimentally implemented in several forms [39, 40]. But developing quantum algorithms that are superior to classical alternatives is a difficult task. Also there was always the possibility that alternative ways of doing quantum computation would be prone to less, or at least different, sources of errors. The hunt for alternative forms of quantum computation was on.

An alternative approach named Adiabatic Quantum Computation (AQC) was proposed in 2000 by Farhi [7] and it was proven to be equivalent to quantum circuit computation with only polynimial overhead [8] and was experimentally implemented in several settings [13, 15, 17, 19–21, 41–43].

AQC consists in the following algorithm to solve a computational problem:

1. Prepare a system in the ground state of a driving Hamiltonian H_D.
2. Choose a Hamiltonian, H_P, which encodes in its ground state the solution to the problem of interest.
3. Evolve this system changing its Hamiltonian from H_D to H_P *slowly enough* so that the system keeps track of the instantaneous ground state of the evolving Hamiltonian.
4. Measure the system, obtaining the desired solution with a given probability.

The Hamiltonian H_D is usually chosen in a way that its ground state is the superposition of all computational states and has no degeneracy. This way ensures that the desired final state is present in the initial superposition [44]. Since H_P encodes the solution to a classical computational problem it will be diagonal in the computational basis, making measuring it simple.

Also, when the system is driven from H_D to H_P it must do so slowly enough so that the adiabatic theorem (AT) applies to this evolution. This theorem is what guarantees that at the final measurement we will have the desired answer with high probability and is explained in the next section.

2.1.1 Adiabatic Theorem

If a system is driven by a time-dependent Hamiltonian its evolution is described by the Schrödinger equation

$$i\hbar\partial_t \left|\psi(t)\right\rangle = H(t) \left|\psi(t)\right\rangle, \tag{2.1}$$

where ∂_t represents the time derivative. Solving this equation is not trivial in general, but for a special case the AT offers a simplified solution.

If $|\psi_n(t)\rangle$ is the n-th eigenstate of H(t), the AT states that if a system is prepared at t=0 as $|\psi_n(0)\rangle$ and the driving Hamiltonian varies slowly enough, then the system will remain close to the instantaneous eigenstate $|\psi_n(t)\rangle$.

This theorem is very useful in our context. It was shown by Farhi et all [7] that it is possible to create a Hamiltonian that encodes the solution of a minimization problem in its final form without the need to know this solution.

The AT was first demonstrated by Born and Fock [28] (and is still present in modern text books [45]) in a way that we will call from now on the traditional version of the AT. It was expanded and improved by Kato [46] and recently similar results were found by Boixo et al [47]. This result points that, for the evolution to be approximately adiabatic, its time scale must be much larger than the inverse of the squared gap times the largest absolute value of the eigenvalues of the time derivative of the Hamiltonian.

This traditional version of the AT has been shown to fail on some occasions and not be necessary on others [48, 49], for this reason the AT has been the focus of a lot of research and refinement lately. There are now several versions of this theorem [44]. We will use the traditional (simplest) version because all adiabatic Hamiltonians of interest in this thesis are real (no geometric phase) and lack oscillatory terms (sines and cosines for example) [50].

2.1.2 Traditional Version of the AT

The proof of the simplest version of this theorem goes as this. Taking H(t) as a Hamiltonian with discrete spectrum and the initial state as $|\Psi(0)\rangle$ and setting $\hbar = 1$ so that its eigenstates and eigenenergies are related by

$$H(t)\,|\psi_n(t)\rangle = E_n(t)\,|\psi_n(t)\rangle\,, \tag{2.2}$$

and the corresponding Schrödinger equation for this system is

$$i\partial_t\,|\Psi(t)\rangle = H(t)\,|\Psi(t)\rangle\,. \tag{2.3}$$

We can express the current state as a superposition of eigenstates:

$$|\Psi(t)\rangle = \sum_n c_n(t)\,|\psi_n(t)\rangle\,e^{i\theta_n(t)}, \tag{2.4}$$

where:

$$\theta_n(t) \equiv -\int_0^t E_n(t')dt'. \tag{2.5}$$

Substituting in (2.3), and omitting the time dependency, we get:

$$i\sum_n \left\{\dot{c}_n \left|\psi_n\right\rangle + c_n|\dot{\psi_n}\rangle + ic_n \left|\psi_n\right\rangle \dot{\theta}_n\right\} e^{i\theta_n} = \sum_n c_n(H\left|\psi_n\right\rangle)e^{i\theta_n}. \tag{2.6}$$

The two rightmost terms cancel each other, so:

$$\sum_n \dot{c}_n \left|\psi_n\right\rangle e^{i\theta_n} = -\sum_n c_n|\dot{\psi_n}\rangle e^{i\theta_n}. \tag{2.7}$$

Taking the inner product with $\langle\psi_m|$:

$$\sum_n \dot{c}_n\delta_{nm}e^{i\theta_n} = -\sum_n c_n \left\langle\psi_m\middle|\dot{\psi}_n\right\rangle e^{i\theta_n}, \tag{2.8}$$

which is equivalent to

$$\dot{c}_m(t) = -\sum_n c_n \left\langle\psi_m\middle|\dot{\psi}_n\right\rangle e^{-i\int_0^t \omega_{nm}(t')dt'}, \tag{2.9}$$

where

$$\omega_{nm}(t) = E_n(t) - E_m(t). \tag{2.10}$$

Now differentiating (2.2) on time we get:

$$\dot{H}\left|\psi_n\right\rangle + H|\dot{\psi_n}\rangle = \dot{E}_n \left|\psi_n\right\rangle + E_n|\dot{\psi_n}\rangle. \tag{2.11}$$

Taking the inner product with $\langle\psi_m|$:

$$\langle\psi_m|\dot{H}|\psi_n\rangle + \left\langle\psi_m\middle|H\middle|\dot{\psi}_n\right\rangle = \dot{E}_n\delta_{nm} + E_n\left\langle\psi_m\middle|\dot{\psi}_n\right\rangle. \tag{2.12}$$

Since this Hamiltonian is Hermitian:

$$\left\langle\psi_m\middle|H\middle|\dot{\psi}_n\right\rangle = E_m\left\langle\psi_m\middle|\dot{\psi}_n\right\rangle. \tag{2.13}$$

Using (2.13) in (2.12) if $m \neq n$ results in:

$$\langle\psi_m|\dot{H}|\psi_n\rangle = (E_n - E_m)\left\langle\psi_m\middle|\dot{\psi}_n\right\rangle. \tag{2.14}$$

By combining (2.9) and (2.14) we get:

$$\dot{c}_m(t) = -c_m(t)\left\langle\psi_m\middle|\dot{\psi}_m\right\rangle - \sum_{n\neq m} c_n(t)\frac{\langle\psi_m|\dot{H}|\psi_n\rangle}{\omega_{nm}}e^{-i\int_0^t \omega_{nm}(t')dt'}. \tag{2.15}$$

To this point the results are all exact, but to simplify (2.15) we need to use the adiabatic approximation. Assuming the Hamiltonian to evolve very slowly, the term $\langle\psi_m|\dot{H}(t)|\psi_n\rangle$ can be neglected, an approximation that will be further explored on next section. So

$$\dot{c}_m(t) = -c_m\left\langle\psi_m\middle|\dot{\psi}_m\right\rangle. \tag{2.16}$$

Solving this ODE:

$$c_m(t) = c_m(0)e^{i\gamma_m(t)}, \tag{2.17}$$

where $\gamma(t)$ is

$$\gamma_m(t) \equiv i\int_0^t \left\langle\psi_m\middle|\frac{\partial}{\partial t'}\psi_m\right\rangle dt'. \tag{2.18}$$

It's clear that γ is a real number for:

$$\langle\psi_m|\psi_m\rangle = 1 \rightarrow \frac{d}{dt}\langle\psi_m|\psi_m\rangle = 0, \tag{2.19}$$

and

$$\frac{d}{dt}(\langle\psi_m|\psi_m\rangle) = \left\langle\dot{\psi}_m\middle|\psi_m\right\rangle + \left\langle\psi_m\middle|\dot{\psi}_m\right\rangle = 2\,\mathrm{Re}\left(\left\langle\psi_m\middle|\dot{\psi}_m\right\rangle\right) = 0. \tag{2.20}$$

It is shown that if a system starts at some n-th eigenstate and its Hamiltonian changes slowly enough for the evolution to be adiabatic, then the system will remain on the same n-th eigenstate up to a phase.

$$|\Psi(t)\rangle = |\psi_n\rangle\, e^{i[\theta_n(t)+\gamma_n(t)]}. \tag{2.21}$$

2.1.3 Quantum Adiabaticity Condition

Now to see when this approximation is valid we notice that on the previous section we used an approximation to solve equation (2.14).

$$e^{i\gamma_m}(t)\frac{d}{dt}(c_m(t)e^{-i\gamma_m(t)}) = \dot{c}_m(t) + c_m(t)\left\langle \psi_m \middle| \dot{\psi}_m \right\rangle. \tag{2.22}$$

Rewriting (2.15):

$$e^{i\gamma_m}(t)\frac{d}{dt}(c_m(t)e^{-i\gamma_m(t)}) = -\sum_{n\neq m} c_n(t)\frac{\langle\psi_m|\dot{H}|\psi_n\rangle}{\omega_{nm}(t)}e^{-i\int_0^t \omega_{nm}(t')dt'}. \tag{2.23}$$

Now parametrizing time:

$$s = t/T, \tag{2.24}$$

where T is the usual total evolution time. This way as we plug (2.24) in (2.23) it results in:

$$e^{i\gamma_m}(s)\frac{d}{ds}(c_m(s)e^{-i\gamma_m(s)}) = -\sum_{n\neq m} c_n(s)\frac{\langle\psi_m|\frac{d}{ds}H|\psi_n\rangle}{\omega_{nm}(s)}e^{-iT\int_0^s \omega_{nm}(s')ds'}. \tag{2.25}$$

Now we define:

$$F_{nm}(s) = c_n(s)e^{-i\gamma_m}\left\langle \psi_m \middle| \frac{d}{ds}H \middle| \psi_n \right\rangle. \tag{2.26}$$

Plugging this definition in (2.25), and integrating over time results in

$$c_m(s)e^{-i\gamma_m(s)} = c_m(0) - \sum_{n\neq m}\int_0^s \frac{F_{nm}}{\omega_{nm}}e^{-iT\int_0^{s'} \omega_{nm}(s')ds'}. \tag{2.27}$$

Integrating by parts we get:

$$\begin{aligned} c_m(s)e^{-i\gamma_m(s)} = c_m(0) - \frac{i}{T}\sum_{n\neq m}\Big[\frac{F_{mn}(s)}{\omega_{mn}^2(s)}e^{-iT\int_0^s \omega_{nm}(s')ds'} - \frac{F_{mn}(0)}{\omega_{mn}^2(0)} - \\ - \int_0^s e^{-iT\int_0^{s'} \omega_{nm}(s'')ds''}\frac{d}{ds'}\Big(\frac{F_{mn}(s')}{\omega_{mn}^2(s')}\Big)ds'\Big]. \end{aligned} \tag{2.28}$$

On the right hand side of (2.28) the Riemann-Lebesgue lemma shows that for large T the oscillating integral will be equal to zero. Now only the first two terms in the summation

make this a coupled evolution. So the condition for adiabaticity to hold is that T be much greater then the absolute value of the summation. Also, as the complex exponential has absolute value constant and equal to 1, and we discard $c_n(s)$ for $|c_n(s)| \leq 1$. Therefore, a decoupled evolution requires:

$$T \gg \underset{0 \leq s \leq 1}{Max} \left| \frac{\langle \psi_m(s) | \frac{d}{ds} H(s) | \psi_n(s) \rangle}{\omega_{nm}^2(s)} \right| = \frac{\varepsilon}{g_{min}^2}, \tag{2.29}$$

or, as a function of time, alternatively:

$$1 \gg \underset{0 \leq t \leq T}{Max} \left| \frac{\langle \psi_m(t) | \dot{H}(t) | \psi_n(t) \rangle}{\omega_{nm}^2(t)} \right|. \tag{2.30}$$

So, we see that the total evolution time must scale with the square of the inverse of the energy gap between the current state and its closest neighboring states. Since we will be working with the ground state only the gap between this and the first excited state (ω_{01}) will be relevant. This result is only exact when the algorithm's execution time approaches infinity.

It is known that this quantum adiabaticity condition in general is neither necessary nor sufficient [51]. Adiabatic conditions more general than (2.30), such as in Refs. [50,52], are beyond the scope of this thesis.

2.2 Circuit Quantum Search Algorithm

The original quantum circuit algorithm searches through an unstructured list of size N looking for a state that satisfies some property, usually referred as the marked state. Given a black box function f, if m is the marked state then $f(m) = a$, but if $y \neq m$ then $f(y) = b$, where $a \neq b$. Such function f is said to be an oracle that recognizes the solution m. Grover's algorithm goes to prove that such function needs to be evaluated $O(\sqrt{N})$ times by a quantum computer to find m, the marked state. This is remarkable because a classical computer would need $O(N)$ evaluations to execute the same search (for more details on the big-O notation see Appendix:A).

To describe the oracle as a mathematical function without explaining its inner workings is quite abstract and may give the impression that this oracle already has to know the answer in the first place in order to work. It is important to notice however that there is a distinction between recognizing a solution and knowing it ahead of time. It is possible to achieve the first without necessarily achieving the second. A simple everyday example is a lock: looking at one will not reveal enough information to figure which is the correct key for opening it from a large keyring, but slotting the right key and twisting it unlocks the door, thus the lock recognizes the proper answer (the key in this case). Notice that we do not need to know how a lock works to use it.

Assuming a single marked state m, the circuit based algorithm works by first initializing the system in the $|\psi_0\rangle = |0\rangle^{\otimes n}$ state then applying a Hadamard gate (for details on this and many other gates see [53]) to all qubits $H^{\otimes n}$. This puts the system in an equal superposition of all states $|+\rangle = N^{-\frac{1}{2}} \sum |i\rangle$. Now we have repeated applications of the Grover operator (G), which consists of several operators and one evaluation of the oracle so that $G = (2\,|+\rangle\langle+| - \mathbb{1})O$. In this case the oracle is taken to have the property of doing a phase shift on the solution only, as in $O\,|z\rangle = (-1)^{\delta_{z,m}}\,|z\rangle$, so $O = (\mathbb{1} - 2\,|m\rangle\langle m|)$. The whole algorithm is illustrated by Figure 2.1, taken from [53].

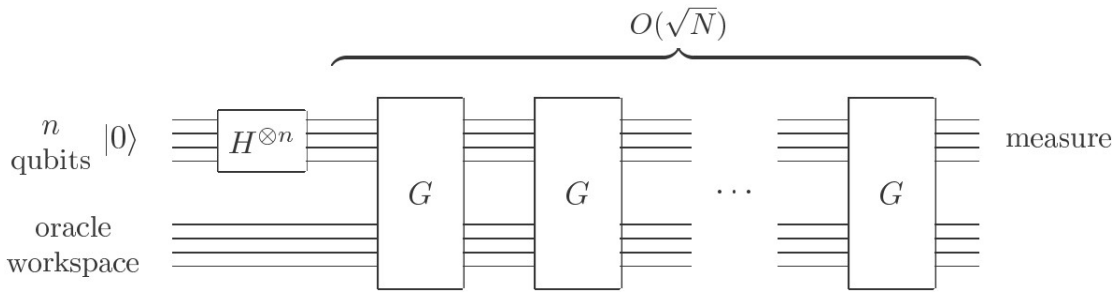

Figure 2.1: Representation of the quantum circuit implementation of the quantum search algorithm.

The Grover operator can be best understood by its geometric interpretation. If we define a vector that is the uniform superposition of all base states that are not the answer to our problem we have $|\psi_n\rangle = \sqrt{1 - 1/N} \sum_{i \neq m} |i\rangle$, we can then see that:

$$|+\rangle = \sqrt{1/N}\,|m\rangle + \sqrt{1-1/N}\,|\psi_n\rangle\,. \tag{2.31}$$

Seeing how O acts on a vector spanned by $|m\rangle$ and $|\psi_n\rangle$: $O(a\,|m\rangle + b\,|\psi_n\rangle) = -a\,|m\rangle + b\,|\psi_n\rangle$ we can see that it implements a reflexion about $|\psi_n\rangle$. Also, the remainder of G is clearly similar to O and is a rotation about $|+\rangle$. Knowing that the product of two reflexions is a rotation we see that G is a rotation by looking at its matrix form:

$$G = \begin{pmatrix} 1-2/N & \frac{2\sqrt{1-1/N}}{\sqrt{N}} \\ -\frac{2\sqrt{1-1/N}}{\sqrt{N}} & 1-2/N \end{pmatrix}. \tag{2.32}$$

Defining θ so that $cos(\theta/2) = \sqrt{1-1/N}$, gives $|+\rangle = cos(\theta/2)\,|\psi_n\rangle + sin(\theta/2)\,|m\rangle$, and with a bit of trigonometry:

$$G = \begin{pmatrix} cos(\theta) & sin(\theta) \\ -sin(\theta) & cos(\theta) \end{pmatrix}, \tag{2.33}$$

so

$$G^k\,|+\rangle = cos(\frac{1+2k}{2}\theta)\,|\psi_n\rangle + sin(\frac{1+2k}{2}\theta)\,|m\rangle\,, \tag{2.34}$$

where k is an integer that represents how many iterations occurred. So our uniform superposition vector gets rotated closer to the solution at every iteration, that is until it is in its closest position, after that further iterations would rotate it away from the desired answer. To see how many iterations are necessary for maximal probability of success we first remember that for $\theta \approx 0$ we have $cos(x) \approx 1 - x^2/2$, along with our definition of $cos(\theta/2)$ it gives us

$$\theta \approx 2/\sqrt{N}, \tag{2.35}$$

which agrees with our assumption of N being large. Now, for maximal probability we want $(1/2 + k)\theta \approx \pi/2$ so

$$k \approx \frac{\pi}{4}\sqrt{N} - 1/2. \tag{2.36}$$

This proves that the circuit quantum search scales as $O(\sqrt{N})$.

2.3 Adiabatic Quantum Search

The adiabatic version can be achieved by employing a Hamiltonian of the form:

$$H(s) = f(s)(\mathbb{1} - |+\rangle\langle+|) + g(s)(\mathbb{1} - |m\rangle\langle m|), \tag{2.37}$$

where $|m\rangle$ is again the marked state, s is the normalized time ($0 \leq s \leq 1$), and $|+\rangle = N^{-1/2}\sum_{i=0}^{N-1}|i\rangle$, and $f(0) = g(1) = 1$ and $f(1) = g(0) = 0$. Notice that $H_P = \mathbb{1} - |m\rangle\langle m|$ and $H_D = \mathbb{1} - |+\rangle\langle+|$ as seen in section 2.1.

This algorithm is simple and powerful. The simplicity comes from the straight forward nature of (2.37), so the spectrum and eigenvectors of this Hamiltonian can be analytically derived. And despite superior performance by classical algorithms to some important problems, like the NP-Complete 3-SAT [54] (with $O(1.33^n) < O(\sqrt{N}) \approx O(1.41^n)$) for example, it is also powerful because it is applicable to NP-Hard problems [55] (for more details on algorithmic complexity see appendix A) with better execution time scaling than the best known classical alternatives for unstructured search [5, 56, 57] (also known as exhaustive search). Unstructured search is the default solution when we don't have access to a specialist algorithm based on the problem's particular characteristics.

2.3.1 Spectrum and Eigenstates

In this section the demonstrations are original, but their results are already known in the literature.

Taking the eigenvectors to be of the form

$$|E(s)\rangle = \sum_i b_i(s)\,|i(s)\rangle\,, \tag{2.38}$$

if $b_m = 0$ then

$$H\,|E_{dg}(s)\rangle = (f(s) + g(s))\,|E_{dg}(s)\rangle - \frac{f(s)}{N}\sum_i b_i(s)\,|i\rangle = E_{dg}(s)\,|E_{dg}(s)\rangle\,. \tag{2.39}$$

So defining $|u\rangle = \sum_i |i\rangle$, we have that

$$\langle u|E_{dg}(s)\rangle = E_{dg}(s)\sum_i b_i(s) = (f(s)+g(s))\sum_i b_i(s) - \frac{f(s)}{N}(N-1)\sum_i b_i(s). \quad (2.40)$$

So, after some simple calculations

$$E_{dg}(s) = g(s) + \frac{f(s)}{N} \longrightarrow E_{dg}(s=0) = \frac{f(0)}{N}, \quad (2.41)$$

which is absurd, from (2.37) we know that $E_{dg}(s=0) = f(0)$ or $E_{dg}(s=0) = 0$. So we conclude that $\sum_{i=1}^{N-1} b_i(s) = 0$. From the previous equations we can show that $E_{dg} = f+g$, and from the summation constraint we can see that this subspace can be spanned by an eigenbasis of exactly $N-2$ vectors.

Now, to find the remaining 2 eigenvectors we study the case $b_m \neq 0$. From (2.37) symmetry we now assume that $b_j = b\ \forall j \neq m$ and $b_m = 1$ so that the eigenvector is written as

$$|E(s)\rangle = \mathrm{N}(s)\big(|m\rangle + b(s)\,|\phi\rangle\,\big),$$

where the normalization constant is $\mathrm{N}(s) = 1/\sqrt{1+(N-1)b(s)^2}$, $|\phi\rangle = \sum_{i\neq m}|i\rangle$. And we use again the fact that $|E\rangle$ is an eigen vector to obtain

$$E = f - \frac{1+(N-1)b}{N}f, \text{ and} \quad (2.42)$$

$$Eb = (f+g)b - \frac{1+(N-1)b}{N}f. \quad (2.43)$$

We find that there are two values of b and E that solve these equations. Naming these values with subindex minus for the lowest energy (ground state) and plus for the highest (first excited state) results in

$$|E_\pm(s)\rangle = \mathrm{N}_\pm(s)\big(|m\rangle + b_\pm(s)\,|\phi\rangle\,\big), \quad (2.44)$$

and

$$b_\pm(s) = 1 - \frac{E_\pm(s)}{f(s)\overline{N}}, \quad (2.45)$$

with $\overline{N} = 1 - 1/N$, and the corresponding energies $E_{\pm}(s)$ given by

$$E_{\pm}(s) = \frac{f(s) + g(s) \pm \sqrt{[f(s) + g(s)]^2 - 4f(s)g(s)\overline{N}}}{2}. \tag{2.46}$$

This result is also noticeable because, if we had a degenerated ground state with degeneracy p, then the only change in the previous set of equations would be the redefinition of the parameter $\overline{N}$ to $\overline{N} = 1 - p/N$.

The other higher-energy eigenstates form an $(N-2)$-fold degenerate eigenspace, whose energy is given by

$$E_{\mathrm{dg}} = [f(s) + g(s)]\,. \tag{2.47}$$

In order to explicitly provide the eigenstates $|E^k_{\mathrm{dg}}\rangle$ $(k = 1, \cdots, N-2)$ associated with the eigenenergy E_{dg}, we write

$$|E^k_{\mathrm{dg}}\rangle = \sum_{n=0}^{N-1} c^k_n |n\rangle. \tag{2.48}$$

Then, from the eigenvalue equation for $H(s)$ (2.37), it directly follows that the set $\{c^k_n\}$ is just required to satisfy the constraints $\sum_{n=0}^{N-1} c^k_n = 0$ and $c^k_m = 0$. As a consequence, the states $|E^k_{\mathrm{deg}}\rangle$ can be suitably chosen as *time-independent* vectors.

2.3.2 Local Adiabaticity

By imposing a local adiabatic evolution [32, 58], i.e. by requiring adiabaticity at each infinitesimal time interval, the runtime is minimized for the path (see also, e.g., Ref. [59])

$$f(s) = 1 - g(s), \qquad g(s) = \frac{1}{2} - \frac{\tan\left[\arctan\left(\sqrt{N-1}\right)(1-2s)\right]}{2\sqrt{N-1}}. \tag{2.49}$$

This results in a quadratic speedup over the classical search, i.e., we obtain the time complexity $O(\sqrt{N})$ expected from the quantum circuit Grover quantum search [32, 58].

To see this, first we substitute our previous adiabatic condition (2.29) (known as global adiabatic condition due to its dependency on the global minimum of the gap) by its local alternative in which we integrate over an infinite number of (2.29)

$$1 \gg \int_0^T \frac{|\,\langle E_+|\partial_t H|E_-\rangle\,|}{(E_+ - E_-)^2} dt. \tag{2.50}$$

Instantaneously we see that the integrand is bounded and we can write

$$\frac{|\langle E_+|\partial_t H|E_-\rangle|}{(E_+ - E_-)^2} \leq \epsilon, \tag{2.51}$$

for some ϵ. Since $s = t/T$ we have $\partial_t H = \partial_g H \partial_s g \partial_t s = \partial_g H \partial_s g/T$ and it can be shown that the numerator does not scale with the problem size, we can see that

$$\partial_s g \leq T\epsilon(E_+ - E_-)^2.$$

If we choose the case described by the equality signal

$$\partial_s g = T\epsilon(1 - 4g(1-g)\overline{N}). \tag{2.52}$$

Moving the infinitesimals and integrating on both sides gives

$$s = \frac{1}{2T\epsilon}\frac{N}{\sqrt{N-1}}\left[arctan(\sqrt{N-1}(2g-1)) + arctan(\sqrt{N-1}),\right] \tag{2.53}$$

but with the countour condition $g(1) = 1$ we can see that

$$\epsilon T\frac{\sqrt{N-1}}{N} = arctan(\sqrt{N-1}). \tag{2.54}$$

So the inverse of (2.53) is exactly (2.49).

To prove the time scaling we see, with some calculations, that (2.50) gives

$$T \gg \int_0^1 \frac{\sqrt{N-1}}{N}\frac{ds}{(1-4s(1-s)\overline{N})^{3/2}} = \sqrt{N-1}, \tag{2.55}$$

and we have just proven that this local adiabatic condition leads to the equivalent best time scaling for the quantum circuit paradigm of computation.

2.3.3 Experimental Implementation Difficulties

The possibility of shifting through unstructured databases in better time than classically possible is a powerful motivator for building quantum computers. Ultimately all computational problem's solutions can be described by a string of zeros and ones, so we can try to solve these problems with an unstructured search algorithm.

The actual implementation of the algorithm is hampered by the non-locality of the oracle, $H_P = \mathbb{1} - |m\rangle\langle m|$, as seen at (2.37). This will be explored in the next section.

To study the oracle we now consider a system with n spins-$\frac{1}{2}$ interacting, thus its more plausible immediate implementability. With X, Y and Z being the usual Pauli matrices, we define $Z_{\vec{k}} = Z_0^{k_0} \otimes Z_1^{k_1} \otimes ... \otimes Z_{n-1}^{k_{n-1}}$ where each k_i may be 0 or 1, we defined the vector $\vec{k} = \{k_0, k_1, ..., k_{N-1}\}$ and we assumed that any invertible matrix to the power of zero equals the identity. We notice that there are $N = 2^n$ $Z_{\vec{k}}$ matrices and that they are linearly independent, so they form a basis for the elements of any diagonal $N \times N$ matrix.

So we can expand:

$$\mathbb{1} - |0\rangle\langle 0| = \sum_{\vec{k}} C_{\vec{k}} Z_{\vec{k}}, \tag{2.56}$$

where we assumed the marked state to be $|0\rangle$ without loss of generality and $C_{\vec{k}}$ represents a constant for each $\vec{k}$. We can decompose this matrix equation into $N = 2^n$ scalar equations, for on both matrices only the diagonal elements are relevant.

The equation for the marked element:

$$\sum_{\vec{k}} C_{\vec{k}} = 0, \tag{2.57}$$

and all others:

$$\sum_{\vec{k}} (-1)^{\mathcal{P}(\vec{k},p)} C_{\vec{k}} = 1, \tag{2.58}$$

where p is a counter that ranges from 1 to $N-1$ and $\mathcal{P}(\vec{k}, p)$ is a function that is all ways 0 for $\vec{k} = \vec{0}$, $\vec{0}$ is the null vector and for all other values of $\vec{k}$ it is 0 half of the times and 1 on the other half. Also, for each value of p $\mathcal{P}(\vec{k}, p)$ is 0 half of the times and 1 on the other half.

The properties of $\mathcal{P}(\vec{k}, p)$ are easy to see after you notice that $Z_{\vec{k}}$ is a tensor product of matrices with only 1 and -1 in their diagonals and the identity matrix. Excluding $Z_{\vec{0}}$ which is an identity matrix it self, all other matrices will have half their diagonal elements being -1. Also, every time we change the value of one of the k_i exponents from 1 to 0 (or vice versa) half the elements of the corresponding $Z_{\vec{k}'}$ change sign.

By summing all eqs: $C_{\vec{0}} = \overline{N}$ and by summing a convenient half and then subtracting the other half of the equations we see that for each other term all reduce to $C_{\vec{k} \neq \vec{0}} = -1/N$.

So, individually, the coefficient $C_{\vec{1}}$ (all $k_i = 1$) is exponentially approaching zero and the term $Z_0 \otimes Z_1 \otimes ... \otimes Z_{N-1}$ vanishes along with it, meaning that "all-bodies" interactions are not relevant in large systems. But if we count the number of terms representing 3 or more bodies interactions we get how many interactions are difficult to implement. To get this total we remember that there are N interaction terms, 1 being a '0-body' ($k_i = 0 \forall i$), n 1-body interactions and C_2^n 2-body interactions, the difference is

$$N - 1 - \frac{n!}{1!(n-1)!} - \frac{n!}{2!(n-2)!} \approx N, \tag{2.59}$$

which grows exponentially!

So even though the many-body interactions are exponentially small they are also exponentially many. This leads to an infinite dimension model. Despite these difficulties there are proposals on how to circumvent this non-locality problem. One such proposal is in spatial search [60]. It is argued in this case that a single bosonic particle on a 3D lattice allowed to adiabaticaly hop between neighboring sites would find the marked site faster than any classical algorithm could.

2.4 Quantum Phase Transitions

A phase transition happens when a parameter of the system passes through its critical point and one or more properties show a sudden difference of value. For example, when water at sea level pressure has its temperature increased from just below 100 °C (212 °F) to just above it, the water starts boiling and goes from liquid to vapor, showing significant sudden change in density.

In classical systems temperature fluctuations govern the systems behaviour. But at (or very close to) $T = 0K$ these fluctuations lose strength and quantum fluctuations become dominant. In this case as we tune some parameter, other than temperature, through its critical point we have a quantum phase transition (QPT). An example is the quantum Ising model, in which neighboring spins belonging to a lattice interact between themselves and with a tunnable external magnetic field. The driving Hamiltonian is

$$H_I(g) = g\sum_i X_i + \sum_{<i,j>} Z_i Z_j, \tag{2.60}$$

where g>0 defines the coupling strength and the sum over $< i, j >$ means that we sum over pairs of nearest neighbors only. X, Y and Z are the usual Pauli matrices and the index i refers to the spin they act upon. In this model there is a QPT at the *critical point* g=1. A critical point is the parameters value ($g = 1$ in this case) at which an excited state becomes the fundamental state and creates a nonanalycity of the ground state energy. For g>1 the spin chain behaves as a paramagnetic material, and for g<1 it behaves as a magnet. This means that at g=1 an spontaneous magnetization takes place, making this the critical point of this QPT.

AQC and QPTs are intimately related. For a quantum adiabatic algorithm to generate speedup over classical analogues, it is expected that a QPT must take place [61]. As defined in Sachdev's work [29], a QPT is said to happen when, by changing some external parameter, there is a nonanalycity in the ground state energy of a infinite lattice. This happens when the ground state and the first excited state (and perhaps more states besides) become degenerated at a level crossing for example.

A trivial Hamiltonian that exhibits a level crossing is $H_T(g) = H_1 + gH_2$ where H_1 and H_2 commute, meaning they can be diagonalized simultaneously and the eigenvectors of $H_T(g)$ do not depend on g. For the Hamiltonians that interest us the level crossings will only happen at the thermodynamic limit $n \to \infty$, with n being the number of particles. But even if we don't observe a QPT in finite sized latices we can observe their asymptotic behavior as their size scales, as Figure 2.2 illustrates. It is clear that the gap between the ground and first excited energies depends on the size of the system, and the nature of this dependence is used to classify different kinds of QPT.

QPTs are classified in first order or continuous order transitions. In first order transitions the ground state energy has a discontinuity in its first derivative at the critical point. In continuous transitions it is a higher derivative that has de discontinuity. Continuous QPTs are characterized by diverging correlation lengths and correlation times, meaning

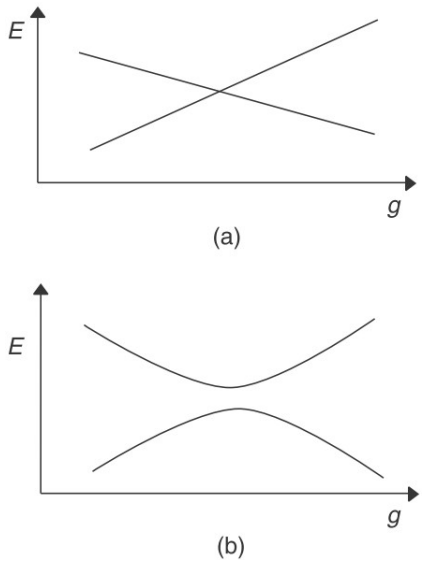

Figure 2.2: (a) A level crossing signaling a QPT in a infinite lattice (trivial systems excluded). (b) Finite size system and avoided level crossing, as the systems grows it will asymptotically converge to what is shown in (a).

that faraway particles are more likely to be correlated and remain so for longer times. First order QPTs are characterized by the coexistence on the critical point of both the phase bellow it and the one above it. Both kinds of QPTs can generate speedups over classical algorithms, but only continuous QPTs might generate exponential speedups [62].

To study the QPT on the adiabatic quantum search algorithm we need the two lowest energy states seen at (2.46), from there it is easy to obtain the gap between these levels:

$$gap(s) = \sqrt{[f(s) + g(s)]^2 - 4f(s)g(s)\overline{N}}. \tag{2.61}$$

At the thermodynamic limit $N \to \infty$ and for both local and global adiabaticity interpolations we can see that

$$gap\left(\frac{1}{2}\right)_{N\to\infty} = 0. \tag{2.62}$$

To see the order of this QPT we look at its two lowest energy levels as shown in Figure 2.3, and also to the parameter b defined at (2.38) and shown in Figure 2.4. In both cases it is easy to see that the first derivative is discontinuous, thus we are dealing with a first order QPT.

First order QPTs have been the object of studies [63] and experimental observation [64], even if less so than continuous QPTs. In AQC this is due to the impossibility of achieving polynomial time solutions for NP-Hard problems [62].

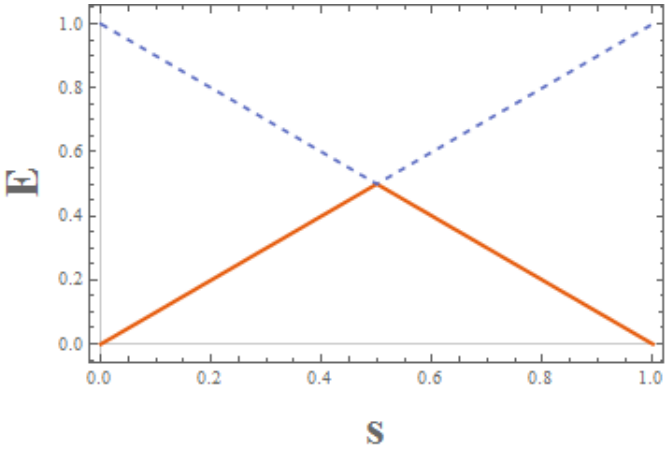

Figure 2.3: Energies of the two lowest energy eigenstates at the thermodynamic limit for the adiabatic quantum search. The ground level is the full line and the first excited state is the dashed line. Notice the obvious discontinuity of the first derivative at $s = \frac{1}{2}$.

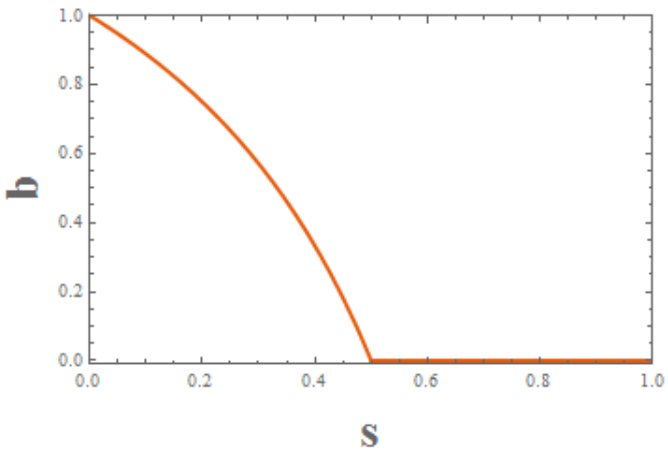

Figure 2.4: Parameter b at thermodynamic limit. Again we can see the discontinuity of the first derivative at $s = \frac{1}{2}$.

2.5 Counterdiabatic Driving

The idea of designing finite-time protocols that reach the same final state as strictly adiabatic evolutions has been termed shortcuts to adiabaticity [65]. One way to achieve a shortcut is to choose a reference Hamiltonian with a desirable adiabatic evolution and mimic it in finite-time by adding another term to it that turns the ideal adiabatic dynamics into the actual system dynamics, this has been termed Counterdiabatic Driving (CD) [66] or transition-less driving [67]. This method can be understood as an analogy to watching a movie going "fast-forward": the system will have the exact same dynamics as the reference system, only much faster.

Considering a slow varying Hamiltonian $H(t)$ with eigenstates $|\psi_n(t)\rangle$ we know that the dynamics of a system initially in the n-th eigenstate will follow

$$|\psi_n(t)\rangle = e^{-i\int_0^t \varepsilon_n(t')dt'} |n(t)\rangle \,, \tag{2.63}$$

up to the geometric phase. The goal now is finding a new Hamiltonian, $H_{CD}(t)$ for which the adiabatic approximation of $H(t)$ gives the exact solution of the finite-time dynamics, e.g. the solution to the Schrödinger equation of $H_{CD}(t)$. We begin by direct construction of the desired evolution operator

$$U_{CD}(t,0) = \sum_n |\psi_n(t)\rangle \langle n(0)| \,, \tag{2.64}$$

remembering we defined $\hbar = 1$ we can now obtain the respective Hamiltonian H_{CD}

$$\begin{aligned} H_{CD} &= i\partial_t U_{CD} U_{CD}^\dagger, && (2.65)\\ &= i\sum_{n,m} |\partial_t \psi_n\rangle\langle\psi_m| \langle n(0)|m(0)\rangle \,, && (2.66)\\ &= i\sum_n |\partial_t \psi_n\rangle\langle\psi_n| \,, && (2.67)\\ &= \sum_n \varepsilon_n |n(t)\rangle\langle n(t)| + i\sum_n |\partial_t n(t)\rangle\langle n(t)| \,, && (2.68)\\ &= H(t) + H_1(t), && (2.69) \end{aligned}$$

where the auxiliary term $H_1(t) = i\sum_n |\partial_t n(t)\rangle\langle n(t)|$ is added to the original Hamiltonian we wish to accelerate.

This method has been successfully applied to speed up quantum gates [68] and thermodynamic processes [69]. In the quantum search algorithm the application of this scheme is problematic for H_1 does not posses an desirable property called oracularity [31]. An oracle is an entity that can be used to verify if an attempt to answer a problem is correct or not, but it provides no hints to the correct answer if the attempt presented is wrong [53, 56]. We now show that in the quantum search while H_P is an oracular Hamiltonian, H_1 is not. First we define an oracular operator $H_P = O_m = \mathbb{1} - |m\rangle\langle m|$ and a not oracular one $H_1 = \overline{O}_m = |+\rangle\langle m| + |m\rangle\langle +|$ ($|+\rangle = N^{-\frac{1}{2}}\sum_{i=0}^{N-1}|i\rangle$), now we check the result of their operations on a computational basis state $|i\rangle$:

$$O_m|i\rangle = (\mathbb{1} - |m\rangle\langle m|)|i\rangle = \begin{cases} 0 & (i = m), \\ |i\rangle & (i \neq m), \end{cases} \tag{2.70}$$

$$\overline{O}_m|i\rangle = (|+\rangle\langle m| + |m\rangle\langle +|)|i\rangle = \begin{cases} \frac{1}{\sqrt{N}}|m\rangle + |+\rangle & (i = m), \\ \frac{1}{\sqrt{N}}|m\rangle & (i \neq m). \end{cases} \tag{2.71}$$

We see that operating O_m on a random state will most likely give us no new information, while operating $\overline{O}_m$ on any undesired state will return the desired state. Farhi's initial paper on AQC [7] has a simple proof that it is possible to build an oracle to an interesting problem (3-sat) without knowing its answer while this non-oracular entity, to my best knowledge, has not been proved to have the same property. Also, if built, this operator would find the solution to its target problem in $O(1)$, which it is reasonable to believe is impossible for most problems of interest.

2.6 Quantum Correlations

In Statistics two variables are correlated if by knowing one I can make predictions about the other. The more exact these predictions get, the more correlated the variables are. In Physics when variables describing different quantities are statistically correlated,

we say that those quantities are correlated as well. In classical physics if you have a box with N marbles moving randomly inside and measure that N_L marbles are on the left side at a given moment, you know that there will be $N_R = N - N_L$ on the right side. Then, the number of marbles on the left side is a variable correlated with the number of marbles on the right side of the box. The extension to quantum mechanics is intuitive in that now we are correlating quantum degrees of freedom. If we observe a quantum system and find correlations that cannot be detected by traditional classical statistics, then we usually attribute them to quantum effects, and hence label them *quantum correlations* [70].

2.6.1 Entanglement

One kind of quantum correlation is known as *entanglement*. Entanglement between subsystems of a pure composite system is observed when it is not possible to describe each subsystem by a pure state, only the total system with all its components can be described by a pure state. We can take a Bell state of two qubits as an example

$$|\psi_{Bell}\rangle = \frac{|10\rangle + |01\rangle}{\sqrt{2}}. \tag{2.72}$$

The states of both qubits are certainly correlated. If we measure the first and find it on the state $|1\rangle$, we can be sure that measuring the second will find it on the state $|0\rangle$. Moreover, each qubit can be shown to be in a maximally mixed state if analyzed on its own. This is an example of a maximally entangled state. On the other hand, an unentangled state, referred as a separable state usually, is one in which we can describe the subsystems independently, like

$$|\Psi\rangle = |\phi\rangle \otimes |\psi\rangle \,. \tag{2.73}$$

Assuming we do not have classical correlations, in this case knowledge about one qubit does not help us making predictions about the other. But between maximally entangled and separable quantum states we can have a whole range of intermediately entangled subsystems. To quantify how correlated these subsystems are we define the von Neumann entropy $S(\rho)$

$$S(\rho) = -Tr[\rho \, log \, (\rho)], \tag{2.74}$$

where ρ denotes the density operator describing the subsystem of the composite pure original system, Tr is the trace operation and log is the base 2 logarithm. It is easier to obtain the von Neumann entropy directly from the eigenvalues of ρ (if they are known) from the equivalent form

$$\begin{aligned} S(\rho) &= -Tr[\rho \, log \, (\rho)], \\ &= -\sum_{i}^{d} \langle \psi_i | \rho \, log \, (\rho) | \psi_i \rangle \, , \\ &= -\sum_{i}^{d} \lambda_i \langle \psi_i | log \, (\rho) | \psi_i \rangle \, , \\ &= -\sum_{i}^{d} \lambda_i \, log \, (\langle \psi_i | \rho | \psi_i \rangle) \, , \\ &= -\sum_{i}^{d} \lambda_i \, log \, (\lambda_i) \, , \end{aligned} \tag{2.75}$$

where d is the dimension of the square matrix ρ, $|\psi_i\rangle$ its eigenvectors, λ_i are its eigenvalues and $\sum_i \lambda_i = 1$. From this alternative form it follows that $S(\rho)$ is invariant under a change of basis since we know that such transformation leaves eigenvalues unchanged.

The von Neumann entropy measures how much uncertainty we have about a system. For composite pure states $S(\rho_{pure}) = 0$ for we know exactly which state we are dealing with. But if we calculate the entropy of a subsystem of a pure state we might find a surprise: we do not have all the information about it. This leads to the natural conclusion that we lost information about one subsystem by ignoring another subsystem. To show this point we first define the partial trace operation, in which we discard one subsystem and describe only the remainder subsystem. Given a density matrix ρ_{AB} describing a system composed of two subsystems named A and B, the respective density matrix describing subsystem A is given by tracing out B as

$$\rho_A = Tr_B \rho_{AB} = \sum_{i} \langle i_b | \rho_{AB} | i_b \rangle \, , \tag{2.76}$$

where $|i_b\rangle = \mathbb{1}_A \otimes |i\rangle$. The definition for tracing over A is analogous.

To use the von Neumann entropy as a measure of entanglement we trace out part of a system and see how much information was lost about the remainder. That loss, if not null, is a clear indication of entanglement. For example we can use eq (2.75) to quantify the entanglement in (2.72). First we obtain $S(\rho_{Bell} = 0)$ which is not surprising since it is a pure state. Now we trace out the second qubit and get

$$\rho_a = \frac{1}{2}\begin{bmatrix} 1 & 0 \\ 0 & 1 \end{bmatrix}, \tag{2.77}$$

with the eigenvalues $\frac{1}{2}, \frac{1}{2}$. So $S(\rho_a) = log(2) = 1$, indicating that we now know less about the state of subsystem A than we know about the whole system AB.

2.6.2 Quantum Discord and Classical States

Entanglement is deeply tied to separability, but even separable states can display some quantum correlations. This is in general attributed to quantum superpositions, which escape detection by entanglement [33]. The "quantumness" associated with the impossibility of measuring a state with no disturbance in any basis is captured by the quantum discord, which we will define shortly after presenting some necessary background.

In classical information theory the amount of information contained in a random variable x is quantified by the Shannon entropy (H),

$$H(x) = -\sum_x p_x log p_x, \tag{2.78}$$

where p_x is the probability of occurrence of an event x. When H(x)=0, the random variable x is completely determined and no new information is gained by measuring it. A classical way of measuring correlations between two subsystems A and B is by their mutual information $I(A:B)$ defined as

$$I(A:B) = H(A) + H(B) - H(A,B), \tag{2.79}$$

with an alternative but equivalent formulation

$$I(A:B) = H(A) - H(A|B), \tag{2.80}$$

where $H(A|B) = H(A,B) - H(B)$ is the conditional entropy (for more details see [53]). Now we have two ways of thinking about classical correlations: one is that they are difference of the sum of local entropies and the total entropy; and the other is that they tell us by how much we can reduce the entropy of one variable by measuring the other.

To generalize these concepts to quantum information theory we simply substitute the Shannon entropy by the von Neumann entropy,

$$I_Q(\rho_{AB}) = S(\rho_A) + S(\rho_B) - S(\rho_{AB}). \tag{2.81}$$

But an analogous expression to (2.80) is more difficult to get, because the quantity $S(A/B)$ involves a measurement and measurements in quantum theory are basis dependent and also may change the state of the system [71]. A way out is to define the quantum conditional entropy as the average entropy of A after a measurement of B

$$S(A/B) = \sum_j p_j S(\rho_{A,j}). \tag{2.82}$$

Since there are infinite ways to measure B we will choose one which minimizes $S(A/B)$. Defining the measurement on B as $\Pi_j^B = |j_B\rangle\langle j_B|$ the system's density matrix after the measurement is given by

$$\rho_{AB|_j} = \frac{\left(\mathbb{1}_A \otimes \Pi_j^B\right) \rho_{AB} \left(\mathbb{1}_A \otimes \Pi_j^B\right)}{Tr\left[\left(\mathbb{1}_A \otimes \Pi_j^B\right) \rho_{AB} \left(\mathbb{1}_A \otimes \Pi_j^B\right)\right]}, \tag{2.83}$$

and $\rho_{A,j} = Tr_B[\rho_{AB|_j}]$. So we get a new expression for the mutual information that reads

$$J_Q(\rho_{AB}) = S(\rho_A) - \underset{\Pi_j^B}{Min}\ S(\rho_{AB}|\Pi_j^B). \tag{2.84}$$

In general expressions (2.81) and (2.84) are not equal [33,71] and we define the *quantum discord* to be their difference

$$Q(\rho_{AB}) = I_Q(\rho_{AB}) - J_Q(\rho_{AB}). \tag{2.85}$$

This difference is interpreted as a consequence of the impossibility of measuring a quantum state without disturbing it, and quantifies this disturbance. So we can define *classical states* as those states with no discord, which means that there is a basis in which we can measure them without disturbance.

There are other measurements for quantum correlations that are equivalent to quantum discord and are referred to as "discord like". One such measurement is the local quantum uncertainty (LQU) analyzed in chapter 3 which was proposed and demonstrated to have a physical interpretation in the context of quantum metrology [34].

Chapter 3

Scaling of the local quantum uncertainty at a first-order quantum phase transition

The interplay between quantum information theory and statistical mechanics has brought emerging connections between these research fields [72–74]. In particular, it has provided a deeper understanding about the role played by correlations in quantum phase transitions (QPTs). A seminal result in this direction is a link between the scaling of pairwise entanglement and QPTs in quantum spin chains [75, 76]. This has been further developed by introducing a distinction between the characterization of first-order and continuous QPTs [77, 78]. For a block analysis, entanglement entropy has been found to be related to the central charge of the Virasoro algebra associated with the conformal field theory behind the critical model [79–81]. More generally, it has been shown that quantum correlation measures such as provided by the quantum discord [33] are also able to identify quantum criticality [82, 83]. Remarkably, pairwise quantum discord may exhibit a more robust characterization of QPTs than pairwise entanglement in certain cases. For instance, pairwise quantum discord between distant sites in a quantum chain may indicate a quantum critical point, while entanglement is absent already for very short distances [84, 85]. In addition, for finite temperatures, pairwise quantum discord is able

to reveal the QPT by non-analyticities in its derivatives, while the pronounced behavior in two-qubit entanglement disappears for even small temperatures [86].

In this chapter, we aim at investigating the behavior of the LQU [34] at quantum criticality. The LQU has been introduced as a quantum discord-like measure, which is primarily related with the skew information [87, 88]. In particular, it plays a role in the characterization of quantum metrology protocols [34, 89]. The behavior of LQU between pairs of spins in a quantum spin chain has been recently considered [90, 91]. Here, we generalize this analysis by considering the LQU for blocks of arbitrary dimension $D \times 2$ and also by discussing its finite-size behavior in first-order QPT.

More specifically, we will evaluate the LQU between a block of L quantum bits (qubits) and one single qubit in a composite system of n qubits. We will consider a Hamiltonian implementation of the quantum search, which is designed to find out a marked element in an unstructured search space of $N = 2^n$ elements. By analytical evaluation, we will show that the LQU exponentially saturates to a constant value at the critical point as we increase the block length L. This saturation is found to be enhanced by the system size n. On the other hand, at non-critical points, the LQU will be shown to vanish for large n. We also consider the LQU as a function of the coupling parameter, showing that the LQU exhibits a pronounced behavior at the quantum critical point independently of the block sizes of L qubits. In particular, this pronounced behavior is sensitive to n, showing a scaling behavior as we increase the size of the system.

3.1 Local quantum uncertainty

The uncertainty of an observable K in a quantum state ρ is usually quantified by the variance $V(\rho, K) = Tr\rho K^2 - (Tr\rho K)^2$. It may exhibit contributions from both quantum and classical sources. Quantum uncertainty comes from the noncommutativity between K and ρ, being quantified by the skew (not commuting) information [87, 88]

$$I(\rho, K) = Tr\rho K^2 - Tr\rho^{1/2} K \rho^{1/2} K. \tag{3.1}$$

Indeed, suppose ρ and K commute. Then, ρ and K have a common basis of eigenstates $\{|k\rangle\}$, which means that the uncertainty of K in an individual eigenstate $|k\rangle$ vanishes. Hence, a nonvanishing uncertainty $V(\rho, K)$ is only possible if ρ is a classical mixing of $\{|k\rangle\}$. Therefore, the commutation of ρ and K implies that $V(\rho, K)$ has a classical origin.

The quantum uncertainty is intrinsically connected with the concept of quantum correlation. For example, let us consider a Bell state of two qubits, namely, $|\psi\rangle = (|00\rangle + |11\rangle)/\sqrt{2}$, where $\{|0\rangle, |1\rangle\}$ denotes the computational basis. This is an eigenstate of the global observable $\sigma_z \otimes \sigma_z$, so there is no uncertainty on the result of a measurement of such an observable. On the other hand, the measurement of local spin observables is intrinsically uncertain for the density operator $|\psi\rangle\langle\psi|$, since an entangled state cannot be an eigenstate of a local observable. In particular, the variance $V(\rho, K)$ for a local observable K will vanish if and only if the state is uncorrelated.

The concept of quantum uncertainty can be extended to mixed states. In this case, the skew information $I(\rho, K)$ vanishes if and only if ρ is not disturbed by the measurement of K. If K is a local observable, the states left invariant by local measurement are the states with zero quantum discord with respect to that local subsystem [92]. The quantum uncertainty on local observables is then intimately related to the notion of quantum discord and, as shown in Ref. [34], it can be used as a discord-like quantifier. We are now ready to define the local quantum uncertainty (LQU). Let $\rho = \rho_{AB}$ be the state of a bipartite system, and let K^Γ denote a local observable on B (K is represented by a Hermitian operator on B with nondegenerate spectrum Γ). The LQU as defined in [75], is given by

$$Q(\rho) = min_{K^\Gamma} I(\rho, K^\Gamma). \tag{3.2}$$

Notice that Q is the minimum quantum uncertainty associated to a single measurement on subsystem B. If there is a K for which $Q = 0$ then there is no quantum correlation between the two parts of the state ρ. As proved in Ref. [34], the LQU satisfies all the good properties of a discord-like measure. An analytical expression for Q can be obtained if we consider a bipartite $D \times 2$ system (for more details see appendix B). In this case

$$Q(\rho_{AB}) = 1 - \lambda_{max}(W_{AB}), \tag{3.3}$$

where λ_{max} is the maximum eigenvalue of the 3×3 symmetric matrix W whose elements are given by

$$(W_{AB})_{ij} = Tr[\rho_{AB}^{1/2}(I_A \otimes \sigma_{iB})\rho_{AB}^{1/2}(I_A \otimes \sigma_{jB})]. \tag{3.4}$$

In this work, we will consider a set of n qubits aligned in a chain, with the bipartition in subsystems A and B chosen as shown in Fig. 3.1.

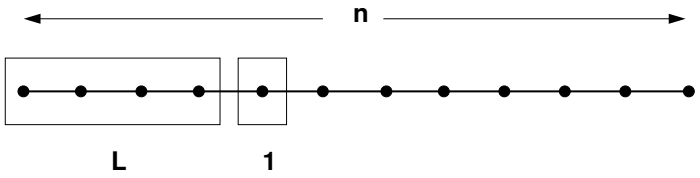

Figure 3.1: Bipartition used to define the subsystems A and B for the LQU evaluation. The size L of the block A is arbitrarily chosen and subsystem B is taken as one qubit.

3.2 LQU for the quantum search

The aim of the search problem is to find out a marked element in an unstructured list of N candidates. In a quantum setting, it is possible to solve the search problem with scaling $\sqrt{N}$, as proved by Grover [5]. Here, we consider a Hamiltonian implementation through a quantum system composed of n qubits, whose Hilbert space has dimension $N = 2^n$. We denote the computational basis by the set $\{|i\rangle\}$ $(0 \leq i \leq N-1)$. Without loss of generality, we can assume an oracular model such that the marked element is the state $|0\rangle$. So the implementation of the quantum search can be achieved through the projective Hamiltonian

$$H(s) = (1-s)(\mathbb{1} - |+\rangle\langle+|) + s(\mathbb{1} - |0\rangle\langle 0|), \tag{3.5}$$

where $|+\rangle = (1/\sqrt{N})\sum_{i=0}^{N-1}|i\rangle$, and s denotes the normalized time $0 \leq s \leq 1$. By preparing the system in its ground state at time $t = 0$ and by considering an adiabatic dynamics, it evolves to the corresponding instantaneous ground state at later times. In particular, the system exhibits a first-order QPT at $s = 1/2$. The ground state energy in

terms of the normalized time s reads

$$E(s) = \frac{1 - \sqrt{1 - 4s(1-s)\overline{N}}}{2}, \tag{3.6}$$

with $\overline{N} = 1 - 1/N$. For the ground state vector $|\psi(s)\rangle$, we obtain

$$|\psi(s)\rangle = \sqrt{a(s)}|0\rangle + \sqrt{c(s)}\sum_{i=1}^{N-1}|i\rangle, \tag{3.7}$$

where we have defined the quantities $a(s) = \frac{1}{1+(N-1)k_s^2}$, $c(s) = \frac{k_s^2}{1+(N-1)k_s^2}$, and $k_s = 1 - \frac{E(s)}{(1-s)\overline{N}}$. Note that, in the thermodynamic limit $n \to \infty$, the structure of the Hamiltonian implies that the LQU can only be non-vanishing at the quantum critical point, even though its scaling is nontrivial at finite sizes. This can observed from Eq. (3.5), where both $|0\rangle$ and $|+\rangle$ are product states that become orthogonal for $n \to \infty$. In this limit, the ground state is $|+\rangle$ for $0 \leq s < 1/2$, with energy $E(s) = s$, while the ground state is $|0\rangle$ for $1/2 < s \leq 1$, with energy $E(s) = 1 - s$. At $s = 1/2$ the ground state is degenerate. From Eq. (3.7), $|\psi(1/2)\rangle$ will be an equal superposition of $|0\rangle$ and $|+\rangle$ for $n \to \infty$. It then follows that $Q = 0$ everywhere except at $s = 1/2$.

In order to determine the scaling at finite size n, we consider the density matrix $\rho = |\psi(s)\rangle\langle\psi(s)|$ describing the system in the ground state, which can be written as

$$\rho(s) = \begin{bmatrix} a & b & b & \dots & b \\ b & c & c & \dots & c \\ \vdots & \vdots & \vdots & \ddots & \vdots \\ b & c & c & \dots & c \end{bmatrix}, \tag{3.8}$$

where $b = \sqrt{a(s)c(s)}$. As we trace out n' qubits of the system, the resulting partial density matrix $\rho'(s)$ will be given by

$$\rho'(s) = \begin{bmatrix} a' & b' & b' & \dots & b' \\ b' & c' & c' & \dots & c' \\ \vdots & \vdots & \vdots & \ddots & \vdots \\ b' & c' & c' & \dots & c' \end{bmatrix}, \tag{3.9}$$

where $a' = a + (2^{n'} - 1)c$, $b' = b + (2^{n'} - 1)c$, and $c' = 2^{n'}c$. We observe that ρ' is an $N' \times N'$ matrix, with $N' = 2^{n-n'}$. Taking the square root from Eq. (3.9), we obtain

$$\sqrt{\rho'} = \begin{bmatrix} a_r & b_r & b_r & \dots & b_r \\ b_r & c_r & c_r & \dots & c_r \\ \vdots & \vdots & \vdots & \ddots & \vdots \\ b_r & c_r & c_r & \dots & c_r \end{bmatrix}, \tag{3.10}$$

where we have defined

$$a_r = \lambda^+ + \lambda^-, \tag{3.11}$$

$$b_r = \lambda^+\beta^+ + \lambda^-\beta^-, \tag{3.12}$$

$$c_r = \lambda^+(\beta^+)^2 + \lambda^-(\beta^-)^2, \tag{3.13}$$

$$\beta^\pm = \frac{c'(N'-1) - a' \pm r}{2b'(N'-1)}, \tag{3.14}$$

$$\lambda^\pm = \frac{\sqrt{\frac{a'+c'(N'-1)\pm r}{2}}}{(1 + (N'-1)(\beta^\pm)^2)}, \tag{3.15}$$

$$r = \sqrt{4(b')^2(N'-1) + (a' - c'(N'-1))^2}. \tag{3.16}$$

By rewriting Eq. (3.10) in block form, we get

$$\sqrt{\rho'} = \begin{bmatrix} A & B & B & \dots & B \\ B^\dagger & C & C & \dots & C \\ \vdots & \vdots & \vdots & \ddots & \vdots \\ B^\dagger & C & C & \dots & C \end{bmatrix}, \tag{3.17}$$

where A, B and C are 2×2 matrices defined as

$$A = \begin{bmatrix} a_r & b_r \\ b_r & c_r \end{bmatrix}, \quad B = \begin{bmatrix} b_r & b_r \\ c_r & c_r \end{bmatrix}, \quad C = \begin{bmatrix} c_r & c_r \\ c_r & c_r \end{bmatrix}. \tag{3.18}$$

Now we define $M_i = \sqrt{\rho'} \cdot (\mathbb{1} \otimes \sigma_i)$, where σ_i are the 2×2 Pauli matrices. We now compute the matrix elements $(W_{AB})_{ij} = Tr[M_i M_j]$. This can be analytically performed

for arbitrary size N, yielding

$$\begin{aligned} W_{1,1} &= 2\left(b_r^2 + c_r a_r + 4q b_r c_r + 2q^2 c_r^2\right), \\ W_{2,2} &= 2\left(c_r a_r - b_r^2\right), \\ W_{3,3} &= a_r^2 - 2b_r^2 + c_r^2, \\ W_{3,1} &= W_{1,3} = 2\left(b_r a_r - b_r c_r + q b_r^2 - q c_r^2\right), \end{aligned} \tag{3.19}$$

with $q = (N'/2 - 1)$ and the remaining matrix elements of W vanishing. We notice that the matrix W would be left unchanged if we interchange blocks A and B, taking block A as the first qubit from the left and B as the L remaining qubits. In order to obtain the LQU, we have to find out the largest eigenvalue of W_{AB} and use it into Eq. (3.3). Since four entries of the matrix W have vanished, this can be done analytically as well.

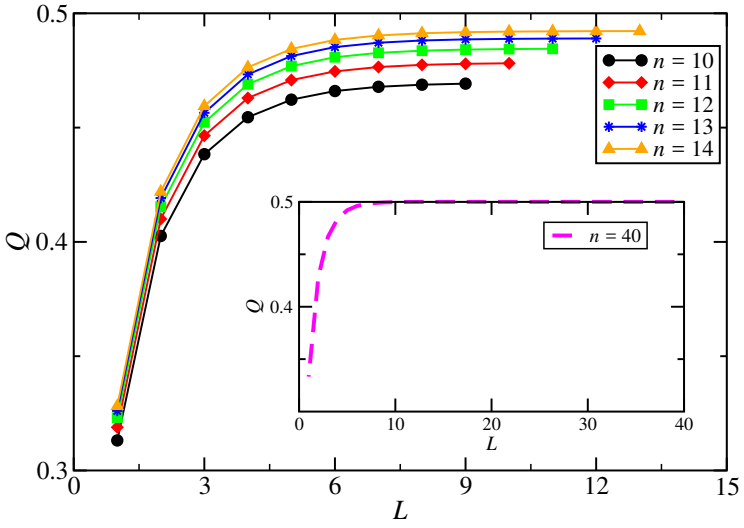

Figure 3.2: LQU between a block of length L and a single qubit at the quantum critical point $s = \frac{1}{2}$. Dots represent calculated results and the continuous lines the respective fit. An exponential saturation as a function of L is observed, with the saturation value enhanced by the system size n. The inset shows the curve for $n = 40$, which approaches the asymptotic form and can be fit by $Q(L) = 1/2 - ae^{-bL}$, with $a \approx 0.29$ and $b \approx 0.71$.

By taking the LQU between a block of length L and a single qubit, we obtain an exponential saturation of the LQU at the quantum critical point. This is illustrated in

Fig. 3.2, where we plot the LQU as a function of L for $s = 1/2$. As we can see, the saturation value is enhanced by n and L, attaining $Q = 1/2$ for $n \to \infty$ and $L \to \infty$. In this regime, the composite system AB is described by a pure state, with the LQU equivalent to bipartite entanglement as measured by the linear entropy [34]. By computing the linear entropy $S(\rho_B) = 2\,(1 - \mathrm{Tr}\rho_B^2)$ from Eq. (3.7) for $n \to \infty$ and $L \to \infty$, we directly obtain $S(\rho_B) = 1/2$, in agreement with the thermodynamic limit in Fig. 3.2. On the other hand, as displayed in Fig. 3.3, the behavior of the LQU displays a "tilde" form if the system is driven to a non-critical point. In this case, as the total number of qubits n grows, the curve tends to vanish independently of the block length L.

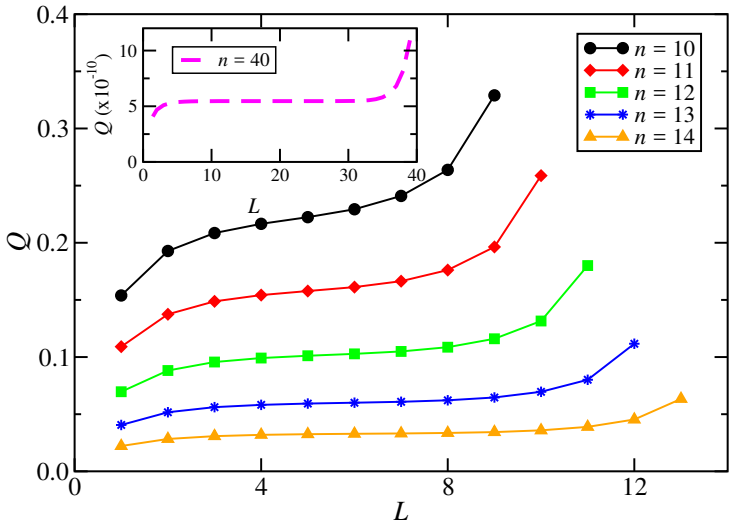

Figure 3.3: LQU between a block of length L and a single qubit at the non-critical point $s = 0.49$. The LQU tends to vanish as we increase the size n of the system (see Inset).

The behavior of the LQU as a function of s for a fixed block size L is also remarkable. Since we have a first order QPT, the LQU itself shows a sharp behavior at $s = 1/2$, as shown in Fig. 3.4.

Indeed, this is exhibited for a pair of qubits for systems of distinct total number n of qubits. Notice that, for $L = 1$, we obtain $Q = 1/3$ in the limit $n \to \infty$. This value comes from the structure of $|\psi(1/2)\rangle$ in Eq. (3.7) for $n \to \infty$, which is an equal superposition

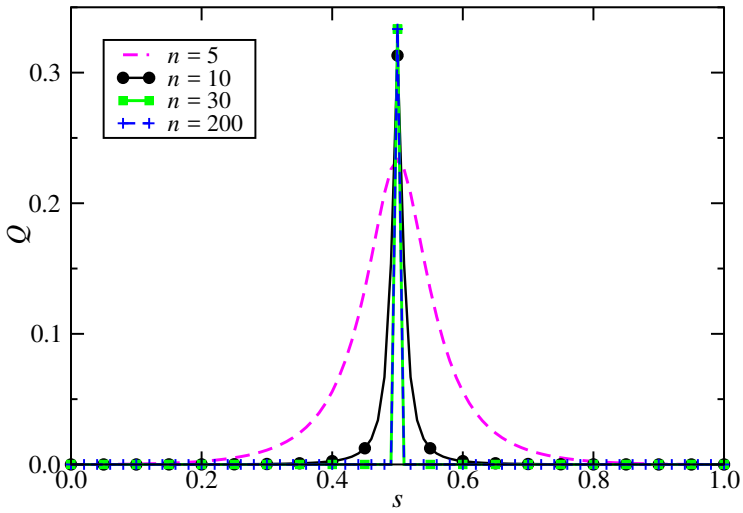

Figure 3.4: LQU between a pair of qubits ($L = 1$) as a function of the normalized time s. The system shows a sharp behavior at the critical point as a function of the system size n. In particular, exponential convergence of the LQU towards its thermodynamical value is obtained for each value of s. Notice that a system with $n = 30$ already has the same behaviour as one with $n = 200$.

of the states $|0\rangle$ and $|+\rangle$. In particular, this maximum value of Q, which is obtained at the critical point $s = 1/2$, strongly depends on L. This is illustrated in Fig. 3.5, where it is shown that the maximum value of the LQU increases along with the total number n of qubits in the system and L for the block, approaching $Q = 1/2$ in the limit of both L and n approaching infinity.

3.3 Results

We have investigated the scaling properties of the LQU at a first-order QPT in the quantum search problem. We have considered the behavior of the LQU in terms of either the block size L or the coupling parameter inducing the QPT. In both cases the QPTs are precisely identified by the LQU, suggesting the measurement of the LQU to be a viable method to find and classify QPTs in other situations as well. We notice that in all cases the observed scaling with problem size was exponential, demonstrating fast convergence

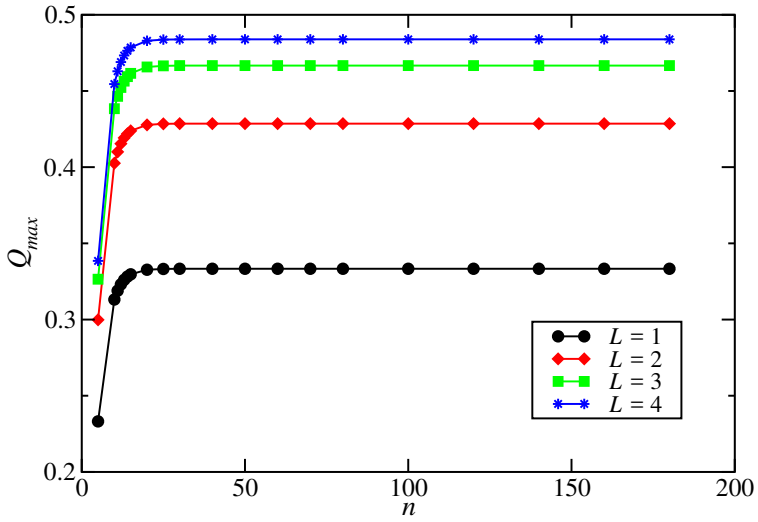

Figure 3.5: The maximum of the LQU for distinct sizes L of blocks.

to saturation. This is in agreement with the well known fact that the quantum search at best scales exponentialy in time with system size, which is related to the exponential shrinking of the energy gap in a first order QPT.

Chapter 4

Dynamics of the quantum search and quench-induced first-order phase transitions

The implementation of quantum technologies is fundamentally based on a precise control of quantum systems. This requires the ability of keeping track of the quantum dynamics along a desired path in Hilbert space. In this direction, a successful strategy is provided by the adiabatic theorem of quantum mechanics [28, 93, 94]. We have seen that it states that a system that is initially prepared in an eigenstate of a time-dependent Hamiltonian $H(t)$ will evolve to the corresponding instantaneous eigenstate at a later time T, provided that $H(t)$ varies smoothly and that T is much larger than (some power of) the relevant minimal inverse energy gap (see, e.g., Ref. [95–97]). The adiabatic theorem is the basis for the paradigm of AQC [98]. A highly related but distinct protocol has currently been implemented and commercially manufactured through QA devices [13, 99], which are based on quantum tunnelling due to interactions with a low temperature bath [100]. Such QA devices constitute a promising approach for quantum information processing (see, e.g. Refs. [20, 21, 101, 102]).

In AQC, the ground state of $H(t)$ adiabatically evolves from an initial simple state to a final state containing the solution of the problem. If the process is performed slowly

enough, the adiabatic theorem ensures that the system stays close to the ground state of $H(t)$ throughout the evolution. At the final time T, measuring the state will give the solution of the original problem with high probability. However, the presence of a quantum phase transition (QPT) [29] will imply in the slowdown of the adiabatic evolution, leading to the appearance of excitations during the quantum dynamics. This phenomenon is well described by the Kibble-Zurek mechanism (KZM) for second-order QPTs [103, 104]. In the quantum realm, a cornerstone lattice model in statistical mechanics illustrating the KZM is the transverse-field Ising spin-1/2 chain [105–107]. In such a case, the ramping from the paramagnetic regime to the ferromagnetic ordering does not asymptotically end up in a fully ferromagnetic state. Instead, the system will be described by a mosaic of ordered domains whose finite size depends on the rate of the transition. In particular, in the case of second-order QPTs, KZM predicts that the size of the ordered domains scales with the transition time as a universal power law, which is provided in terms of a combination of critical exponents. This approach also reveals many-body critical features close to QPTs through the dynamics of the entanglement spectrum [108, 109].

The aim of this chapter is to investigate the excitation dynamics at a first-order QPT. In this direction, we will consider the quench-induced QPT in the quantum search Hamiltonian [32, 58], which implements a quantum algorithm whose target is to find out a marked element in an unstructured list [5]. As a first contribution, we will provide the exact dynamics of the model in terms of a single Riccati differential equation [110]. We will then apply this exact solution in the characterization of the first-order QPT as well as its associated excitation dynamics. For a first-order classical phase transition, KZM has been recently considered in the case of the two-dimensional Potts model [111,112]. In that case, it has been shown that an important role is played by the boundary conditions adopted, which imply different scaling laws for the ordered domains. The search Hamiltonian is translationally invariant, which leads to scaling laws that will be shown to be compatible with those for periodic boundary conditions appearing in the classical case. In particular, we will also discuss the probabilities of success of determining the marked element along the quantum evolution by adopting either global or local adiabaticity strategies.

Moreover, we will determine the disturbance of the quantum criticality as a function of the system size. We will then show that the critical point exponentially converges to its thermodynamic limit even in a fast evolution regime. This will be characterized by both entanglement QPT estimators [113] (see also Ref. [114]) and the Schmidt gap [115]. As in the transverse-field Ising spin-1/2 chain, the excitation pattern will be manifested in terms of quantum domains separated by kinks. However, instead of a power law, the kink density will then be shown to follow an exponential scaling as a function of the evolution speed, which can be interpreted as a KZM for first-order QPTs.

4.1 Dynamics of the quantum search

The search problem aims at finding out a marked element in an unstructured list of N items. In a quantum setting, it can be solved with scaling $\sqrt{N}$, as proven by Grover [5]. Again, we consider a Hamiltonian implementation through a quantum system composed of n quantum bits (qubits), whose Hilbert space has dimension $N = 2^n$. The qubits can be taken here as spin-1/2 degrees of freedom arranged in a chain. We denote the computational basis by the set $\{|i\rangle\}$, with $0 \leq i \leq N-1$. Without loss of generality, we can assume an oracular model such that the marked element is the state $|0\rangle$. So the implementation of the quantum search can be achieved through the projective Hamiltonian

$$H(s) = f(s)(\mathbb{1} - |+\rangle\langle+|) + g(s)(\mathbb{1} - |0\rangle\langle 0|), \tag{4.1}$$

where $|+\rangle = (1/\sqrt{N})\sum_{i=0}^{N-1}|i\rangle$ and s denotes the normalized time $s = t/T$ ($0 \leq s \leq 1$), with T the total time of evolution. The Grover search has motivated a number of small scale experimental realizations in different physical architectures [18, 116–123]. The adiabatic search algorithm starts in $s = 0$ with the quantum system prepared in the uniform superposition provided by $|\psi(0)\rangle = |+\rangle$. This initial state can be split up in the form

$$|\psi(0)\rangle = a(0)\,|0\rangle + p(0)\sum_{i=1}^{N-1}|i\rangle\,, \tag{4.2}$$

with $a(0) = p(0) = 1/\sqrt{N}$. The system dynamics is then governed by Schrödinger equation which, in terms of the normalized time s, can be written as

$$H(s)|\psi(s)\rangle = \frac{i}{T}|\psi'(s)\rangle, \tag{4.3}$$

with $\hbar = 1$ and the *prime* symbol denoting derivative with respect to s. Since the Hamiltonian preserves the form of the initial state given in Eq. (4.2), with $|0\rangle$ as a privileged state, the quantum evolution of $|\psi(0)\rangle$ implies in

$$|\psi(s)\rangle = a(s)\,|0\rangle + p(s)\sum_{i=1}^{N-1}|i\rangle\,, \tag{4.4}$$

with $a(s)$ and $p(s)$ to be determined by the solution of Eq. (4.3). In order to solve Schrödinger equation, we first notice that, by defining $|\psi(s)\rangle \equiv a(s)|\chi(s)\rangle$, Eq. (4.3) becomes

$$\left[H(s) - \frac{i}{T}\frac{a'(s)}{a(s)}\mathbb{1}\right]|\chi(s)\rangle = \frac{i}{T}|\chi'(s)\rangle, \tag{4.5}$$

where

$$|\chi(s)\rangle = |0\rangle + k(s)\sum_{i=1}^{N-1}|i\rangle\,, \tag{4.6}$$

with $k(s) = p(s)/a(s)$. Now, observe that

$$\begin{aligned} H(s)|\chi(s)\rangle &= f(s)\overline{N}\,[1-k(s)]\,|0\rangle \\ &+ \left[-\frac{f(s)}{N}(1-k(s)) + g(s)k(s)\right]\sum_{i=1}^{N-1}|i\rangle\,, \end{aligned} \tag{4.7}$$

with $\overline{N} = 1 - 1/N$. Then, by inserting Eq. (4.7) into Eq. (4.5), we obtain

$$f(s)\overline{N}\,[1-k(s)] - \frac{\alpha(s)}{T} = 0, \tag{4.8}$$

$$-\frac{f(s)}{N}\,[1-k(s)] + g(s)k(s) - \frac{\alpha(s)}{T}k(s) = \frac{i}{T}k'(s), \tag{4.9}$$

with $\alpha(s) = i\,a'(s)/a(s)$. From Eq. (4.8), we can solve the dynamics for $a(s)$, yielding

$$a(s) = \frac{1}{\sqrt{N}}\exp\left\{-iT\int_0^s f(s')\overline{N}\,[1-k(s')]\,ds'\right\}. \tag{4.10}$$

Notice that, in Eq. (4.10), we have the exponential of a complex number, since $k(s)$ may in general exhibit real and imaginary parts. Indeed, the norm of $a(s)$ varies with s, since the

algorithm targets on maximizing this probability amplitude at the end of the evolution. We can also use Eq. (4.8) to eliminate $\alpha(s)$ in Eq. (4.9). It then follows that $k(s)$ can be obtained by solving

$$\begin{aligned} \frac{i}{T}k'(s) &= f(s)\overline{N}k^2(s) + \left[g(s) + f(s) - 2f(s)\overline{N}\right]k(s) \\ &\quad -f(s)(1-\overline{N}), \end{aligned} \tag{4.11}$$

which is a Riccati equation, i.e. a first-order ordinary differential equation for $k(s)$ that is quadratic in $k(s)$ [110]. Provided the solution of Eq. (4.11), we are able to exactly describe the dynamics of the quantum search for an arbitrary number n of qubits. Eq. (4.11) is rather general, holding for any interpolation defined by the functions $f(s)$ and $g(s)$. The choice of such functions affects the energy gap from the ground state to the first excited state, which determines the time scale of the algorithm.

4.2 Success Probabilities

In order to investigate the success probabilities of the adiabatic quantum search via Eq. (4.11), we have to define the interpolation scheme for the functions $f(s)$ and $g(s)$. As a first step, let us consider the lowest eigenvalues of the eigenspectrum of $H(s)$, which are provided by

$$E_{\pm}(s) = \frac{1 \pm \sqrt{1 - 4f(s)g(s)\overline{N}}}{2}, \tag{4.12}$$

where $E_{-}(s)$ denotes the ground state energy, while $E_{+}(s)$ is the energy associated with the first excited state. Their corresponding eigenstates read

$$|E_{\pm}(s)\rangle = \mathcal{N}_{\pm}(s)\left[|0\rangle + b_{\pm}(s)\sum_{i=1}^{N-1}|i\rangle\right], \tag{4.13}$$

where

$$b_{\pm}(s) = 1 - \frac{E_{\pm}(s)}{\overline{N}f(s)}, \tag{4.14}$$

and $\mathcal{N}_{\pm}(s) = 1/\sqrt{1 + (N-1)b_{\pm}(s)^2}$. This implies into a gap given by

$$\Delta E(s) = E_{+}(s) - E_{-}(s) = \sqrt{1 - 4f(s)g(s)\overline{N}}. \tag{4.15}$$

In order to stay close to the ground state of $H(s)$, we will impose the adiabatic condition [94]

$$T \gg \max_s \frac{D(s)}{\Delta E^2(s)}, \tag{4.16}$$

where $D(s) = |\langle E_+(s)| H'(s) |E_-(s)\rangle|$. In order to evaluate the adiabatic time condition and then analyze the success probabilities of the algorithm, we will consider both *global* and *local* adiabatic strategies. In both cases, the system exhibits a first-order QPT at $s_c = 1/2$, with the energy gap from the ground state to the first excited state exponentially shrinking as a function of the input size n. This implies that, no matter how slowly the system is dynamically driven, its evolution cannot follow the time-dependent ground state close to the quantum critical point. More specifically, the system will exhibit excitations manifested through the presence of kinks separating domain walls as the instantaneous vector state undergoes the QPT.

4.2.1 Global adiabatic evolution

The simplest evolution strategy is to adopt *global adiabaticity* through a linear interpolation, namely,

$$\begin{aligned} f(s) &= 1 - s, \\ g(s) &= s. \end{aligned}$$

Therefore, we can directly obtain the running time of the algorithm as $T \gg T_{GA}$, with T_{GA} denoting the characteristic time scale for global adiabaticity, which reads

$$T_{GA} = \max_s \frac{D(s)}{\Delta E^2(s)} = O(N), \tag{4.17}$$

with $O(N)$ denoting asymptotic upper bound N on the growth rate of T_{GA}. Notice then that T_{GA} provides the adiabatic scale for the running time of the algorithm as a function of the size of the list. In the particular case of the global adiabaticity strategy, we obtain a linear scaling $O(N)$, which is equivalent to the expected scaling in a classical search approach [53]. In the quantum setting, we can now analyze the probability of success $P_0(s) = |\langle 0|\psi(s)\rangle|^2$ as a function of time. The results are displayed in Fig. 4.1, where

we consider the dimensionless running ratio $\tau_{GA} = T/T_{GA}$ as a measure of adiabaticity. For fast evolutions compared to T_{GA}, the adiabatic theorem is far from satisfied, which implies into a low probability of success $P_0(s)$. On the other hand, $P_0(s)$ improves as the total time gets much greater than T_{GA}. Notice also that strong oscillations occur close to the critical point $s_c = 1/2$, which are reduced at the end of the evolution. This is a consequence of the stiffness of the ordinary differential equation (ODE) system [124].

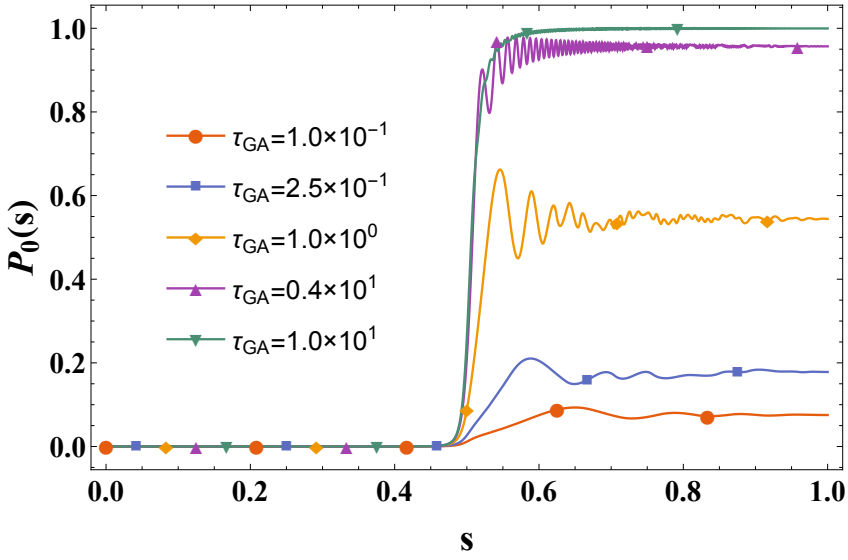

Figure 4.1: Probability of success $P_0(s)$ as a function of the normalized time s for $n = 10$ qubits for several dimensionless running rates τ_{GA}, under a global adiabaticity strategy.

4.2.2 Local adiabatic evolution

We can improve the time scaling by imposing a *local adiabaticity* strategy [32, 58], i.e. by dividing the total time into infinitesimal time intervals and applying the adiabaticity condition given by Eq. (4.16) locally to each of these intervals. By using this procedure, it can be shown that the runtime is minimized for the path (see, e.g. Ref. [59])

$$\begin{aligned} f(s) &= 1 - g(s), \\ g(s) &= \frac{\sqrt{N-1} - \tan\left[\arctan\left(\sqrt{N-1}\right)(1-2s)\right]}{2\sqrt{N-1}}. \end{aligned}$$

This results in a quadratic speedup over the classical search, i.e., we obtain the time complexity $T_{LA} = O(\sqrt{N})$ expected by the Grover quantum search [32, 58].

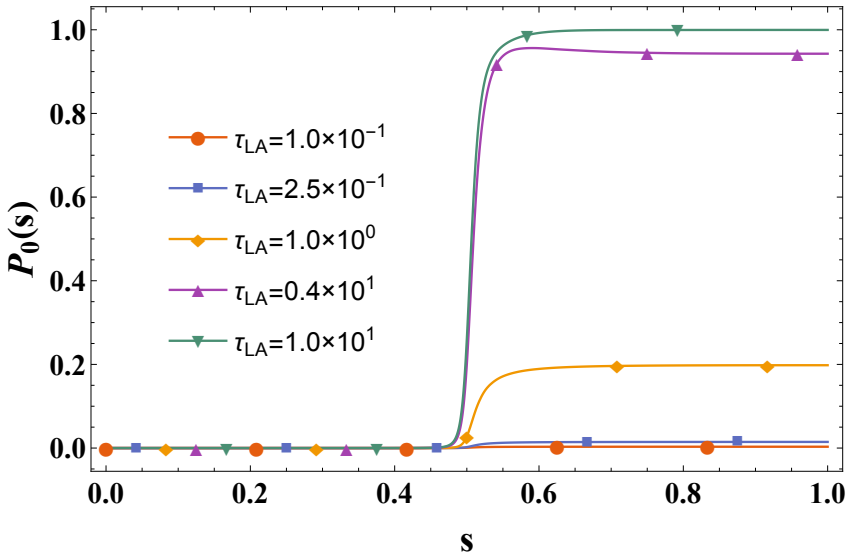

Figure 4.2: Probability of success $P_0(s)$ as a function of the normalized time s for n=10 qubits for several dimensionless running rates τ_{LA}, under a local adiabaticity strategy.

We can now analyze the probability os success $P_0(s) = |\langle 0|\psi(s)\rangle|^2$ as a function of time for the local strategy. The results are displayed in Fig. 4.2, where we consider the dimensionless running ratio $\tau_{LA} = T/T_{LA}$ as a measure of adiabaticity. Notice that the local adiabatic dynamics are more stable, with the success probability converging faster after the critical point $s = 1/2$ to its final value at $s = 1$. Bearing in mind the improved asymptotic scaling $O(\sqrt{N})$ of the local adiabaticity strategy, the absence of stiffness in the ODE system, and the smoothness of its probability of success as a function of s, we will adopt this interpolation in the subsequent analysis of the QPT dynamics and quantum domains formation.

4.3 Quench-induced first-order QPT

4.3.1 QPT Estimator

The characterization of quantum criticality via entanglement estimators [113, 114] is based on the detection of quantum critical points by exploring the distinct behavior of the entanglement entropy in critical and noncritical systems. To begin with, we consider the instantaneous evolved state $|\psi(s)\rangle$ as given by Eq. (4.4). By defining a bipartition

AB in the quantum system, the density operator of the composite system can be written as $\rho_{AB}(s) = |\psi(s)\rangle\langle\psi(s)|$. Then, the von Neumann entropy for the subsystem A reads

$$E(\rho_A) = -\sum_i \lambda_i[\rho_A] \log(\lambda_i[\rho_A]), \tag{4.18}$$

where $\lambda_i[\rho_A]$ denotes the eigenvalues of the reduced density operator $\rho_A = \mathrm{Tr}_B \rho_{AB}$. The entropy $E(\rho_A)$ itself could, in principle, be used to characterize the quantum criticality. However, it usually requires much larger lattices to achieve the same precision as compared with the QPT estimator approach to continuous QPTs [113]. In this scenario, we consider the difference between entanglement entropies for two subsystems with different sizes in a first-order QPT setting and look to compare it with the known continuous QPT behaviour. Here, we will choose blocks of qubits with sizes $n/2$ and $n/4$. Due to the high level of symmetry in this model it is not relevant if these blocks are or not continuous. Then, the QPT estimator $\Delta_E^{(n)}(s)$ is defined as

$$\Delta_E^{(n)}(s) = E(\rho_{n/2}) - E(\rho_{n/4}). \tag{4.19}$$

By adopting the local adiabatic interpolation, we provide in Fig. 4.3 the behavior of the quench-induced QPT estimator for $n = 8$ for several dimensionless times τ_{LA}. As originally observed in Refs. [113,125], $\Delta_E^{(n)}(s)$ locates a first-order QPT through a peak at the quantum critical point for finite sizes lattices, with the peak tending to shrink as the system size is increased. Here, Fig. 4.3 exhibits this peak for $\tau_{LA} > 1$, which means a total evolution time T larger than the Grover scaling $O(\sqrt{N})$. For short times τ_{LA}, the peak disappear. Remarkably, the QPT can still be located through the change of concavity in $\Delta_E^{(n)}(s)$.

We now analyse the scaling behavior of $\Delta_E^{(n)}(s)$ for different system sizes n. We take the local adiabatic strategy in the fast evolution regime. The results are shown in Fig. 4.4. Notice that there is a jump in $\Delta_E^{(n)}(s)$ as a function of s around the critical point $s_c = 1/2$, with the plateau after the critical point decreasing as the size n gets larger. In the upper inset, we show the plateau height obeys an exponential scaling law as a function of n. In the lower inset, we show that that the finite size precursor s_m of the critical point exponentially converges to its thermodynamic limit s_c, with s_m defined as the time s for

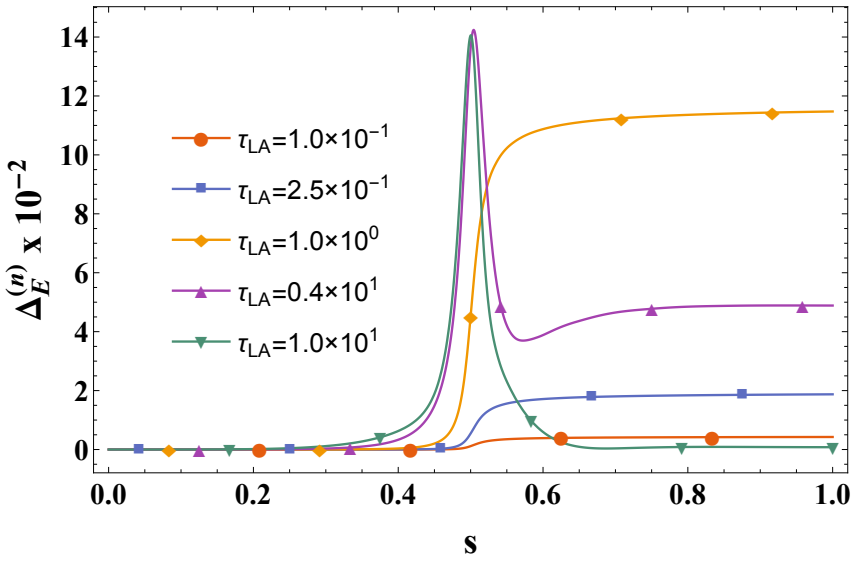

Figure 4.3: QPT estimator $\Delta_E^{(n)}(s)$ for $n = 8$ under local adiabatic evolution for several dimensionless running rates τ_{LA}.

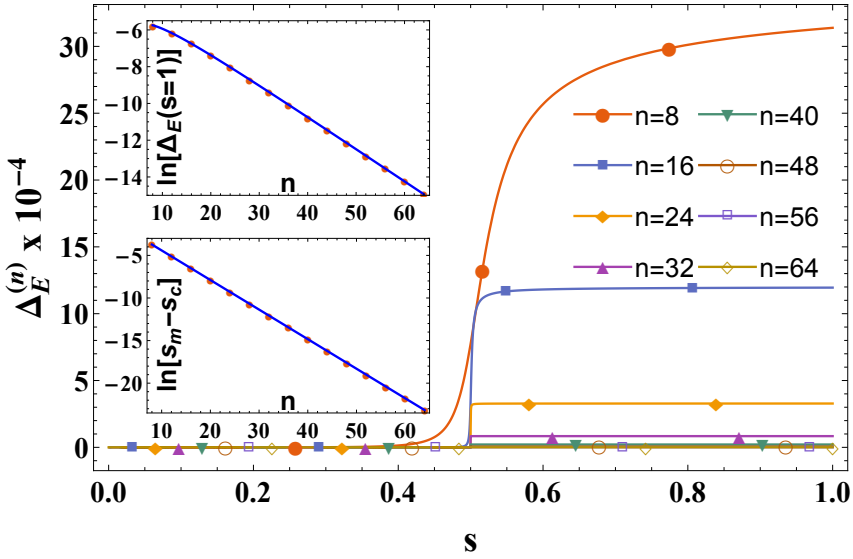

Figure 4.4: Estimator for $n \in [8, 64]$ and dimensionless time $\tau_{LA} = 0.1$ in the local adiabatic regime as a function of the normalized time s. The final plateau height at $s = 1$ can be fit as $\ln[\Delta_E^{(n)}(s = 1)] = -0.18n - 3.5 - 6.7/n$. The precursor s_m of the critical point s_c exponentially converges as $\ln[s_m - s_c] = -0.35n - 0.95$

.

which $\Delta_E^{(n)}(s)$ exhibits an inflection point. This result is remarkable in the sense that the critical point can be precisely detected by the QPT estimator even in the fast evolution

regime, with exponential convergence of s_m towards the critical point s_c for this model.

4.3.2 Schmidt Gap

The Schmidt gap $\Delta_G^{(n)}(s)$ is defined as the difference between the two highest eigenvalues of the reduced density matrix ρ_A in a composite system AB of n qubits described by the density operator ρ_{AB}. Here, we will compute the Schmidt gap by splitting up the system into two continuous parts with equal size $n/2$ and using the reduced density matrix after tracing out one of the parts. When approaching a quantum phase transition, $\Delta_G^{(n)}(s)$ has been shown to signal the critical point and to scale with universal critical exponents [115]. For the first-order QPT of the quantum search Hamiltonian, we can also show that $\Delta_G^{(n)}(s)$ is able to detect the critical point with exponential convergence, as in the case of the QPT estimator. This result is illustrated in Fig. 4.5, where we plot $\Delta_G^{(n)}(s)$ as a function of the normalized time s for several system sizes n. As n increases, $\Delta_G^{(n)}(s)$ shows a behavior closer to a ladder function.

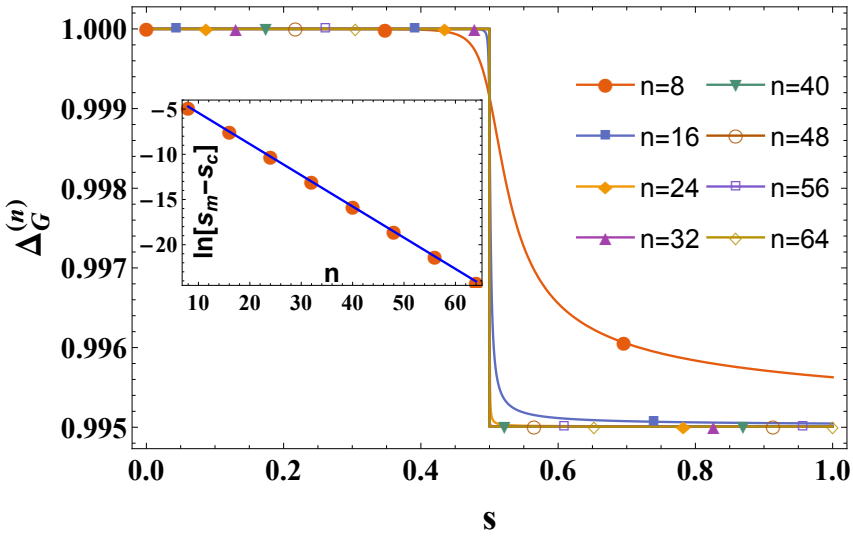

Figure 4.5: Schmidt gap $\Delta_G^{(n)}(s)$ for $n \in [8, 64]$ and dimensionless time $\tau_{LA} = 0.1$ in the local adiabatic regime as a function of the normalized time s. The precursor s_m of the critical point s_c exponentially converges as $\ln[s_m - s_c] = -0.34n - 1.96$

4.4 Quantum domains and kink dynamics

In this Section, we will analyze the formation of defects in the quantum search dynamics. The initial state for the Hamiltonian in Eq. (4.1) is $|\psi(0)\rangle = (1/\sqrt{N})\sum_{i=0}^{N-1}|i\rangle$, which corresponds to a completely polarized state in the Pauli σ_x eigenbasis. The final expected state, after an ideal adiabatic evolution, is the ferromagnetic state $|\psi(s=1)\rangle = |0\rangle$, which is completely polarized in the Pauli σ_z eigenbasis. However, for a quench-induced QPT driven by a finite-time ramping, KZM implies into a final state composed by a mosaic of quantum domains separated by kinks. A quantitative discussion has been provided in details for a second-order QPT, with the kink density following a typical power-law behavior [105–107]. Let us now discuss the kink density behavior for the case of first-order QPTs and verify if it can differentiate it from continuous QPTs. We begin by defining the number of kinks through the following observable:

$$N_k = 1/2\sum_{i=0}^{n-1}(\mathbb{1} - \sigma_i^z\sigma_{i+1}^z). \tag{4.20}$$

Its expectation value as a function of the normalized time s is then

$$n_k(s) = \langle\psi(s)|N_k|\psi(s)\rangle = |a(s)|^2\langle\chi(s)|N_k|\chi(s)\rangle, \tag{4.21}$$

where we have used that $|\psi(s)\rangle = a(s)|\chi(s)\rangle$. From the normalization of the state vector $|\psi(s)\rangle$ in Eq. (4.4), we obtain

$$|a(s)|^2 = \frac{1}{1+(N-1)\,|k(s)|^2}, \tag{4.22}$$

with $k(s) = p(s)/a(s)$. Moreover, by using $|\chi(s)\rangle$ as given in Eq. (4.6), we observe that the operator σ_i^z will act on the state $|\chi(s)\rangle$ by changing the sign of $N/2$ vector elements from $k(s)$ to $-k(s)$. Then

$$\langle\chi(s)|\,\sigma_i^z\sigma_{i+1}^z\,|\chi(s)\rangle = 1 - |k(s)|^2\,. \tag{4.23}$$

In order to investigate the domain formation in terms of the evolution speed, we define the density of kinks as

$$d_k(s) = \frac{1}{n}N_k(s). \tag{4.24}$$

By using Eqs. (4.22) and (4.23) into Eq. (4.21), we obtain

$$d_k(s) = \frac{2^{n-1}|k(s)|^2}{1 + (2^n - 1)|k(s)|^2}, \tag{4.25}$$

Observe that the kink density is completely characterized by the amplitude $k(s)$, as given by Eq. (4.25). This is highly unusual in comparison with the usual KZM. It is a consequence of both the initial superposition required by the quantum algorithm [as in Eq. (4.2)] and the Hamiltonian symmetry, which imposes a uniform superposition of all computational states $|i\rangle$ for $i \neq 0$ throughout the evolution [as in Eq. (4.4)]. Moreover, there is no one-to-one association between the energy cost of a domain configuration and the excitation density, due to the tower of degenerate excited states arising from the projector structure of the Grover Hamiltonian, as given by Eq. (4.1).

The behavior of the kink density as a function of the normalized time s for fast and slow ramps is illustrated in Fig. 4.6, where the local adiabatic strategy is adopted. Notice that, as we increase the dimensionless time τ_{LA}, the kink density tends to decrease at $s = 1$, yielding a final state closer to the ferromagnetic state. On the other hand, in the fast regime, higher excitations are found in the final state, with a kink density closer to its value in the original initial state. This result can be already observed for a small lattice such as $n = 8$ and is shown to hold for larger sizes such as $n = 64$ qubits. In particular, the larger the size, the closer is the kink density to a ladder function. In Fig. 4.7 we consider the kink density as a function of the dimensionless speed $1/\tau_{LA}$ for $n = 64$ qubits. As we can see, the kink density obeys an exponential law for its scaling in terms of $1/\tau_{LA}$. In the inset, we show that the usual power law behavior predicted by KZM for second-order QPTs cannot be applied here. Instead, we obtain a KZM for first-order QPTs, where the quantum domains appear as expected by a finite speed, but with an exponential scaling law. In particular, the convergence of the kink density is now much faster than in the case of the traditional KZM, which is due to the exponential behavior of the first-order QPT.

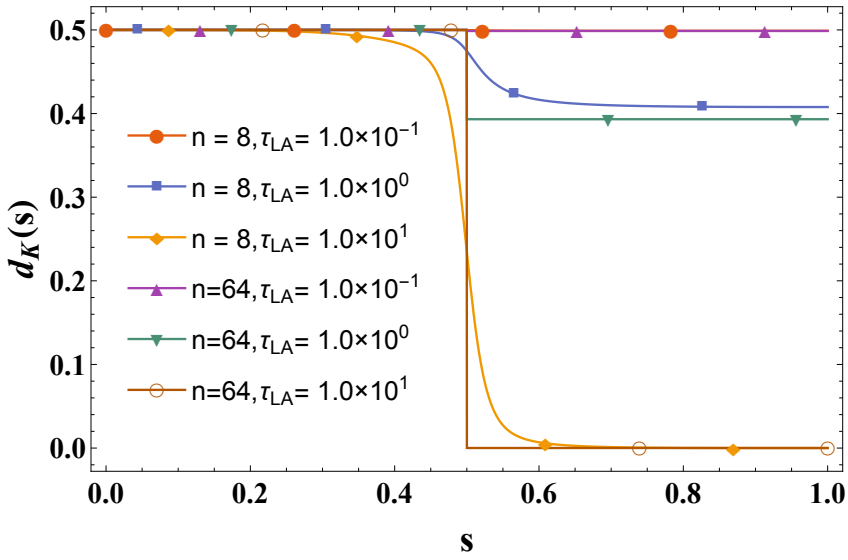

Figure 4.6: Kink density $d_k(s)$ as a function of the normalized time s for $n = 8$ and $n = 64$ qubits, where fast and slow speed regimes in terms of the dimensionless time τ_{LA} are considered.

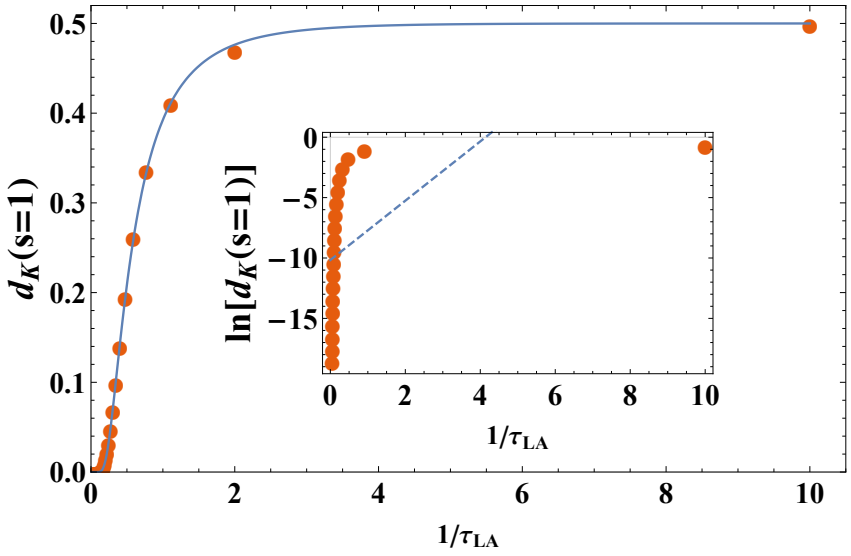

Figure 4.7: Kink density d_k for $s = 1$ as a function of the dimensionless speed $1/\tau_{LA}$ for $n = 64$ qubits. The plot can be fit by the curve $d_k = 1/2(1 - exp[-a/\tau_{LA}])^{b\tau_{LA}}$, with $a = 0.73$ and $b = 0.37$. In the inset, we see a log-plot and its best linear fit, which shows that a power law cannot describe the kink density behavior.

4.5 Results

We have investigated the dynamics of a first-order QPT through the analysis of the quantum search problem. After deriving the exact evolution in terms of a single Riccati equation, we investigated the disturbance of the criticality due to the evolution rate. We have shown that the critical point exponentially converges to its thermodynamic limit as a function of the system size. This scaling law, which is manifested both in QPT entanglement estimators and in the Schmidt gap, holds even in a fast evolution regime. This shows that the characterization of the critical point is robust against quench-induced evolutions. Remarkably, the QPT estimator does not show a peak in a fast regime, as it is usual for an ideal adiabatic transition. However, it indicates a characterization through an inflection point in the QPT estimator measure.

Concerning the excitation dynamics, we have derived a KZM for first-order QPTs, indicating the existence of an exponential law for the kink density in terms of the dimensionless speed. This situation is rather different from the typical (second-order QPT) instances of the KZM, where a polynomial scaling is expected. In particular, this implies that the kink density might be a useful tool to characterize the order of a quench-induced QPT. Moreover, it is related to the disturbance in both the QPT entanglement estimator and Schmidt gap in the dynamical regime. Since there in no association between energy cost and domain sizes (due to the tower of degenerate excited states), the evolution rate mainly determines the presence or absence of domain walls if a detection scheme (measurement) is performed on the system. In any case, for the Grover dynamics, the kink density still reflects an exponential behavior as a function of the evolution rate (as illustrated in Fig. 4.7).

The quantum search Hamiltonian is the main representative of a larger class of projector-based Hamiltonians, which can be used to implement more general quantum algorithms. We expect the pattern of excitation dynamics derived in our work applies to these generalized models as well (including the quench-induced QPT behavior). Naturally, these models are very different from the usual KZM in Ising spin glasses, e.g. in Ref. [126].

Chapter 5

Superadiabatic quantum friction suppression in finite-time thermodynamics

We have seen that, in AQC, finite-time evolution leads to errors in the form of kinks in the spin chain implementing the algorithm. We have also briefly shown in chapter 2 that there is a technique called counterdiabatic driving developed for suppressing these errors. Unfortunately we also showed that such a technique may require previous knowledge of the answer to be applicable to the quantum search Hamiltonian. For an algorithm to be able to benefit from this technique we know it must be complex enough to be programmable and simple enough for us to be able to implement counterdiabatic driving without previous knowledge of the solution and without many-body interaction terms in the Hamiltonian. Looking for a first step in this direction we turn now to the thermodynamics of a quantum engine, which despite not being programmable is challenging enough to be of interest and simple enough to be currently achievable in laboratory conditions.

The quest for the optimal performance of thermal machines and efficient use of energy resources has motivated the development of finite-time thermodynamics. At the macroscale, thermodynamic cycles are operated in finite time to enhance the output power, at the expense of inducing friction and reducing efficiency. Analyzing the trade-

off between efficiency and power has guided efforts in design and optimization [127–129]. The advent of unprecedented techniques to experimentally control and engineer quantum devices at the nanoscale has shifted the focus to the quantum domain. A quantum engine is an instance of a thermal machine in which heat [130, 131] and other quantum resources [132, 133] can be used to produce work. The experimental realization of a single-atom heat engine [134] and a quantum absorption refrigerator [135] have been demonstrated using trapped ions.

The adiabatic theorem [93] dictates that excitations are formed during fast driving of the working substance, leading to the emergence of quantum friction, which we quantify by the extra energy spent in expanding the trap from the same initial configuration to the same final configuration, but in an adiabatic evolution. Trading efficiency and power remains a predominant strategy in finite-time quantum thermodynamics, e.g., of ground-state cooling [136–139]. In parallel, new efforts have been devoted to completely suppress friction in finite-time quantum processes. A systematic way of achieving this goal is provided by shortcuts to adiabaticity (STA): fast nonadiabatic processes that reproduce adiabatic dynamics, e.g., in the preparation of a target state [140]. The use of STA provides a disruptive approach in finite-time thermodynamics and has motivated proposals for superadiabatic thermal machines, operating at maximum efficiency and arbitrarily high output power [69,141–143] at the cost of implementing more complex evolutions. STA engineering is facilitated by counterdiabatic driving [66, 67], whereby an auxiliary control field speeds up the evolution of the system through an adiabatic reference trajectory in a prescheduled amount of time. Experimental demonstrations of counterdiabatic driving have focused on effectively single-particle systems at zero temperature [144–147]. Tailoring excitation dynamics is expected to be a daunting task in complex systems. Yet efficient quantum thermal machines offering scalability require the superadiabatic control of the finite-time thermodynamics in many-particle systems [69]. In this chapter we describe and report the suppression of quantum friction in the finite-time thermodynamics of a strongly-coupled quantum fluid. In our experiment, we implement friction-free superadiabatic strokes with a unitary Fermi gas in an anisotropic time-dependent trap as a working

medium.

The unitary regime is reached when the scattering length governing the short-range interactions in a spin-1/2 ultracold Fermi gas at resonance greatly surpasses the interparticle spacing [148,149]. This strongly-interacting state of matter is described by a nonrelativistic conformal field theory [150]. The controllability of the external trap potential and interatomic interactions in this system allows for the preparation of well-defined many-body states and the precise engineering of time-dependent Hamiltonians. This provides unprecedented opportunities for studying strongly interacting nonequilibrium phenomena [151].

In particular, the emergent scale-invariance symmetry at unitarity facilitates the realization of superadiabatic strokes by the counterdiabatic driving scheme. The work done in a stroke induced by a modulation of the trap frequency can be described by a probability distribution [152]. The mean work equals the difference between the energy of the cloud brought out of equilibrium at the end of the stroke and its initial equilibrium value. For a unitary dynamics, the emergent scaling symmetry at strong coupling [153] dictates the evolution of the nonadiabatic energy in terms of the cloud density profile.

5.1 Finite-time thermodynamics of a unitary Fermi gas in a time-dependent anisotropic trap

The Hamiltonian of a unitary Fermi gas confined in a 3D anisotropic harmonic trap whose frequency is time dependent is given by

$$H(t) = \sum_{i=1}^{N} \sum_{j=\{x,y,z\}} \left[\frac{p_{i,j}^2}{2m} + \frac{1}{2} m\omega_j^2(t) x_{i,j}^2 \right] + \sum_{k<l} U(\mathbf{r}_k - \mathbf{r}_l), \tag{5.1}$$

where ω_j $(j = x, y, z)$ is the corresponding trapping frequency along the j-axis and $p_{i,j}$ $(x_{i,j})$ is the momentum (position) of the i-th particle in the j-axis, m is the particle mass, U is a two-body interacting potential and the vector $\mathbf{r_q}$ represent the 3D position of the q-th particle. The short-range pair-wise interaction potential becomes a homogeneous

function of degree -2 in the unitary regime, satisfying [149]

$$U(\lambda \mathbf{r}) = \frac{1}{\lambda^2} U(\mathbf{r}), \tag{5.2}$$

where λ is a scalar. In what follows it is convenient to rewrite the total Hamiltonian $H(t)$ as the sum

$$H(t) = H_0 + H_{\rm trap}(t), \tag{5.3}$$

where

$$H_0 = \sum_{i=1}^{N} \sum_{j=\{x,y,z\}} \left[\frac{p_{i,j}^2}{2m} \right] + \sum_{k<l} U(\mathbf{r}_k - \mathbf{r}_l), \tag{5.4}$$

$$H_{\rm trap}(t) = \sum_{i=1}^{N} \sum_{j=\{x,y,z\}} \left[\frac{1}{2} m \omega_j^2(t) x_{i,j}^2 \right]. \tag{5.5}$$

For an exact treatment of the finite-time thermodynamics we compute the nonadiabatic evolution of the mean work. To this end, we note that in the Heisenberg picture

$$\begin{aligned}
\frac{d}{dt} H_0 &= \frac{1}{i\hbar} \left[H_0, H(t) \right] \\
&= \frac{1}{i\hbar} \left[H_0, H_{\rm trap}(t) \right] \\
&= \frac{1}{i\hbar} \left[\sum_{i=1}^{N} \sum_{j=\{x,y,z\}} \left(\frac{p_{i,j}^2}{2m} \right) + \sum_{k<l} U(\mathbf{r}_k - \mathbf{r}_l), \sum_{i=1}^{N} \sum_{j=\{x,y,z\}} \left(\frac{1}{2} m \omega_j^2(t) x_{i,j}^2 \right) \right] \\
&= \frac{1}{4i\hbar} \left[\sum_{i=1}^{N} \sum_{j=\{x,y,z\}} p_{i,j}^2, \sum_{i=1}^{N} \sum_{j=\{x,y,z\}} \omega_j^2(t) x_{i,j}^2 \right] \\
&= \frac{1}{4i\hbar} \sum_{i=1}^{N} \sum_{j=\{x,y,z\}} \omega_j^2(t) \left[p_{i,j}^2, x_{i,j}^2 \right] \\
&= \frac{1}{4i\hbar} \sum_{i=1}^{N} \sum_{j=\{x,y,z\}} \omega_j^2(t) \left(-2i\hbar \{ x_{i,j}, p_{i,j} \} \right) \\
&= -\frac{1}{2} m \sum_{i=1}^{N} \sum_{j=\{x,y,z\}} \omega_j^2(t) \frac{d}{dt} x_{i,j}^2,
\end{aligned} \tag{5.6}$$

where we used that $\frac{d}{dt} x_{i,j}^2 = 1/m \{ x_{i,j}, p_{i,j} \}$ in the last step. We now introduce the collective coordinate operators

$$R_j^2 = \sum_{i=1}^{N} x_{i,j}^2, \quad j = x, y, z, \tag{5.7}$$

and define via their expectation values the scaling factors

$$b_j(t) = \left[\frac{\langle R_j^2(t)\rangle}{\langle R_j^2(0)\rangle}\right]^{1/2}. \tag{5.8}$$

Since the system is at equilibrium at $t = 0$ and lacks any intrinsic scale we can argue that its ground state energy can only be a function of $\hbar$ and the trap frequencies ω_j [154]. If we expand such function in a Laurent series we know by dimensional analysis that it must be of the form

$$\langle H(0)\rangle = \hbar \sum_{a,b} k_{a,b}\omega_x^a \omega_y^b \omega_z^{1-a-b}, \tag{5.9}$$

with $k_{a,b}$ being some constant. We notice that

$$\begin{aligned}\sum_j \omega_j \partial_{\omega_j} \langle H(0)\rangle &= \hbar \sum_{a,b} a k_{a,b}\omega_x^a \omega_y^b \omega_z^{1-a-b} + b k_{a,b}\omega_x^a \omega_y^b \omega_z^{1-a-b} + (1-a-b) k_{a,b}\omega_x^a \omega_y^b \omega_z^{1-a-b},\\ &= \hbar \sum_{a,b} k_{a,b}\omega_x^a \omega_y^b \omega_z^{1-a-b},\\ &= \langle H(0)\rangle .\end{aligned} \tag{5.10}$$

Then we can use Hellmann-Feyman theorem [155] (for a proof of the theorem see appendix C) to see that

$$\partial_{\omega_j} \langle H(0)\rangle = \left\langle \partial_{\omega_j} H(0)\right\rangle = m\omega_{j,0} \left\langle R_j^2(0)\right\rangle . \tag{5.11}$$

Now combining (5.10) and (5.11) we get

$$\langle H(0)\rangle = \sum_j m\omega_{j,0}^2 \left\langle R_j^2(0)\right\rangle . \tag{5.12}$$

Along with the equipartition of energy approximation, we find that

$$\langle R_j^2(0)\rangle = \frac{1}{3m\omega_{j,0}^2}\langle H(0)\rangle, \quad j = x, y, z. \tag{5.13}$$

Using (5.13) and (5.8) the expectation value of Eq. (5.6) can thus be written as

$$\begin{aligned}\frac{d}{dt}\langle H_0\rangle &= -\frac{1}{2}m \sum_{j=x,y,z} \omega_j^2(t) \frac{d\langle R_j^2(t)\rangle}{dt}\\ &= -\frac{1}{6} \sum_{j=x,y,z} \frac{\omega_j^2(t)}{\omega_{j,0}^2} \frac{db_j^2}{dt} \langle H(0)\rangle\\ &= -\frac{1}{3} \sum_{j=x,y,z} \frac{\omega_j^2(t)}{\omega_{j,0}^2} b_j \dot{b}_j \langle H(0)\rangle.\end{aligned} \tag{5.14}$$

For a 3D unitary Fermi gas, the scaling factors are coupled via the evolution equations [156]

$$\ddot{b}_j + \omega_j^2(t) b_j = \frac{\omega_{j,0}^2}{b_j \Gamma(t)^{2/3}}, \quad j = x, y, z, \tag{5.15}$$

where the volume scaling factor is given by $\Gamma(t) = \prod_j b_j(t)$.

Combining (5.15) and (5.14) to substitute $\frac{\omega_j^2(t)}{\omega_{j,0}^2} b_j$, we rewrite the rate of change of the expectation value of H_0 as

$$\begin{aligned} \frac{d}{dt}\langle H_0 \rangle &= \frac{1}{3} \sum_{j=x,y,z} \left(\frac{\dot{b}_j \ddot{b}_j}{\omega_{j,0}^2} - \frac{\dot{b}_j}{b_j \Gamma^{2/3}} \right) \langle H(0) \rangle \\ &= \frac{d}{dt} \left(\frac{1}{2\Gamma^{2/3}} + \frac{1}{6} \sum_{j=x,y,z} \frac{\dot{b}_j^2}{\omega_{j,0}^2} \right) \langle H(0) \rangle. \end{aligned} \tag{5.16}$$

As for the variation of the expectation value of the trapping potential term, from (5.5) and (5.7) it simply reads

$$\frac{d}{dt}\langle H_{\mathrm{trap}}(t) \rangle = \frac{d}{dt} \left(\frac{1}{6} \sum_{j=x,y,z} \frac{\omega_j^2(t)}{\omega_{j,0}^2} b_j^2 \right) \langle H(0) \rangle. \tag{5.17}$$

The exact expression for the nonadiabatic mean energy directly follows from integrating the differential equation

$$\frac{d}{dt}\langle H \rangle = \frac{d}{dt}\langle H_0 + H_{\mathrm{trap}}(t) \rangle, \tag{5.18}$$

with the initial boundary condition $\langle H(t=0) \rangle = \langle H(0) \rangle$ and reads

$$\langle H(t) \rangle = \left[\frac{1}{2\Gamma^{2/3}} + \frac{1}{6} \sum_{j=x,y,z} \frac{\dot{b}_j^2 + \omega_j^2(t) b_j^2}{\omega_{j,0}^2} \right] \langle H(0) \rangle, \tag{5.19}$$

which is the central result of this section, from which all finite-time thermodynamics can be derived. In the adiabatic limit under slow driving ($\dot{b_j} = 0$ and since b_j is a well behaved function, $\ddot{b_j}$=0 in (5.15)), the adiabatic scaling factor reads

$$b_{j,ad}(t) = \frac{1}{\Gamma_{ad}^{1/3}} \frac{\omega_{j,0}}{\omega_j(t)}, \tag{5.20}$$

$$\Gamma_{ad}(t) = \prod_j b_{j,ad}(t). \tag{5.21}$$

Therefore, the instantaneous adiabatic mean energy reads

$$\langle H(t)\rangle_{ad} = \frac{1}{\Gamma_{ad}^{2/3}}\langle H(0)\rangle. \tag{5.22}$$

In characterizing the finite-time thermodynamics of isolated quantum systems, the ratio of the nonadiabatic and adiabatic mean energies plays a crucial role and is known as the nonadiabatic factor [157, 158]

$$Q^*(t) = \langle H(t)\rangle / \langle H_{ad}(t)\rangle_{ad}. \tag{5.23}$$

Then, the nonadiabatic factor is calculated from (5.22) and (5.19) to be

$$Q^*(t) = \Gamma_{ad}(t)^{2/3}\left[\frac{1}{2\Gamma^{2/3}} + \frac{1}{6}\sum_{j=x,y,z}\frac{\dot{b}_j^2 + \omega_j^2(t)b_j^2}{\omega_{j,0}^2}\right], \tag{5.24}$$

and determines the nonadiabatic mean work

$$\langle W(t)\rangle = \langle H(t)\rangle - \langle H(0)\rangle = (Q^*(t)/\Gamma_{ad}^{2/3}(t) - 1)\langle H(0)\rangle, \tag{5.25}$$

where we used that since we only dealt with unitary transformations there was no heat transfer between system and environment. The attentive reader will notice that all results in this section were given as a function of $\langle H(0)\rangle$. This is necessary because of the unknown exact number of atoms in the trap after the evaporative cooling phase and the complex nature of the interaction U of which our model only states the scaling property (5.2). These two constraints make it impossible to give a theoretical prediction on the ground state energy. But if this ground state energy is given, we have just shown how to obtain its change as function of time.

5.2 Local counterdiabatic control of the finite-time thermodynamics of a unitary Fermi gas

When a system undergoes a process in which it goes from one state to another by spending more energy then the necessary by adiabatic evolution we name this extra energy to be lost by quantum friction. Quantum friction is evidenced during dynamical

processes by values of $Q^*(t) > 1$, showing that some energy is being lost by becoming disordered motion inside the cloud instead of being used to produce work. To suppress friction, the counterdiabatic driving technique [66, 67] can be exploited in combination with dynamical scaling laws [30, 159] to set $Q^* = 1$. We refer to such superadiabatic control as counterdiabatic driving (CD).

Our approach to achieve superadiabatic control relies on first designing a desirable reference trajectory by specifying the modulation of the parameters of the Hamiltonian, i.e., $\omega_j(t)$. Subsequently, we consider an alternative protocol with frequencies $\omega_j(t) \to \Omega_j(t)$ that lead to the same final state than the adiabatic evolution corresponding to $\omega_j(t)$. The modified protocol with trap frequencies $\Omega_j(t)$ can be found for an arbitrary value T of the duration of the stroke, provided that $\Omega_j(t)$ can be implemented.

To design the reference evolution of the cloud we impose the following boundary conditions

$$\begin{aligned} \omega_j(0) &= \omega_{j,0}, \quad \omega_j(T) = c_{j,f}^{-2}\omega_j(0), \\ \dot{\omega}_{j,0} &= 0, \qquad \dot{\omega}_{j,f} = 0, \\ \ddot{\omega}_{j,0} &= 0, \qquad \ddot{\omega}_{j,f} = 0, \end{aligned} \tag{5.26}$$

and $c_{f,j} = \omega_j(T)/\omega_j(0)$ is set by the ratio of the initial and final target trap frequency. We determine a possible choice for the time-dependent scaling factors via the polynomial ansatz $\omega_j(t) = \omega_{j,0}\sum_n k_n(t/T)^n$. Specifically,

$$\omega_j(t) = \omega_j(0)\{1 + (c_{f,j}^{-2} - 1)[10s^3 - 15s^4 + 6s^5]\}, \tag{5.27}$$

where $s = t/T$. Consequently, the reference expansion factor is set by the adiabatic consistency equations

$$\begin{aligned} b_j(t) &= \frac{\omega_{j,0}}{\omega_j(t)\Gamma_{ad}^{1/3}(t)} \\ &= \frac{\omega_{j,0}}{\omega_{j,t}}\left[\frac{\nu(t)}{\nu(0)}\right]^{1/2}, \end{aligned} \tag{5.28}$$

where the geometric mean frequency equals $\nu(t) = [\omega_x(t)\omega_y(t)\omega_z(t)]^{1/3}$.

The above equations describe the evolution of the scaling factors in the adiabatic limit under slow driving. Nonetheless, they describe as well the exact nonadiabatic dynamics

under a modified driving protocol with a different time-dependence of the trapping frequencies, i.e., replacing $\omega_j(t) \to \Omega_j(t)$, where the explicit form of $\Omega_j(t)$ is to be determined and the Hamiltonian will remain the same as in (5.1). For a unitary Fermi gas in a 3D anisotropic trap, the requiring driving frequencies obtained from (5.15) are given by

$$\begin{aligned}\Omega_j^2(t) &= \frac{\omega_{j,0}^2}{b_j^2\Gamma^{2/3}} - \frac{\ddot{b}_j}{b_j} \\ &= \omega_j^2(t) - \frac{\ddot{b}_j}{b_j}\,, \end{aligned} \tag{5.29}$$

where $b_j(t)$ are given by Eqs. (5.28), but since this is a finite time implementation $\ddot{b_j} = 0$ no longer applies. The explicit expression for $\Omega_j^2(t)$ reads

$$\begin{aligned}\Omega_j^2(t) &= \omega_j^2 - 2\left(\frac{\dot{\omega}_j}{\omega_j}\right)^2 + \frac{\ddot{\omega}_j}{\omega_j} - \frac{4}{9}\left(\frac{\dot{\Gamma}}{\Gamma}\right)^2 + \frac{1}{3}\frac{\ddot{\Gamma}}{\Gamma} - \frac{2}{3}\frac{\dot{\omega}_j\dot{\Gamma}}{\omega_j\Gamma} \\ &= \omega_j^2 - 2\left(\frac{\dot{\omega}_j}{\omega_j}\right)^2 + \frac{\ddot{\omega}_j}{\omega_j} + \frac{1}{4}\left(\frac{\dot{\nu}}{\nu}\right)^2 - \frac{1}{2}\frac{\ddot{\nu}}{\nu} + \frac{\dot{\omega}_j\dot{\nu}}{\omega_j\nu}\,, \end{aligned} \tag{5.30}$$

which includes counterdiabatic corrections arising from ω_j, the geometric mean ν, and their coupling. The nonadiabatic factor for a unitary Fermi gas under local counterdiabatic driving obtained from (5.30), (5.29) and (5.24) reads

$$\begin{aligned}Q^*(t) &= 1 + \frac{1}{6}\Gamma(t)^{2/3}\sum_{j=\{x,y,z\}}\frac{\dot{b}_j^2 - b_j\ddot{b}_j}{\omega_{j,0}^2} \\ &= 1 + \frac{1}{6}\sum_{j=\{x,y,z\}}\left(\frac{\ddot{\omega}_j}{\omega_j^3} - \frac{\dot{\omega}_j^2}{\omega_j^4} - \frac{\ddot{\nu}}{2\nu\omega_j^2} + \frac{\dot{\nu}^2}{2\nu^2\omega_j^2}\right). \end{aligned} \tag{5.31}$$

When the scaling factors are isotropic so that $b_j(t) = b(t)$, the axis subindex j can be dropped out, the volume scaling factor simplifies to $\Gamma(t) = b(t)^3 = [\omega_0/\omega(t)]^{\frac{3}{2}}$ and

$$\Omega^2(t) = \omega^2(t) - \frac{3}{4}\left[\frac{\dot{\omega}(t)}{\omega(t)}\right]^2 + \frac{1}{2}\frac{\ddot{\omega}(t)}{\omega(t)}\,, \tag{5.32}$$

in agreement with [30,159]. Similarly, in the isotropic case the nonadiabatic factor reduces to

$$Q^*(t) = 1 + \frac{1}{4}\left(\frac{\ddot{\omega}}{\omega^3} - \frac{\dot{\omega}^2}{\omega^4}\right), \tag{5.33}$$

which agrees for the result in one-dimensional harmonically trapped systems [69, 143]. Note that while for nonadiabatic processes $Q^*(t)$ is expected to exceed unity, values of $Q^*(t) < 1$ can be reached whenever $\ddot{\omega} < \dot{\omega}^2/\omega$.

The engineering of a STA by CD requires the nonadiabatic modulation of the trap frequencies

$$\Omega_j^2(t) = \omega_j^2 - 2\left(\frac{\dot{\omega}_j}{\omega_j}\right)^2 + \frac{\ddot{\omega}_j}{\omega_j} + \frac{1}{4}\left(\frac{\dot{\nu}}{\nu}\right)^2 - \frac{1}{2}\frac{\ddot{\nu}}{\nu} + \frac{\dot{\omega}_j\dot{\nu}}{\omega_j\nu}, \tag{5.34}$$

where $\nu(t) = [\omega_x(t)\omega_y(t)\omega_z(t)]^{1/3}$ denotes the geometric mean frequency.

5.3 The experiment

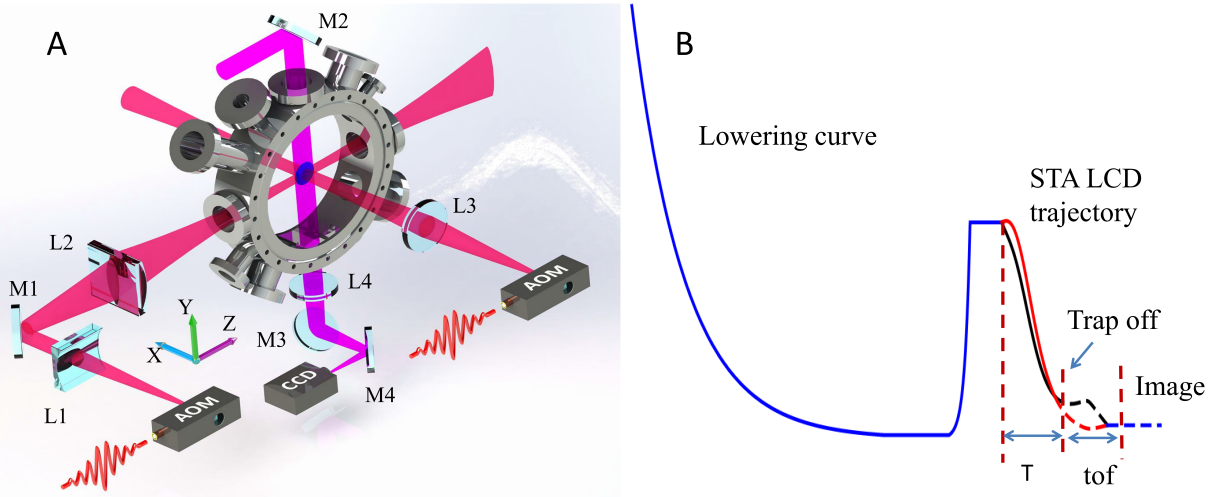

Figure 5.1: Schematic of the experimental setup (A) and the experimental procedure (B). A specially designed optical crossed-dipole trap is formed by two orthogonal far-off resonance laser beams, providing a highly controllable trap frequency. M1-M4, Mirrors; L1-L2, cylindrical lenes; L3-L4, achromatic lenses; AOM, acousto-optic modulator; tof, time-of-flight.

The experiment described here was executed by Professor's Haibin group [37] and theoreticaly described by us, it probes the nonadiabatic expansion dynamics in an anisotropically-trapped unitary quantum gas, a balanced mixture of fermionic ^{6}Li atoms in the lowest two hyperfine states $|\uparrow\rangle \equiv |F = 1/2, M_F = -1/2\rangle$ and $|\downarrow\rangle \equiv |F = 1/2, M_F = 1/2\rangle$. The experimental setup is similar to that in Ref. [160, 161], with a new configuration of the dipole trap consisting in an elliptic beam generated by a cylindrical lens along the x-axis and a nearly-ideal Gaussian beam along the z-axis. The resulting potential has a

cylindrical symmetry around x. This trap facilitates the control of the anisotropy and geometric frequency. Fermionic atoms are loaded into a cross-dipole trap used for evaporative cooling. A Feshbach resonance is used to tune the interactomic interaction to the unitary limit, reached at $B = 832\,\mathrm{G}$. The system is initially prepared in a stationary state of a normal fluid, with $\omega_x(0) = 2\pi \times 1200$ Hz and $\omega_y(0) = \omega_z(0) = 2\pi \times 300$ Hz. The initial energy of Fermi gas at unitarity is $E = 0.8(0.1)\,E_F$, corresponding to a temperature $Temp = 0.25(0.02)\,T_F$, where E_F and T_F are the Fermi energy and temperature of an ideal Fermi gas, respectively. Each data point is obtained from averaging 5 runs of measurements with identical parameters.

Fig. 5.2 shows the expansion stroke of the unitary Fermi gas with $b_{f,x} = 1/4$, $b_{f,y} = b_{f,z} = 1$ in $T = 800\mu s$. The trap frequencies are changed from the initial values $\omega_x(0) = 2\pi \times 1200$ Hz and $\omega_y(0) = \omega_z(0) = 2\pi \times 300$ Hz to the target values $\omega_x(T) = 2\pi \times 300$ Hz and $\omega_y(T) = \omega_z(T) = 2\pi \times 300$ Hz in 800 μs. The Fermi gas is initially confined in an anisotropic harmonic trap with a frequency aspect ratio of 4. Due to the engineering of frequencies, the size of the cloud gas is mostly expanded in the x axis, the changes in the y and z directions being small (Fig. 5.2A) during the driving processes. While the Fermi gas is anisotropic during the nonadiabatic, CD drive, it becomes isotropic at the final target state, in which both the frequency and cloud size aspect ratio are close to 1; see Fig. 5.2B(iii) and Fig. 5.2C(iii). Also in Fig 5.2 we include de results for the implementation of expansion attempting to follow the adiabatic schedule we are mimicing by CD. We name this finite-time approximation of an adiabatic evolution the *reference driving* which we shown to be a better approximation as the parameter T grows.

5.4 Results

The measured nonadiabatic factor $Q^*(t)$ and mean work during the expansion stroke are shown in Fig. 5.3. For the reference driving, the $Q^*(t)$ of the strongly interacting Fermi gas monotonically increases, witnessing quantum friction induced by excitations that emerge from the nonadiabatic dynamics. At time $T = 800\mu s$, $Q^*(T)$ approaches to 1.17 for the experimental parameters (brown dots in Fig. 5.3A). Quantum friction

decreases the mean work of the stroke (see Fig. 5.3B), defined as

$$\kappa(t) = \langle W(t)\rangle / \langle H(0)\rangle. \tag{5.35}$$

By contrast, quantum friction is greatly suppressed with the local counterdiabatic driving scheme. Indeed, $Q^*(t)$ reduces to 1 after completion of the superadiabatic stroke (blue dots in Fig. 5.3A), revealing that it is a friction-free process. Using STA by CD thus allow reaching $Q^*(T) = 1$, enhancing the work output. Its maximum value is reached at T and is determined by the geometric mean frequency according to

$$\langle W(T)\rangle_{\rm CD} = \left(\left(\frac{\nu(T)}{\nu(0)} \right)^{1/3} - 1 \right) \langle H(0)\rangle. \tag{5.36}$$

The measured value of the mean work κ in the experiment is about -0.37 in units of $\langle H(0)\rangle$ (blue dots in Fig. 5.3B), which is in very good agreement with the theoretical prediction, $(2^{-2/3} - 1) = -0.370$. Compared to the case of reference driving process, the mean work in the the local counterdiabatic driving process is increased by nearly 42.3%.

As seen from Eq. 5.36, in a STA by CD quantum friction is suppressed and the final mean work depends only on the ratio of geometric mean frequency between the initial state and the target state. For processes satisfying $\nu(T) = \nu(0)$, such as a change of the anisotropy of the cloud, the mean work vanishes. We verify this prediction experimentally. The strongly interacting Fermi gas is first prepared in a quantum state with frequencies of $\omega_x(0) = 2\pi \times 1200$ Hz and $\omega_y(0) = \omega_z(0) = 2\pi \times 300$ Hz. Then the trap frequencies are changed to $\omega_x(T) = \omega_y(T) = \omega_z(T) = 2\pi \times (\prod_j \omega_j(0))^{1/3} = 2\pi \times 476.22$ Hz, modifying the aspect ratio of the cloud. The measured nonadiabatic factor $Q^*(t)$, mean work and cloud expansion images are presented in Fig. 5.4. It is apparent that there is no friction for $Q^*(T) = 1$ (blue dots in Fig. 5.4B) and that the mean work vanishes $W(T) = 0$ (blue dots in Fig. 5.4C) when manipulating the quantum state using STA by CD. For the nonadiabatic reference driving, quantum friction is however induced and causes $Q^*(T) > 1$ (brown dots in Fig. 5.4B), signaling energy dispersion in the final state. The mean work is then increased to a positive value of $1.22\langle H(0)\rangle$ (brown dots in Fig. 5.4C).

A global measure of the nonadiabatic character of a superadiabatic stroke can be quantified by the time-average deviation of the mean work $\langle W(t)\rangle$ from the adiabatic

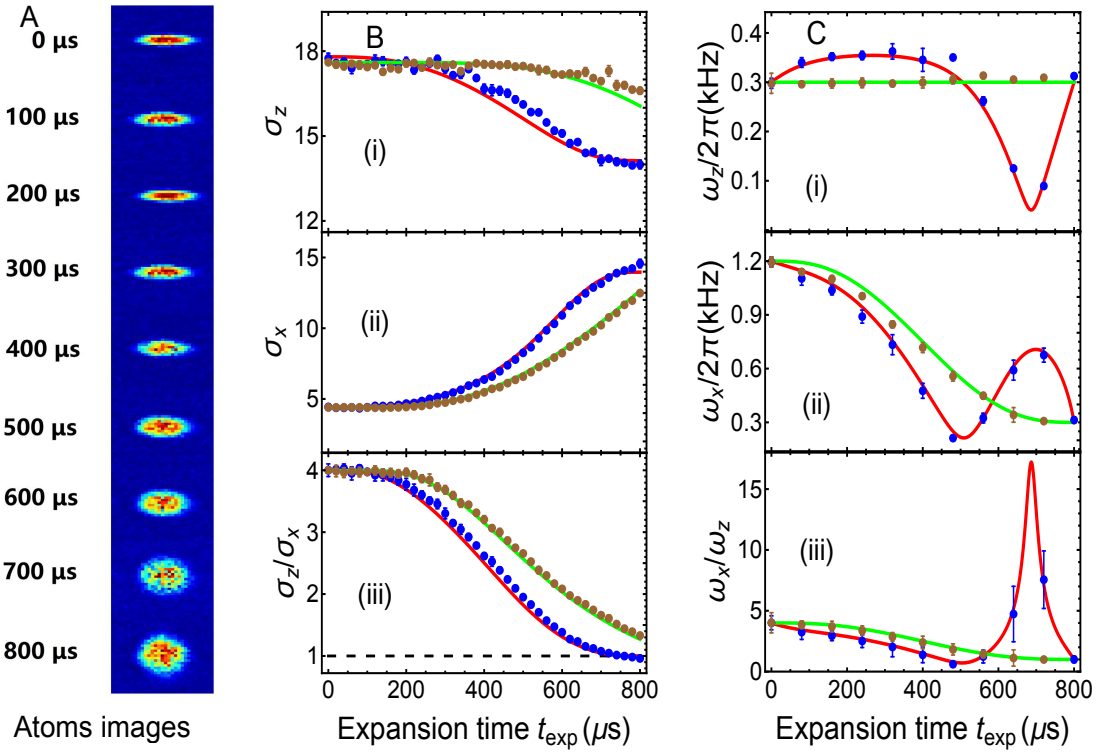

Figure 5.2: The expansion stroke of the unitary Fermi gas for STA of CD and reference driving case with $b_{f,x} = 4$, keeping $b_{f,y} = b_{f,z} = 1$ in $T = 800\mu s$: the atoms images of CD driving (A), the measured cloud size (the σs being the Gaussian waists in μm) and cloud aspect ratio (B), and the measured frequencies and frequency aspect ratio (C). Blue dots and brown dots are the measured results for CD and reference driving case, respectively. The red line and green line are theoretical predictions. The black dashed line in (Biii) denotes for the aspect ratio of 1, indicating an isotropic trap for Fermi gas. Error bars represent the standard deviation of the statistic.

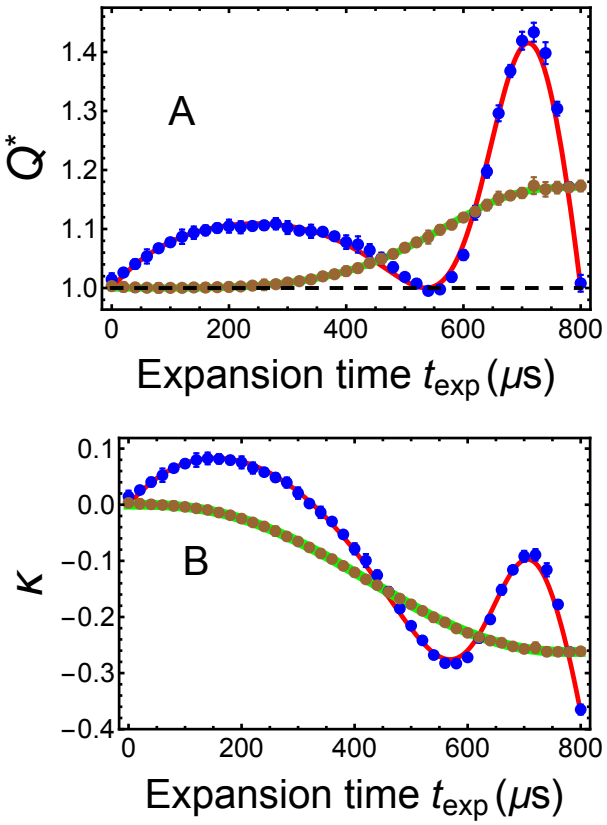

Figure 5.3: Nonadiabatic factor Q^* (A) and the mean work (B) in an expansion stroke. Blue and brown dots denote the measured data for STA of local counterdiabatic driving and nonadiabatic reference driving case while the red and green lines are the corresponding theoretical predictions. $\kappa(t) = \langle W(t)\rangle/\langle H(0)\rangle$ is the ratio of the mean work and the initial energy. The black dashed line represents $Q^* = 1$ where there is no quantum friction. Error bars represent the standard deviation of the statistic.

value $\langle W_{ad}(t)\rangle$ as a function of the total time T

$$\delta W = \frac{1}{T}\int_0^T dt\,[\langle W(t)\rangle - \langle W_{ad}(t)\rangle]\,. \tag{5.37}$$

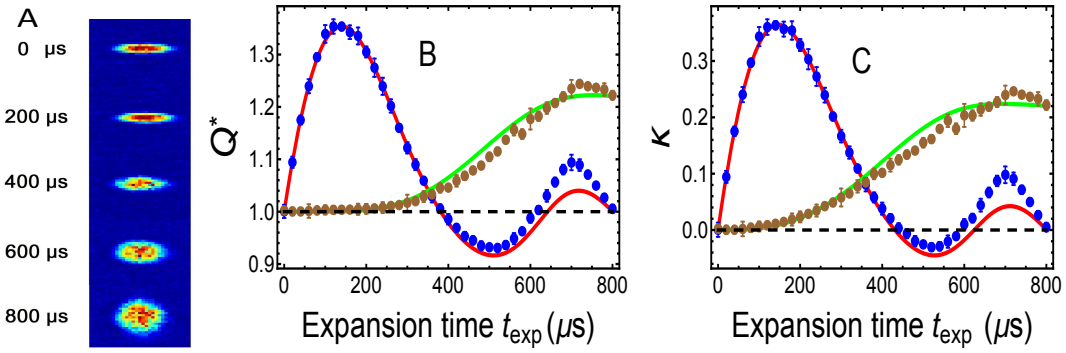

Figure 5.4: Cloud expansion images (A), nonadiabatic factor Q^* (B) and mean work (C) of unitary Fermi gas during a change of the cloud aspect ratio that preserves the geometric mean frequency, $\nu(T) = \nu(0)$. Blue and brown dots represent the measured results for STA of CD and nonadiabatic driving case, respectively. Red and green lines denote the corresponding theoretical predictions. Black dashed lines denote the friction-free $Q^*(T) = 1$ and the zero mean work $\kappa = 0$. Error bars represent the standard deviation of the statistic.

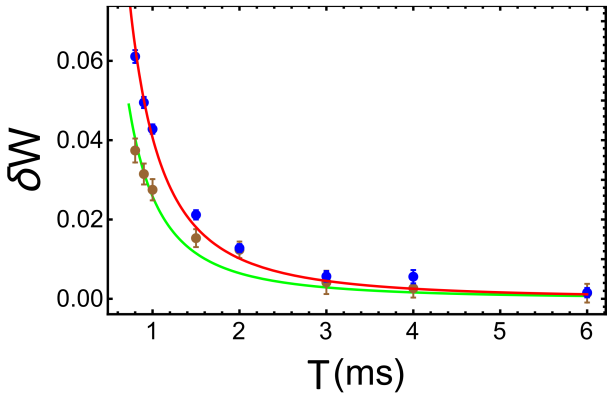

Figure 5.5: Time-averaged mean work deviation δW in units of $\langle H(0)\rangle$ as a function of T. Blue and brown dots denote the measured data for STA by CD driving and the nonadiabatic reference driving case, while the red and green lines are the fits with a function of $1/T^2$. Error bars represent the standard deviation of the measurement data.

In the experiment, we measure the mean work deviation in both a STA based on CD driving and a nonadiabatic reference protocol for the expansion strokes. The initial and final geometric frequencies are fixed to 4.8 and 1.2, respectively. The trap frequencies are changed from the initial frequencies $\omega_x = 2\pi \times 1440$ Hz, $\omega_y = \omega_z = 2\pi \times 300$ Hz to $\omega_x = 2\pi \times 360$ Hz, $\omega_y = \omega_z = 2\pi \times 300$ Hz in different time T. For STA by CD driving, the mean work $\langle W(T) \rangle$ does not change no matter how short the time T is. However, $\langle W(t) \rangle$ at $t < T$ keeps changing to reflect how large the excess work needed to implement STA at different stages. The measured results are shown in Fig. 5.5. The shorter the time T, the greater the deviation of mean work δW. The solid curves are the fits with a power-law $1/T^2$ as a function of the duration of the stroke T.

The experiment presented here demonstrate the suppression of quantum friction and enhancement of the mean work output in superadiabatic strokes, when compared to diabatic strokes, with a strongly interacting quantum fluid as a working medium. The control of the finite-time quantum thermodynamics is achieved using shortcuts to adiabaticity that exploit the emergent scale-invariance of a unitary Fermi gas. In combination with cooling and heating steps, superadiabatic strokes can be used to engineer quantum heat engines [69, 141–143, 162] and refrigerators [163–165], e.g., based on a quantum Otto cycle, that operate at maximum efficiency with high output and cooling power.

Chapter 6

Conclusions

Throughout this thesis we have studied many-body systems of interest to AQC. We began by considering the quantum search algorithm, which can be built upon a solvable quantum Hamiltonian. It exhibits quantum advantage through a run-time scaling $O(\sqrt{N})$ as we increase the dimension N of the search space. This behavior can be associated with a first-order quantum phase transition as the system undergoes the adiabatic evolution.

Our first work was a numeric and analytic evaluation of quantum correlations measured by the LQU in the adiabatic quantum search. We have shown that these correlations converge exponentially fast to saturation as a function of the block length L. Moreover, at the limit $n \to \infty$, the LQU vanishes everywhere except at the critical point $s = \frac{1}{2}$. This behavior has been shown to precisely characterize the first-order QPT in the model.

In our second work we explored not the perfect adiabatic execution of the quantum search algorithm, but its dynamics in a finite-time implementation. Any Hamiltonian quantum algorithm with speed up over classical algorithms is expected to go through a quantum phase transition [61] which implies that the total time needed to drive the system will scale with the size of the problem. Driving the system at feasible speeds will result in excitations, which can be measured by the number of kinks shown in the system. We observed an exponential behavior in the amount of excitations in relation to the speed of the driving Hamiltonian and noticed that the quantum phase transition can be observed even on small systems if they are not driven too fast.

In our third and final work, noticing that the fast driving of quantum algorithms

causes them to be less reliable, we contributed to bridge the gap between theory and experiment in a technique originally proposed to speed up AQC. Shortcuts to adiabaticity are proposed as a way to find finite time implementations of driven Hamiltonians without causing excitations. Despite its obvious value to AQC, implementing it on large scale problems has been difficult due to non-locality of the interactions, non-oracularity of the Hamiltonian or other requirements. So we took a step back and found a system in which we could work around these requirements. The system we found was a unitary Fermi gas in an anisotropic time-dependent trap as a medium for transformations that could take place in a thermal machine. We have shown that for this case we were able to control the dynamics of the expansion of the atom cloud and obtained higher efficiency than a traditional adiabatic machine would present.

As future perspectives the works presented on this thesis have several possibilities. It would be interesting to investigate possible universal properties of LQU, e.g. analyzing its behavior for quantum critical spin chains belonging to distinct universality classes. A relevant point would be a possible scaling related to the central charge of the Virasoro algebra behind the critical chain, similarly as it occurs for entanglement [79–81]. Other points of interest would be the investigation of the quantum critical behavior for finite temperatures as well as the effect of boundary conditions over the scaling of the LQU for systems $D \times 2$.

We also intend to consider decoherence effects [166] in dynamical first-order QPTs. Moreover, we are also interested in the exchange between power-law and exponential-law behaviors as a consequence of boundary conditions [111] and Hamiltonian symmetries.

Besides all that, finding physical systems more suitable to adiabatic quantum computation that still allows implementation of shortcuts remains a challenge. This thesis has provided contributions in this direction and opens the possibility of further developments in this field.

Appendix

A Computational Complexity Theory Recap

Frequently in computer science more than one algorithm can be used to solve the same problem. Their time efficiency is frequently a parameter of great interest in deciding which to use, besides exactness and memory efficiency, to name a few.

Comparing time and memory efficiency of two algorithms may not be trivial, and to aid with that there is the big-O notation. This notation allows us to see at a glance how fast an algorithm's consumption of a resource diverges.

For example lets assume that the execution time for algorithm A_1 is $O(n^3)$ and for A_2 it is $O(n^1)$, n being the number of bits necessary to store the problem. We know that for large inputs a cubic polinom grows faster tham a linear one, so we expect that A_2 will be faster for large values of n.

A.1 Big-O Notation

Definition. Given two functions $f(n)$ and $g(n)$, $f(n) = O(g(n))$ if there are constants n_0 and c > 0 such that $|f(n)| <$ c $|g(n)|$ for all n $> n_0$, where $|\square|$ represents the absolute value of $\square$. [56]

This definition thus gives an upper bound on the quantity measured by $f(n)$. Which is useful because when we run an algorithm in a computer the exact amount of resources consumed (time, memory, etc) as a function of the problem size is represented by a very complicated function. Knowing this function exactly isn't important, only it's scaling is important. Further, we are mostly interested in knowing the resources consumed in the

computation of large problems.

A good rule of thumb to obtain the big-O order of a function is to keep only the term that diverges to infinity the fastest as the problem's size grows, ignoring any multiplicative prefactors. For example

$$\begin{aligned} \text{if } f = 5n^3 + n + e^{-n} &\longrightarrow f = O(n^3), \\ \text{if } f = 4e^n + n^5 &\longrightarrow f = O(e^n). \end{aligned} \tag{A.1}$$

A.2 Complexity

This section closely follows [56], but only gives an intuition on the concepts presented. For a rigorous analysis see the reference.

A complexity class is a set of problems that the best algorithms we know to solve them exactly demand resources that scale similarly. Also some subsets of classes have useful relationships with each other. The classes of interest to us are:

- P is the class of problems whose solutions can be found with a amount of resources that scales as a polynomial of the input size (number of bits used to input the problem).
- NP is the class of problems that, if presented by a possible solution, this candidate can be verified in polynomial time.
- NP-Hard is the class of problems to which all problems in NP can be reducted efficiently (reduction is defined bellow).
- NP-Complete is the intersection of NP with NP-Hard.

A problem P_1 is said to be reductible to another problem P_2 iff there are functions f and g that can be used to turn an algorithm A_2 that solves P_2 into an algorithm that solves P_1 in the following way: the input x_1 is transformed in $x_2 = f(x_1)$ and fed to A_2 to obtain the result $r_2 = A_2(x_2)$ and finally this response is transformed in $r_1 = g(r_2)$, which is the solution to P_1. A reduction is said to be efficient if both f and g require computational resources that scale with polynomial functions on the size of their inputs.

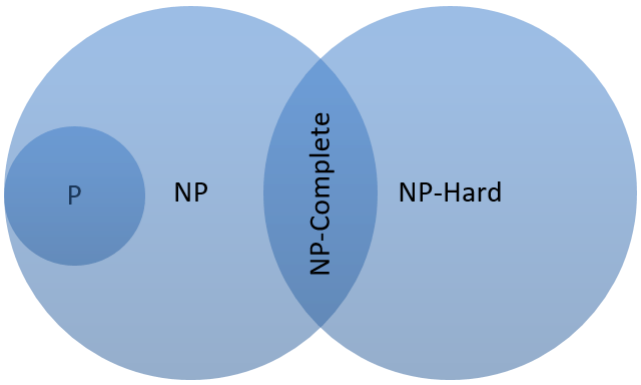

Figure A.1: A diagram representation of what most experts believe are the relationships between P, NP, NP-Complete and NP-Hard.

B LQU for 2 × D Systems

The change from equation (3.2) to (3.3) is the central result in [34], enabling us to have a closed form calculation that delivers a quantification of discord between a qubit and a larger system. We now prove this transformation.

The LQU (Q) is defined as a minimization of the skew-information (I) of a system (ρ) related to a measurement (K) of one qubit (the first spin in a chain in our case). In mathematical language:

$$Q(\rho) = min_K I(\rho, K), \tag{B.1}$$

$$I(\rho, K) = Tr\rho K^2 - Tr\rho^{1/2} K \rho^{1/2} K, \tag{B.2}$$

with $K = K_B \otimes \mathbb{1}$, and since this measurement can be in any direction

$$K_B = \langle n|\vec{\sigma}\rangle = Sin(\theta)Z + Cos(\theta)Sin(\gamma)X + Cos(\theta)Cos(\gamma)Y, \tag{B.3}$$

where X, Y and Z are the usual Pauli matrices and θ , γ are real parameters and $|n\rangle = (Cos(\theta)Sin(\gamma), Cos(\theta)Cos(\gamma), Sin(\theta))$ is a unit vector. We notice that $K_B^2 = \mathbb{1}$ and that allows us to rewrite (B.2) as

$$I(\rho, K) = 1 - \overline{I}, \tag{B.4}$$

$$\overline{I} = Tr[M], \tag{B.5}$$

$$M = \rho^{1/2} K \rho^{1/2} K, \tag{B.6}$$

if we make $Z_B = Z \otimes \mathbb{1}$ and anlogously for the other Pauli matrices, then

$$\begin{aligned} M &= \rho^{1/2}(Sin(\theta)Z_B + Cos(\theta)Sin(\gamma)X_B + Cos(\theta)Cos(\gamma)Y_B)\rho^{1/2}(Sin(\theta)Z_B + \\ &+Cos(\theta)Sin(\gamma)X_B + Cos(\theta)Cos(\gamma)Y_B), \\ &= Sin(\theta)^2\rho^{1/2}Z_B\rho^{1/2}Z_B + Cos(\theta)^2Sin(\gamma)^2\rho^{1/2}X_B\rho^{1/2}X_B + \\ &+Cos(\theta)^2Cos(\gamma)^2\rho^{1/2}Y_B\rho^{1/2}Y_B + Sin(\theta)Cos(\theta)Sin(\gamma)\{\rho^{1/2}Z_B, \rho^{1/2}X_B\} + \\ &+Sin(\theta)Cos(\theta)Cos(\gamma)\{\rho^{1/2}Z_B, \rho^{1/2}Y_B\} + Cos(\theta)Sin(\gamma)Cos(\gamma)\{\rho^{1/2}X_B, \rho^{1/2}Y_B\}. \end{aligned} \tag{B.7}$$

Now we see that

$$\begin{aligned} \overline{I} = Sin(\theta)^2Tr[\rho^{1/2}Z_B\rho^{1/2}Z_B] + Cos(\theta)^2Sin(\gamma)^2Tr[\rho^{1/2}X_B\rho^{1/2}X_B] + \\ +Cos(\theta)^2Cos(\gamma)^2Tr[\rho^{1/2}Y_B\rho^{1/2}Y_B] + 2Sin(\theta)Cos(\theta)Sin(\gamma)Tr[\rho^{1/2}Z_B\rho^{1/2}X_B] + \\ +2Sin(\theta)Cos(\theta)Cos(\gamma)Tr[\rho^{1/2}Z_B\rho^{1/2}Y_B] + 2Cos(\theta)Sin(\gamma)Cos(\gamma)Tr[\rho^{1/2}X_B\rho^{1/2}Y_B]. \end{aligned} \tag{B.8}$$

Its easy to notice that

$$\overline{I} = \langle n|W|n\rangle, \tag{B.9}$$

where

$$W_{ij} = Tr[\rho_{AB}^{1/2}(I_A \otimes \sigma_{iB})\rho_{AB}^{1/2}(I_A \otimes \sigma_{jB})]. \tag{B.10}$$

From (B.1), (B.4) and (B.9) we know that we want:

$$Q(\rho) = 1 - max_{|n\rangle}\, \langle n|W|n\rangle, \tag{B.11}$$

But we know that the highest result from $\langle n|W|n\rangle$ on a Hermitean matrix is its highest eigenvalue (see next section for proof), so:

$$Q(\rho) = 1 - \lambda_{max}\{W\}. \tag{B.12}$$

B.1 Maximum Eigenvalue Formula Demonstration

If A is an Hermitean real matrix and $A = U^{\dagger}DU$ with U a unitary matrix and D a diagonal matrix with its eigenvalues ordered

$$D = \begin{pmatrix} \lambda_{min} & & (0) \\ & \ddots & \\ (0) & & \lambda_{max} \end{pmatrix}. \tag{B.13}$$

Being $|x\rangle$ a unit vector, we define

$$r(\vec{x}) = \langle x|A|x\rangle\,. \tag{B.14}$$

But changing the variables with $|y\rangle = U\,|x\rangle$ we get

$$r(\vec{y}) = \langle y|D|y\rangle\,. \tag{B.15}$$

Its clear that $Max\{r(|x\rangle)\} = Max\{r(|y\rangle)\} = \lambda_{max}$.

C The Hellmann-Feynman Theorem

For the ground state $|\psi_g\rangle$ of a system subjected to the Hamiltonian $H(t,\lambda)$ with t being the time and $\lambda(t)$ a tunnable external paramater (like temperature or a trap frequency), the Hellmann-Feynman Theorem (HFT) states that

$$\partial_\lambda \langle\psi_g|H|\psi_g\rangle = \langle\psi_g|\partial_\lambda H|\psi_g\rangle\,. \tag{C.1}$$

The proof follows. First we use the multiplication rule for derivatives

$$\partial_\lambda \langle\psi_g|H|\psi_g\rangle = \langle\partial_\lambda\psi_g|H|\psi_g\rangle + \langle\psi_g|H|\partial_\lambda\psi_g\rangle + \langle\psi_g|\partial_\lambda H|\psi_g\rangle\,, \tag{C.2}$$

and since $|\psi_g\rangle$ is the ground state we can use the fact that $H\,|\psi_g\rangle = E_g\,|\psi_g\rangle$

$$\partial_\lambda \langle\psi_g|H|\psi_g\rangle = E_g\,\langle\partial_\lambda\psi_g|\psi_g\rangle + E_g\,\langle\psi_g|\partial_\lambda\psi_g\rangle + \langle\psi_g|\partial_\lambda H|\psi_g\rangle\,, \tag{C.3}$$

$$= E_g\,[\langle\partial_\lambda\psi_g|\psi_g\rangle + \langle\psi_g|\partial_\lambda\psi_g\rangle] + \langle\psi_g|\partial_\lambda H|\psi_g\rangle\,. \tag{C.4}$$

But we also know that taking the derivative of $\langle\psi_g|\psi_g\rangle = 1$ results in $\langle\partial_\lambda\psi_g|\psi_g\rangle + \langle\psi_g|\partial_\lambda\psi_g\rangle = 0$. So the two first terms in the right hand side of (C.3) cancel each other and we have

$$\partial_\lambda \langle\psi_g|H|\psi_g\rangle = \langle\psi_g|\partial_\lambda H|\psi_g\rangle\,. \tag{C.5}$$

and the proof is finished.

Bibliography

[1] Paul Benioff. The computer as a physical system: A microscopic quantum mechanical hamiltonian model of computers as represented by Turing machines. *Journal of Statistical Physics*, 22(5):563–591, 1980. DOI: 10.1007/BF01011339.

[2] R. Feynman. Simulating physics with computers. *Int. J. Theor. Phys.*, 21(467), 1982.

[3] D. Deutsch. Quantum theory, the Church-Turing principle and the universal quantum computer. *Proc. R. Soc. Lond*, A(400), 1985.

[4] P. Shor. Algorithms for quantum computacion: discrete logarithm and factoring. *Proc. 35th Annual Symposium Of Foundations Of Computer Science*, pages 124 – 134, 1994.

[5] L. K. Grover. Quantum mechanics helps in searching for a needle in a haystack. *Phys. Rev. Lett.*, 79(325), 1997. DOI: 10.1103/PhysRevLett.79.325.

[6] Christof Zalka. Grover's quantum searching algorithm is optimal. *Phys. Rev. A*, 60:2746–2751, 1999. DOI: 10.1103/PhysRevA.60.2746.

[7] E. Farhi, J. Goldstone, S. Gutmann, and M. Sipser. Quantum computation by adiabatic evolution. *Technical Report MIT-CTP-2936*, 2000.

[8] D. Aharonov, W. van Dam, J. Kempe, Z. Landau, S. Lloyd, and O. Regev. Adiabatic quantum computation is equivalent to standard quantum computation. *SIAM Journal of Computing*, 37(1):166–194, 2007. DOI: 10.1137/080734479.

[9] A. M. Childs, E. Farhi, and J. Preskill. Robustness of adiabatic quantum computation. *Phys. Rev. A*, 65:012322, 2001. DOI: 10.1103/PhysRevA.65.012322.

[10] V. Martin-Mayor and I. Hen. Unraveling quantum annealers using classical hardness. *Scientific Reports*, 5:15324, 2015. DOI: 10.1038/srep15324.

[11] Kebiao Xu, Tianyu Xie, Zhaokai Li, Xiangkun Xu, Mengqi Wang, Xiangyu Ye, Fei Kong, Jianpei Geng, Changkui Duan, Fazhan Shi, and Jiangfeng Du. Experimental adiabatic quantum factorization under ambient conditions based on a solid-state single spin system. *Phys. Rev. Lett.*, 118:130504, 2017. DOI: 10.1103/PhysRevLett.118.130504.

[12] A J Berkley, M W Johnson, P Bunyk, R Harris, J Johansson, T Lanting, E Ladizinsky, E Tolkacheva, M H S Amin, and G Rose. A scalable readout system for a superconducting adiabatic quantum optimization system. *Superconductor Science and Technology*, 23(10):105014, 2010.

[13] M. W. et al. Johnson. Quantum annealing with manufactured spins. *Nature*, 473:194, 2011. DOI: 10.1038/nature10012.

[14] A. W. Glaetzle, R. M. W. van Bijnen, P. Zoller, and W. Lechner. A coherent quantum annealer with rydberg atoms. *Nature Communications*, 8:15813, 2017. DOI: 10.1038/ncomms15813.

[15] Matthias Steffen, Wim van Dam, Tad Hogg, Greg Breyta, and Isaac Chuang. Experimental implementation of an adiabatic quantum optimization algorithm. *Phys. Rev. Lett.*, 90:067903, 2003. DOI: 10.1103/PhysRevLett.90.067903.

[16] Avik Mitra, Arindam Ghosh, Ranabir Das, Apoorva Patel, and Anil Kumar. Experimental implementation of local adiabatic evolution algorithms by an NMR quantum information processor. *Journal of Magnetic Resonance*, 177(2):285–298, 2005. DOI: 10.1016/j.jmr.2005.08.004.

[17] Yu Long, Guanru Feng, Yongchao Tang, Wei Qin, and Guilu Long. Nmr realization of adiabatic quantum algorithms for the modified simon problem. *Phys. Rev. A*, 88:012306, 2013. DOI: 10.1103/PhysRevA.88.012306.

[18] M.S. Anwar, D. Blazina, H.A. Carteret, S.B. Duckett, and J.A. Jones. Implementing grover's quantum search on a para-hydrogen based pure state nmr quantum computer. *Chemical Physics Letters*, 400(1):94 – 97, 2004. DOI: 10.1016/j.cplett.2004.10.078.

[19] P. Richerme, C. Senko, J. Smith, A. Lee, S. Korenblit, and C. Monroe. Experimental performance of a quantum simulator: Optimizing adiabatic evolution and identifying many-body ground states. *Phys. Rev. A*, 88:012334, 2013. DOI: 10.1103/PhysRevA.88.012334.

[20] S. Boixo, T. Albash, F. M. Spedalieri, N. Chancellor, and D. A. Lidar. Experimental signature of programmable quantum annealing. *Nature Comm.*, 4:3067, 2013. DOI: 10.1038/ncomms3067.

[21] S. Boixo, T. F. Ronnow, S. V. Isakov, Z. Wang, D. Wecker, D. A. Lidar, J. M. Martinis, and M. Troyer. Evidence for quantum annealing with more than one hundred qubits. *Nature Physics*, 10:218, 2014. DOI: 10.1038/nphys2900.

[22] Kristen L. Pudenz, Tameem Albash, and Daniel A. Lidar. Error-corrected quantum annealing with hundreds of qubits. *Nature Communications*, 5, 2014. DOI: 10.1038/ncomms4243.

[23] S. W. Shin, G. Smith, J. A. Smolin, and U. Vazirani. How "Quantum" is the D-Wave Machine? *eprint arXiv:quant-ph/1401.7087*, 2014.

[24] Troels F. Rønnow, Zhihui Wang, Joshua Job, Sergio Boixo, Sergei V. Isakov, David Wecker, John M. Martinis, Daniel A. Lidar, and Matthias Troyer. Defining and detecting quantum speedup. *Science*, 345(6195):420–424, 2014. DOI: 10.1126/science.1252319.

[25] Oxford english dictionary, 2008.

[26] R. Orús and J. I. Latorre. Universality of entanglement and quantum-computation complexity. *Phys. Rev. A*, 69:052308, 2004. DOI: 10.1103/PhysRevA.69.052308.

[27] E. Biham, G. Brassard, D. Kenigsberg, and T. Mor. Quantum computing without entanglement. *Theoretical Computer Science*, 320(1):15 – 33, 2004. DOI: 10.1016/j.tcs.2004.03.041.

[28] M. Born and V. Fock. Beweis des adiabatensatzes. *Zeitschrift für Physik*, 51(3):165–180, 1928. DOI: 10.1007/BF01343193.

[29] S. Sachdev. *Quantum Phase Transitions*. Cambridge University Press, Cambridge, England, 2001.

[30] Adolfo del Campo. Shortcuts to adiabaticity by counterdiabatic driving. *Physical Review Letters*, 111(10), 2013. DOI: 10.1103/physrevlett.111.100502.

[31] I. B. Coulamy, A. C. Santos, I. Hen, and M. S. Sarandy. Energetic cost of superadiabatic quantum computation. *Frontiers in ICT*, 3:19, 2016. DOI: 10.3389/fict.2016.00019.

[32] Jérémie Roland and Nicolas J. Cerf. Quantum search by local adiabatic evolution. *Phys. Rev. A*, 65:042308, 2002. DOI: 10.1103/PhysRevA.65.042308.

[33] H. Ollivier and W. H. Zurek. Quantum discord: A measure of the quantumness of correlations. *Phys. Rev. Lett.*, 88:017901, 2001. DOI: 10.1103/PhysRevLett.88.017901.

[34] Davide Girolami, Tommaso Tufarelli, and Gerardo Adesso. Characterizing nonclassical correlations via local quantum uncertainty. *Phys. Rev. Lett.*, 110:240402, 2013. DOI: 10.1103/PhysRevLett.110.240402.

[35] I.B. Coulamy, J.H. Warnes, M.S. Sarandy, and A. Saguia. Scaling of the local quantum uncertainty at quantum phase transitions. *Physics Letters A*, 380(20):1724 – 1728, 2016. DOI: 10.1016/j.physleta.2016.03.026.

[36] I. B. Coulamy, A. Saguia, and M. S. Sarandy. Dynamics of the quantum search and quench-induced first-order phase transitions. *Phys. Rev. E*, 95:022127, 2017. DOI: 10.1103/PhysRevE.95.022127.

[37] Shujin Deng, Aurélia Chenu, Pengpeng Diao, Fang Li, Shi Yu, Ivan Coulamy, Adolfo del Campo, and Haibin Wu. Superadiabatic quantum friction suppression in finite-time thermodynamics. *Science Advances*, 4(4), 2018. DOI: 10.1126/sciadv.aar5909.

[38] A. Steane. Quantum computing. *Reports on Progress in Physics*, 61(2):117, 1998.

[39] C. Figgatt, D. Maslov, K. A. Landsman, N. M. Linke, S. Debnath, and C. Monroe. Complete 3-qubit grover search on a programmable quantum computer. *Nature Communications*, 8(1):1918, 2017. DOI: 10.1038/s41467-017-01904-7.

[40] Lieven M. K. Vandersypen, Matthias Steffen, Gregory Breyta, Costantino S. Yannoni, Mark H. Sherwood, and Isaac L. Chuang. Experimental realization of shor's quantum factoring algorithm using nuclear magnetic resonance. *Nature*, 414:883 EP –, 2001.

[41] Nanyang Xu, Jing Zhu, Dawei Lu, Xianyi Zhou, Xinhua Peng, and Jiangfeng Du. Quantum factorization of 143 on a dipolar-coupling nuclear magnetic resonance system. *Phys. Rev. Lett.*, 108:130501, 2012. DOI: 10.1103/PhysRevLett.108.130501.

[42] Xinhua Peng, Zeyang Liao, Nanyang Xu, Gan Qin, Xianyi Zhou, Dieter Suter, and Jiangfeng Du. Quantum adiabatic algorithm for factorization and its experimental implementation. *Physical Review Letters*, 101(22), 2008. DOI: 10.1103/physrevlett.101.220405.

[43] Zhengbing Bian, Fabian Chudak, William G. Macready, Lane Clark, and Frank Gaitan. Experimental determination of ramsey numbers. *Phys. Rev. Lett.*, 111:130505, 2013. DOI: 10.1103/PhysRevLett.111.130505.

[44] Tameem Albash and Daniel A. Lidar. Adiabatic quantum computation. *Rev. Mod. Phys.*, 90:015002, 2018. DOI: 10.1103/RevModPhys.90.015002.

[45] K. Gottfried and T.-M. Yan. *Quantum Mechanics: Fundamentals*. Springer, New York, 2003.

[46] Tosio Kato. On the adiabatic theorem of quantum mechanics. *Journal of the Physical Society of Japan*, 5(6):435–439, 1950. DOI: 10.1143/jpsj.5.435.

[47] S. Boixo and R. D. Somma. Necessary condition for the quantum adiabatic approximation. *Phys. Rev. A*, 81:032308, 2010. DOI: 10.1103/PhysRevA.81.032308.

[48] D. M. Tong, K. Singh, L. C. Kwek, and C. H. Oh. Quantitative conditions do not guarantee the validity of the adiabatic approximation. *Phys. Rev. Lett.*, 95:110407, 2005. DOI: 10.1103/PhysRevLett.95.110407.

[49] Karl-Peter Marzlin and Barry C. Sanders. Inconsistency in the application of the adiabatic theorem. *Phys. Rev. Lett.*, 93:160408, 2004. DOI: 10.1103/PhysRevLett.93.160408.

[50] Daniel Comparat. General conditions for quantum adiabatic evolution. *Phys. Rev. A*, 80:012106, 2009. DOI: 10.1103/PhysRevA.80.012106.

[51] Jiangfeng Du, Lingzhi Hu, Ya Wang, Jianda Wu, Meisheng Zhao, and Dieter Suter. Experimental study of the validity of quantitative conditions in the quantum adiabatic theorem. *Phys. Rev. Lett.*, 101:060403, 2008. DOI: 10.1103/PhysRevLett.101.060403.

[52] Zhen-Yu Wang and Martin B. Plenio. Necessary and sufficient condition for quantum adiabatic evolution by unitary control fields. *Phys. Rev. A*, 93:052107, 2016. DOI: 10.1103/PhysRevA.93.052107.

[53] M. A. Nielsen and I. L. Chuang. *Quantum Computation and Quantum Information*. Cambridge University Press, Cambridge, England, 2000.

[54] R. A. Moser and D. Scheder. A full derandomization of schöning's k-SAT algorithm. In *Proceedings of the 43rd annual ACM symposium on Theory of computing - STOC 11*. ACM Press, 2011.

[55] Nicolas J. Cerf, Lov K. Grover, and Colin P. Williams. Nested quantum search and NP-hard problems. *Applicable Algebra in Engineering, Communication and Computing*, 10(4-5):311–338, 2000. DOI: 10.1007/s002000050134.

[56] M. R. Garey and D. S. Johnson. *Computers and Intractability: A Guide to the Theory of NP-Completeness*. Series of Books in the Mathematical Sciences. W. H. Freeman, 1979.

[57] Gerhard J. Woeginger. Exact algorithms for NP-hard problems: A survey. In *Combinatorial Optimization — Eureka, You Shrink!*, pages 185–207. Springer Berlin Heidelberg, 2003.

[58] W. van Dam, M. Mosca, and U. Vazirani. How powerful is adiabatic quantum computation? In *Proceedings 2001 IEEE International Conference on Cluster Computing*, pages 279–287, 2001.

[59] M. Kieferová and N. Wiebe. On the power of coherently controlled quantum adiabatic evolutions. *New Journal of Physics*, 16(12):123034, 2014. DOI: 10.1088/1367-2630/16/12/123034.

[60] I. Hen. Realizable quantum adiabatic search. *EPL (Europhysics Letters)*, 118(3):30003, 2017.

[61] J. I. Latorre and R. Orús. Adiabatic quantum computation and quantum phase transitions. *Phys. Rev. A*, 69:062302, 2004. DOI: 10.1103/PhysRevA.69.062302.

[62] E. Farhi, J. Goldstone, S. Gutmann, and D. Nagaj. How to make the quantum adiabatic algorithm fail. *International Journal of Quantum Information*, 06(03):503–516, 2008. DOI: 10.1142/S021974990800358X.

[63] C. Pfleiderer. Why first order quantum phase transitions are interesting. *Journal of Physics: Condensed Matter*, 17(11):S987, 2005.

[64] J. M. Fink, A. Dombi, A. Vukics, A. Wallraff, and P. Domokos. Observation of the photon-blockade breakdown phase transition. *Phys. Rev. X*, 7:011012, 2017. DOI: 10.1103/PhysRevX.7.011012.

[65] Xi Chen, A. Ruschhaupt, S. Schmidt, A. del Campo, D. Guéry-Odelin, and J. G. Muga. Fast optimal frictionless atom cooling in harmonic traps: Shortcut to adiabaticity. *Physical Review Letters*, 104(6), 2010. DOI: 10.1103/physrevlett.104.063002.

[66] M. Demirplak and S. A. Rice. Adiabatic population transfer with control fields. *The Journal of Physical Chemistry A*, 107(46):9937–9945, 2003. DOI: 10.1021/jp030708a.

[67] M. V. Berry. Transitionless quantum driving. *Journal of Physics A: Mathematical and Theoretical*, 42(36):365303, 2009. DOI: 10.1088/1751-8113/42/36/365303.

[68] Alan C. Santos and Marcelo S. Sarandy. Superadiabatic controlled evolutions and universal quantum computation. *Scientific Reports*, 5(1), 2015. DOI: 10.1038/srep15775.

[69] M. Beau, J. Jaramillo, and A. del Campo. Scaling-up quantum heat engines efficiently via shortcuts to adiabaticity. *Entropy*, 18(12):168, 2016. DOI: 10.3390/e18050168.

[70] M. B. Plenio and S. Virmani. An introduction to entanglement measures. *eprint arXiv:quant-ph/0504163*, 2005.

[71] V. Vedral. Foundations of Quantum Discord. *eprint arXiv:quant-ph/1702.01327*, 2017.

[72] Luigi Amico, Rosario Fazio, Andreas Osterloh, and Vlatko Vedral. Entanglement in many-body systems. *Rev. Mod. Phys.*, 80:517–576, 2008. DOI: 10.1103/RevModPhys.80.517.

[73] Koji Maruyama, Franco Nori, and Vlatko Vedral. Colloquium. *Rev. Mod. Phys.*, 81:1–23, 2009. DOI: 10.1103/RevModPhys.81.1.

[74] I. M. Georgescu, S. Ashhab, and Franco Nori. Quantum simulation. *Rev. Mod. Phys.*, 86:153–185, 2014. DOI: 10.1103/RevModPhys.86.153.

[75] A. Osterloh, Luigi Amico, G. Falci, and Rosario Fazio. Scaling of entanglement close to a quantum phase transition. *Nature*, 416, 2002. DOI: 10.1038/416608a.

[76] Tobias J. Osborne and Michael A. Nielsen. Entanglement in a simple quantum phase transition. *Phys. Rev. A*, 66:032110, 2002. DOI: 10.1103/PhysRevA.66.032110.

[77] L.-A. Wu, M. S. Sarandy, and D. A. Lidar. Quantum phase transitions and bipartite entanglement. *Phys. Rev. Lett.*, 93:250404, 2004. DOI: 10.1103/PhysRevLett.93.250404.

[78] L.-A. Wu, M. S. Sarandy, D. A. Lidar, and L. J. Sham. Linking entanglement and quantum phase transitions via density-functional theory. *Phys. Rev. A*, 74:052335, 2006. DOI: 10.1103/PhysRevA.74.052335.

[79] G. Vidal, J. I. Latorre, E. Rico, and A. Kitaev. Entanglement in quantum critical phenomena. *Phys. Rev. Lett.*, 90:227902, 2003. DOI: 10.1103/PhysRevLett.90.227902.

[80] V. E. Korepin. Universality of entropy scaling in one dimensional gapless models. *Phys. Rev. Lett.*, 92:096402, 2004. DOI: 10.1103/PhysRevLett.92.096402.

[81] Pasquale Calabrese and John Cardy. Entanglement entropy and quantum field theory. *Journal of Statistical Mechanics: Theory and Experiment*, 2004(06):P06002, 2004.

[82] Raoul Dillenschneider. Quantum discord and quantum phase transition in spin chains. *Phys. Rev. B*, 78:224413, 2008. DOI: 10.1103/PhysRevB.78.224413.

[83] M. S. Sarandy. Classical correlation and quantum discord in critical systems. *Phys. Rev. A*, 80:022108, 2009. DOI: 10.1103/PhysRevA.80.022108.

[84] J. Maziero, L.C. Céleri, R.M. Serra, and M.S. Sarandy. Long-range quantum discord in critical spin systems. *Physics Letters A*, 376(18):1540 – 1544, 2012. DOI: 10.1016/j.physleta.2012.03.029.

[85] Yichen Huang. Scaling of quantum discord in spin models. *Phys. Rev. B*, 89:054410, 2014. DOI: 10.1103/PhysRevB.89.054410.

[86] T. Werlang, C. Trippe, G. A. P. Ribeiro, and Gustavo Rigolin. Quantum correlations in spin chains at finite temperatures and quantum phase transitions. *Phys. Rev. Lett.*, 105:095702, 2010. DOI: 10.1103/PhysRevLett.105.095702.

[87] Shunlong Luo. Wigner-yanase skew information and uncertainty relations. *Phys. Rev. Lett.*, 91:180403, 2003. DOI: 10.1103/PhysRevLett.91.180403.

[88] E. P. Wigner and Mutsuo M. Yanase. Information contents of distributions. *Proceedings of the National Academy of Sciences*, 49(6):910–918, 1963.

[89] Chang shui Yu, Shao xiong Wu, Xiaoguang Wang, X. X. Yi, and He shan Song. Quantum correlation measure in arbitrary bipartite systems. *EPL (Europhysics Letters)*, 107(1):10007, 2014.

[90] G. Karpat, B. Çakmak, and F. F. Fanchini. Quantum coherence and uncertainty in the anisotropic xy chain. *Phys. Rev. B*, 90:104431, 2014. DOI: 10.1103/PhysRevB.90.104431.

[91] Thiago M Carrijo, Ardiley T Avelar, and Lucas C Céleri. Quantum uncertainty in critical systems with three spins interaction. *Journal of Physics B: Atomic, Molecular and Optical Physics*, 48(12):125501, 2015.

[92] Nan Li and Shunlong Luo. Classical states versus separable states. *Phys. Rev. A*, 78:024303, 2008. DOI: 10.1103/PhysRevA.78.024303.

[93] T. Kato. On the adiabatic theorem of quantum mechanics. *Journal of the Physical Society of Japan*, 5(6):435–439, 1950. DOI: 10.1143/JPSJ.5.435.

[94] A. Messiah. *Quantum Mechanics*, volume II. North- Holland Publishing Company, Amsterdam, 1962.

[95] S. Teufel. *Adiabatic perturbation theory in quantum dynamics, Lecture Notes in Mathematics*. Springer-Verlag Berlin Heidelberg, 2003.

[96] S. Jansen, M.-B. Ruskai, and R. Seiler. Bounds for the adiabatic approximation with applications to quantum computation. *Journal of Mathematical Physics*, 48(10):102111, 2007. DOI: 10.1063/1.2798382.

[97] M. S. Sarandy, L.-A. Wu, and D. A. Lidar. Consistency of the adiabatic theorem. *Quantum Information Processing*, 3(6):331–349, 2004. DOI: 10.1007/s11128-004-7712-7.

[98] Edward Farhi, Jeffrey Goldstone, Sam Gutmann, Joshua Lapan, Andrew Lundgren, and Daniel Preda. A quantum adiabatic evolution algorithm applied to random instances of an np-complete problem. *Science*, 292(5516):472–475, 2001. DOI: 10.1126/science.1057726.

[99] A. J. Berkley, A. J. Przybysz, T. Lanting, R. Harris, N. Dickson, F. Altomare, M. H. Amin, P. Bunyk, C. Enderud, E. Hoskinson, M. W. Johnson, E. Ladizinsky, R. Neufeld, C. Rich, A. Yu. Smirnov, E. Tolkacheva, S. Uchaikin, and A. B. Wilson. Tunneling spectroscopy using a probe qubit. *Phys. Rev. B*, 87:020502, 2013. DOI: 10.1103/PhysRevB.87.020502.

[100] Arnab Das and Bikas K. Chakrabarti. Colloquium. *Rev. Mod. Phys.*, 80:1061–1081, 2008. DOI: 10.1103/RevModPhys.80.1061.

[101] Troels F. Rønnow, Zhihui Wang, Joshua Job, Sergio Boixo, Sergei V. Isakov, David Wecker, John M. Martinis, Daniel A. Lidar, and Matthias Troyer. Defining and detecting quantum speedup. *Science*, 345(6195):420–424, 2014. DOI: 10.1126/science.1252319.

[102] R. et al Barends. Digitized adiabatic quantum computing with a superconducting circuit. *Nature*, 534:222 EP –, 2016. DOI: 10.1038/nature17658.

[103] T. W. B. Kibble. *J. Phys. A* **9**, *1387 (1976); Phys. Rep.* **67**, *183 (1980).*

[104] W. H. Zurek. *Nature (London)* **317**, *505 (1985); Acta Phys. Pol. B* **24**, *1301 (1993); Phys. Rep.* **276**, *177 (1996).*

[105] Wojciech H. Zurek, Uwe Dorner, and Peter Zoller. Dynamics of a quantum phase transition. *Phys. Rev. Lett.*, 95:105701, 2005. DOI: 10.1103/PhysRevLett.95.105701.

[106] Jacek Dziarmaga. Dynamics of a quantum phase transition: Exact solution of the quantum ising model. *Phys. Rev. Lett.*, 95:245701, 2005. DOI: 10.1103/PhysRevLett.95.245701.

[107] Anatoli Polkovnikov. Universal adiabatic dynamics in the vicinity of a quantum critical point. *Phys. Rev. B*, 72:161201, 2005. DOI: 10.1103/PhysRevB.72.161201.

[108] Elena Canovi, Elisa Ercolessi, Piero Naldesi, Luca Taddia, and Davide Vodola. Dynamics of entanglement entropy and entanglement spectrum crossing a quantum phase transition. *Phys. Rev. B*, 89:104303, 2014. DOI: 10.1103/PhysRevB.89.104303.

[109] G Torlai, L Tagliacozzo, and G De Chiara. Dynamics of the entanglement spectrum in spin chains. *Journal of Statistical Mechanics: Theory and Experiment*, 6:P06001, 2014.

[110] W. T. Reid. *Riccati differential equations, Volume 86 (Mathematics in Science and Engineering).* Academic Press, 1972.

[111] Haralambos Panagopoulos and Ettore Vicari. Off-equilibrium scaling behaviors across first-order transitions. *Phys. Rev. E*, 92:062107, 2015. DOI: 10.1103/PhysRevE.92.062107.

[112] Andrea Pelissetto and Ettore Vicari. Dynamic off-equilibrium transition in systems slowly driven across thermal first-order phase transitions. *Phys. Rev. Lett.*, 118:030602, 2017. DOI: 10.1103/PhysRevLett.118.030602.

[113] J. C. Xavier and F. C. Alcaraz. Precise determination of quantum critical points by the violation of the entropic area law. *Phys. Rev. B*, 84:094410, 2011. DOI: 10.1103/PhysRevB.84.094410.

[114] A. Saguia. Study of the 1d anisotropic kondo necklace model at criticality via an entanglement entropy estimator. *Physics Letters A*, 377(37):2288 – 2292, 2013. DOI: 10.1016/j.physleta.2013.06.043.

[115] G. De Chiara, L. Lepori, M. Lewenstein, and A. Sanpera. Entanglement spectrum, critical exponents, and order parameters in quantum spin chains. *Phys. Rev. Lett.*, 109:237208, 2012. DOI: 10.1103/PhysRevLett.109.237208.

[116] Isaac L. Chuang, Neil Gershenfeld, and Mark Kubinec. Experimental implementation of fast quantum searching. *Phys. Rev. Lett.*, 80:3408–3411, 1998. DOI: 10.1103/PhysRevLett.80.3408.

[117] Jonathan A. Jones, Michele Mosca, and Rasmus H. Hansen. Implementation of a quantum search algorithm on a quantum computer. *Nature*, 393:344 EP –, 1998.

[118] P. G. Kwiat, J. R. Mitchell, P. D. D. Schwindt, and A. G. White. Grover's search algorithm: An optical approach. *Journal of Modern Optics*, 47(2-3):257–266, 2000. DOI: 10.1080/09500340008244040.

[119] J. Ahn, T. C. Weinacht, and P. H. Bucksbaum. Information storage and retrieval through quantum phase. *Science*, 287(5452):463–465, 2000. DOI: 10.1126/science.287.5452.463.

[120] N. Bhattacharya, H. B. van Linden van den Heuvell, and R. J. C. Spreeuw. Implementation of quantum search algorithm using classical fourier optics. *Phys. Rev. Lett.*, 88:137901, 2002. DOI: 10.1103/PhysRevLett.88.137901.

[121] K.-A. Brickman, P. C. Haljan, P. J. Lee, M. Acton, L. Deslauriers, and C. Monroe. Implementation of grover's quantum search algorithm in a scalable system. *Phys. Rev. A*, 72:050306, 2005. DOI: 10.1103/PhysRevA.72.050306.

[122] P. Walther, K. J. Resch, T. Rudolph, E. Schenck, H. Weinfurter, V. Vedral, M. Aspelmeyer, and A. Zeilinger. Experimental one-way quantum computing. *Nature*, 434, 2005. DOI: 10.1038/nature03347.

[123] L. DiCarlo, J. M. Chow, J. M. Gambetta, Lev S. Bishop, B. R. Johnson, D. I. Schuster, J. Majer, A. Blais, L. Frunzio, S. M. Girvin, and R. J. Schoelkopf. Demonstration of two-qubit algorithms with a superconducting quantum processor. *Nature*, 460, 2009. DOI: 10.1038/nature08121.

[124] E. Hairer and G. Wanner. *Solving Ordinary Differential Equations II: Stiff and Differential-Algebraic Problems.* Springer, 1996.

[125] B. Boechat, J. Florencio, A. Saguia, and O. F. de Alcantara Bonfim. Critical behavior of a quantum chain with four-spin interactions in the presence of longitudinal and transverse magnetic fields. *Phys. Rev. E*, 89:032143, 2014. DOI: 10.1103/PhysRevE.89.032143.

[126] A. Dutta, G. Aeppli, B. K. Chakrabarti, U. Divakaran, T. F. Rosenbaum, and D. Sen. *Quantum Phase Transitions in Transverse Field Spin Models: From Statistical Physics to Quantum Information.* Cambridge University Press, 2015.

[127] F. L. Curzon and B. Ahlborn. Efficiency of a carnot engine at maximum power output. *American Journal of Physics*, 43(1):22–24, 1975. DOI: 10.1119/1.10023.

[128] Bjarne Andresen, Peter Salamon, and R. Stephen Berry. Thermodynamics in finite time. *Physics Today*, 37(9):62–70, 1984. DOI: 10.1063/1.2916405.

[129] J. P. S. Peterson, T. B. Batalhão, M. Herrera, A. M. Souza, R. S. Sarthour, I. S. Oliveira, and R. M. Serra. Experimental characterization of a spin quantum heat engine. *eprint arXiv:quant-ph/1803.06021*, 2018.

[130] R Alicki. The quantum open system as a model of the heat engine. *Journal of Physics A: Mathematical and General*, 12(5):L103–L107, 1979. DOI: 10.1088/0305-4470/12/5/007.

[131] Ronnie Kosloff. A quantum mechanical open system as a model of a heat engine. *The Journal of Chemical Physics*, 80(4):1625–1631, 1984. DOI: 10.1063/1.446862.

[132] M. O. Scully. Extracting work from a single heat bath via vanishing quantum coherence. *Science*, 299(5608):862–864, 2003. DOI: 10.1126/science.1078955.

[133] J. Rossnagel, O. Abah, F. Schmidt-Kaler, K. Singer, and E. Lutz. Nanoscale heat engine beyond the carnot limit. *Physical Review Letters*, 112(3), 2014. DOI: 10.1103/physrevlett.112.030602.

[134] J. Rossnagel, S. T. Dawkins, K. N. Tolazzi, O. Abah, E. Lutz, F. Schmidt-Kaler, and K. Singer. A single-atom heat engine. *Science*, 352(6283):325–329, 2016. DOI: 10.1126/science.aad6320.

[135] G. Maslennikov, S. Ding, R. Hablutzel, J. Gan, A. Roulet, S. Nimmrichter, J. Dai, V. Scarani, and D. Matsukevich. Quantum absorption refrigerator with trapped ions. *ArXiv e-prints*, 2017.

[136] Eitan Geva and Ronnie Kosloff. On the classical limit of quantum thermodynamics in finite time. *The Journal of Chemical Physics*, 97(6):4398–4412, 1992. DOI: 10.1063/1.463909.

[137] Yair Rezek and Ronnie Kosloff. Irreversible performance of a quantum harmonic heat engine. *New Journal of Physics*, 8(5):83–83, 2006. DOI: 10.1088/1367-2630/8/5/083.

[138] Naoto Shiraishi, Keiji Saito, and Hal Tasaki. Universal trade-off relation between power and efficiency for heat engines. *Physical Review Letters*, 117(19), 2016. DOI: 10.1103/physrevlett.117.190601.

[139] R. Onofrio. Physics of our days: Cooling and thermometry of atomic fermi gases. *Physics-Uspekhi*, 59(11):1129, 2016. DOI: 10.3367/UFNe.2016.07.037873.

[140] Erik Torrontegui, Sara Ibáñez, Sofia Martínez-Garaot, Michele Modugno, Adolfo del Campo, David Guéry-Odelin, Andreas Ruschhaupt, Xi Chen, and Juan Gonzalo

Muga. Shortcuts to adiabaticity. In *Advances In Atomic, Molecular, and Optical Physics*, pages 117–169. Elsevier, 2013.

[141] Jiawen Deng, Qing hai Wang, Zhihao Liu, Peter Hänggi, and Jiangbin Gong. Boosting work characteristics and overall heat-engine performance via shortcuts to adiabaticity: Quantum and classical systems. *Physical Review E*, 88(6), 2013. DOI: 10.1103/physreve.88.062122.

[142] A. del Campo, J. Goold, and M. Paternostro. More bang for your buck: Superadiabatic quantum engines. *Scientific Reports*, 4(1), 2014. DOI: 10.1038/srep06208.

[143] O. Abah and E. Lutz. Energy efficient quantum machines. *EPL (Europhysics Letters)*, 118(4):40005, 2017. DOI: 10.1209/0295-5075/118/40005.

[144] M. G. Bason, M. Viteau, N. Malossi, P. Huillery, E. Arimondo, D. Ciampini, R. Fazio, V. Giovannetti, R. Mannella, and O. Morsch. High-fidelity quantum driving. *Nature Physics*, 8(2):147–152, 2011. DOI: 10.1038/nphys2170.

[145] J. Zhang, J. Hyun Shim, I. Niemeyer, T. Taniguchi, T. Teraji, H. Abe, S. Onoda, T. Yamamoto, T. Ohshima, J. Isoya, and D. Suter. Experimental implementation of assisted quantum adiabatic passage in a single spin. *Physical Review Letters*, 110(24), 2013. DOI: 10.1103/physrevlett.110.240501.

[146] Yan-Xiong Du, Zhen-Tao Liang, Yi-Chao Li, Xian-Xian Yue, Qing-Xian Lv, Wei Huang, Xi Chen, Hui Yan, and Shi-Liang Zhu. Experimental realization of stimulated raman shortcut-to-adiabatic passage with cold atoms. *Nature Communications*, 7:12479, 2016. DOI: 10.1038/ncomms12479.

[147] Shuoming An, Dingshun Lv, Adolfo del Campo, and Kihwan Kim. Shortcuts to adiabaticity by counterdiabatic driving for trapped-ion displacement in phase space. *Nature Communications*, 7:12999, 2016. DOI: 10.1038/ncomms12999.

[148] Cheng Chin, Rudolf Grimm, Paul Julienne, and Eite Tiesinga. Feshbach resonances in ultracold gases. *Rev. Mod. Phys.*, 82:1225–1286, 2010. DOI: 10.1103/RevModPhys.82.1225.

[149] Yvan Castin and Félix Werner. The unitary gas and its symmetry properties. In *The BCS-BEC Crossover and the Unitary Fermi Gas*, pages 127–191. Springer Berlin Heidelberg, 2011.

[150] Y. Nishida and D. T. Son. Nonrelativistic conformal field theories. *Physical Review D*, 76(8), 2007. DOI: 10.1103/physrevd.76.086004.

[151] Wilhelm Zwerger, editor. *The BCS-BEC Crossover and the Unitary Fermi Gas*. Springer Berlin Heidelberg, 2012.

[152] Peter Talkner, Eric Lutz, and Peter Hänggi. Fluctuation theorems: Work is not an observable. *Physical Review E*, 75(5), 2007. DOI: 10.1103/physreve.75.050102.

[153] K. M. O'Hara, S. L. Hemmer, M. E. Gehm, S. R. Granade, and J. E. Thomas. Observation of a strongly interacting degenerate fermi gas of atoms. *Science*, 298(5601):2179–2182, 2002. DOI: 10.1126/science.1079107.

[154] D. T. Son. Three comments on the Fermi gas at unitarity in a harmonic trap. *eprint arXiv:quant-ph/0707.1851*, 2007.

[155] R. P. Feynman. Forces in molecules. *Phys. Rev.*, 56:340–343, 1939. DOI: 10.1103/PhysRev.56.340.

[156] Yu. Kagan, E. L. Surkov, and G. V. Shlyapnikov. Evolution of a bose gas in anisotropic time-dependent traps. *Phys. Rev. A*, 55:R18–R21, 1997. DOI: 10.1103/PhysRevA.55.R18.

[157] K. Husimi. Miscellanea in elementary quantum mechanics, II. *Progress of Theoretical Physics*, 9(4):381–402, 1953. DOI: 10.1143/ptp/9.4.381.

[158] J. Jaramillo, M. Beau, and A. del Campo. Quantum supremacy of many-particle thermal machines. *New Journal of Physics*, 18(7):075019, 2016. DOI: 10.1088/1367-2630/18/7/075019.

[159] Sebastian Deffner, Christopher Jarzynski, and Adolfo del Campo. Classical and quantum shortcuts to adiabaticity for scale-invariant driving. *Physical Review X*, 4(2), 2014. DOI: 10.1103/physrevx.4.021013.

[160] Shu-Jin Deng, Peng-Peng Diao, Qian-Li Yu, and Hai-Bin Wu. All-optical production of quantum degeneracy and molecular bose-einstein condensation of 6li. *Chinese Physics Letters*, 32(5):053401, 2015. DOI: 10.1088/0256-307x/32/5/053401.

[161] S. Deng, Z.-Y. Shi, P. Diao, Q. Yu, H. Zhai, R. Qi, and H. Wu. Observation of the efimovian expansion in scale-invariant fermi gases. *Science*, 353(6297):371–374, 2016. DOI: 10.1126/science.aaf0666.

[162] Peter Salamon, Karl Heinz Hoffmann, Yair Rezek, and Ronnie Kosloff. Maximum work in minimum time from a conservative quantum system. *Phys. Chem. Chem. Phys.*, 11(7):1027–1032, 2009. DOI: 10.1039/b816102j.

[163] Y. Rezek, P. Salamon, K. H. Hoffmann, and R. Kosloff. The quantum refrigerator: The quest for absolute zero. *EPL (Europhysics Letters)*, 85(3):30008, 2009. DOI: 10.1209/0295-5075/85/30008.

[164] Dionisis Stefanatos, Justin Ruths, and Jr-Shin Li. Frictionless atom cooling in harmonic traps: A time-optimal approach. *Physical Review A*, 82(6), 2010. DOI: 10.1103/physreva.82.063422.

[165] K. H. Hoffmann, P. Salamon, Y. Rezek, and R. Kosloff. Time-optimal controls for frictionless cooling in harmonic traps. *EPL (Europhysics Letters)*, 96(6):60015, 2011. DOI: 10.1209/0295-5075/96/60015.

[166] Anirban Dutta, Armin Rahmani, and Adolfo del Campo. Anti-kibble-zurek behavior in crossing the quantum critical point of a thermally isolated system driven by a noisy control field. *Phys. Rev. Lett.*, 117:080402, 2016. DOI: 10.1103/PhysRevLett.117.080402.